

DISSERTATION

Interactions between Fuel Ash from Residues and K-Feldspar Bed Material and their Significance for Fluidised Bed Thermal Conversion Systems

ausgeführt zum Zwecke der Erlangung des akademischen Grades eines
Doktors der technischen Wissenschaften

unter der Leitung von

Univ.Prof.i.R. Dipl.Ing. Dr.techn. Hermann Hofbauer

und unter der Betreuung von

Univ.Lektor Dipl.Ing. Dr.techn. Matthias Kuba

und

Ass.Prof. Docent Nils Skoglund, Ph.D. M.Sc. M.Sc.Eng.

Institut für Verfahrenstechnik,

Umwelttechnik und Technische Biowissenschaften

eingereicht an der Technischen Universität Wien,

Fakultät für Maschinenwesen und Betriebswissenschaften

von

Dipl.Ing. Katharina Fürsatz

Matrikelnummer 1125234

Wien, January 27, 2021

Katharina Fürsatz



Die approbierte gedruckte Originalversion dieser Dissertation ist an der TU Wien Bibliothek verfügbar.
The approved original version of this doctoral thesis is available in print at TU Wien Bibliothek.

Affidativ

I, Katharina Fürsatz, hereby declare

1. that I am the sole author of the present Dissertation "Interactions between Fuel Ash from Residues and K-Feldspar Bed Material and their Significance for Fluidised Bed Thermal Conversion Systems", 184 pages, bound, and that I have not used any sources or tool other than those referenced or any other illicit aid or tool.
2. that I have not prior to this date submitted this Dissertation as an examination paper in any form in Austria or abroad.
3. I acknowledge that the submitted work will be checked electronically-technically using suitable and state-of-the-art means (plagiarism detection software). On the one hand, this ensures that the submitted work was prepared according to the high-quality standards within the applicable rules to ensure good scientific practice "Code of Conduct" at the TU Wien. On the other hand, a comparison with other student theses avoids violations of my personal copyright.

Vienna, January 27,2021

Katharina Fürsatz



Die approbierte gedruckte Originalversion dieser Dissertation ist an der TU Wien Bibliothek verfügbar.
The approved original version of this doctoral thesis is available in print at TU Wien Bibliothek.

Acknowledgements

I want to thank Matthias for providing me with the possibility to work with him in the field of bed materials and fuel layers. You were always supporting me in every way possible and your enthusiasm for every new research question and new solution is contagious. I am really glad I had you as my supervisor in the last years.

I also want to thank Hermann for supervising me as a PhD student in the field of biomass gasification. I was able to choose from a variety of reactors and other infrastructure that were developed under your care. I appreciate all your input during my research and the discussions about results.

Thanks to you, Nils, for being the hardcore chemist always overwhelming me with your knowledge about and excitement for crystals, compounds and shooting lasers. The time spent in Sweden played a big part during my research and made it possible to considerably broaden my topic.

I am also grateful to my external reviewers Pavleta Knutsson and Fabrizio Scala for taking the time to evaluate this thesis and being the external examiners for my PhD examination.

Thanks to the BEST colleagues one could hope for. I always enjoyed our extensive discussions about today's lunch choice and our afternoon chocolate and cake brakes. Thanks to you guys I was always looking forward to the next day at work! I also want to thank the colleagues from TU Wien for performing all the gasification experiments presented throughout this thesis. Special thanks to Josef for providing me with the idea for my last paper and supporting me in finalising it to be published. I also want to thank my colleagues in Sweden, especially Nikki, for supporting me in my week long SEM sessions, and Gustav for spending several days and nights with me in the lab.

I also want to thank all my master students I supervised throughout the years. The experiments you performed helped me in further developing my thesis in a way I couldn't have done alone. You also showed me again that I am really fond of teaching and supervising, even though the students got on my nerves one time or another.

I am really grateful to my parents, siblings, friends and parents-in-law for making me the person I am today. Your support along the way made it easy to tackle everything step by

step. I also thank my husband Marian for supporting me throughout all the years of my studies as well as my thesis. You always listened to all my problems and ideas and even gave me valuable input on my work. Implementing the criticism you had regarding my figures and statistics highly improved my papers and this thesis and made me a more reflective scientist.

Abstract

In dual fluidised bed (DFB) steam gasification the bed material is used to transport heat from the combustion to the gasification reactor and also to act as a catalyst for i.e. tar reduction. Olivine has proven to be a suitable mineral for this application. Various previous studies have shown that during operation a layer is formed on the surface of the bed material, originating from interactions between fuel ash and bed material. This layer improves the catalytic activity of olivine. However, olivine contains traces of heavy metals necessitating the deposition of bottom ash, which is connected to increased operation costs of a plant. A heavy-metal-free material would therefore allow for further use of the bottom ash. Furthermore, until now only woody based fuels have been used in DFB steam gasification, but the use of waste streams would improve the economic feasibility of the system. Studying the behaviour with these more complicated fuels increases the flexibility of the system.

K-feldspar was selected as possible candidate for an alternative bed material and thoroughly studied during this thesis. It was used as bed material in both fluidised bed combustion and DFB steam gasification experiments. A variety of alternative fuels were tested in combination with K-feldspar as bed material to additionally determine the suitability of K-feldspar for the use with alternative fuels with higher ash contents compared to softwood. The fuels tested within this thesis include bark, straw, chicken manure and various mixtures between those fuels. The performance of DFB steam gasification experiments with K-feldspar were benchmarked against experiments with fresh and layered olivine and calcite. Samples collected during the experiments were studied for ash layers that formed on the bed material with scanning electron microscope microscopy combined with energy dispersive X-ray spectroscopy. The samples were additionally used in a micro-scale test-rig to determine and compare their catalytic activity regarding the Water-Gas-Shift (WGS) reaction.

The results obtained from these experiments were summarised to answer three major aspects to bring K-feldspar closer to utilization in DFB steam gasification plants. Firstly, the suitability of K-feldspar as alternative to olivine was evaluated. Secondly, the mechanisms behind fuel ash layer formation with P-lean and P-rich fuels were determined. Thirdly, the catalytic activity of fuel ash layers on K-feldspar and the time-dependent activation towards

gasification reactions, with a focus on the WGS reaction, was described.

It was possible to show the applicability of K-feldspar as bed material both for fluidised bed combustion and DFB steam gasification. Problems with agglomeration and ash accumulation were observed occasionally but could be traced back to the low-melting eutectics originating from the fuel ash composition. The experiments showed that special attention has to be given to ash handling when alternative fuels are used.

Fuel ash layers on K-feldspar were studied originating from a variety of different fuels. Throughout this thesis it was possible to further clarify the mechanisms proposed for layer formation on K-feldspar with P-lean fuels. Additionally, a yet undescribed mechanism was proposed for P-rich fuels. P inhibits the diffusion of Ca into the particle, leading to thinner inner layers. Due to the reduced diffusion of Ca into the particle the diffusion of K out of the particle was reduced as well.

In conclusion, it was possible to show that fuel ash can lead to an increase in catalytic activity of catalytically inactive bed materials like K-feldspar. The use of K-feldspar as bed material in DFB steam gasification in combination with ash-rich fuels is therefore especially promising. More research as well as dedicated long-term experiments will be necessary to further support the role of ash-rich fuels for K-feldspar activation.

Kurzfassung

In der Zweibettwirbelschichtdampfvergasung wird ein Bettmaterial verwendet, um Wärme vom Verbrennungsreaktor zum Vergasungsreaktor zu transportieren. Zeitgleich wirkt es auch als Katalysator für die Teerreduktion in der Vergasung. Hierbei hat sich Olivin als zweckmäßiges Mineral für diese Anwendung erwiesen. Zahlreiche frühere Studien haben gezeigt, dass sich während des Betriebes eine Schicht auf der Oberfläche des Bettmaterials, aufgrund der Interaktion zwischen Bettmaterial und Brennstoffasche, bildet. Diese Schicht verbessert die katalytische Wirkung des Bettmaterials. Das derzeit verwendete Olivin enthält allerdings Spuren von Schwermetallen, die es notwendig machen die produzierte Asche zu deponieren, was die Betriebskosten einer Anlage erhöht. Ein schwermetallfreies Bettmaterial würde eine weitere Nutzung der Asche erlauben und somit die Betriebskosten, durch Wegfall der Deponierungskosten, senken. Weiters wurden bis jetzt nur holzartige Brennstoffe in kommerziellen Zweibettwirbelschichtdampfvergasungsanlagen verwendet, allerdings würde die Verwendung von Abfallströmen hierbei die Wirtschaftlichkeit des Systems verbessern. Wird das Wissen über das Verhalten dieser alternativen Brennstoffe in der Wirbelschicht verbessert, erhöht dies die Flexibilität der Zweibettwirbelschichtdampfvergasung.

K-Feldspat wurde als mögliches alternatives Bettmaterial ausgewählt und umfassend untersucht. Es wurde als Bettmaterial in Wirbelschichtverbrennungsversuchen sowie Versuchen zur Zweibettwirbelschichtdampfvergasung verwendet. Eine Vielzahl an alternativen Brennstoffen wurde gleichzeitig mit K-Feldspat als Bettmaterial untersucht, um dessen Eignung in Kombination mit alternativen Brennstoffen mit einem höheren Aschegehalt als Weichholz zu ermitteln. Die untersuchten Brennstoffe waren Rinde, Stroh, Hühnermist sowie Mischungen zwischen diesen Brennstoffen. Die Zweibettwirbelschichtdampfvergasungsversuche mit K-Feldspat wurden zusätzlich mit Versuchen mit frischen und benutztem Olivin sowie Kalk verglichen. Die gesammelten Proben wurden mit einem Rasterelektronenmikroskop kombiniert mit energiedispersiver Röntgenspektroskopie auf Ascheschichten untersucht. Zusätzlich wurden die Proben in einem Mikro-Prüfstand untersucht um die katalytische Aktivität bezüglich der Wasser-Gas-Shift Reaktion zu ermitteln.

Die erhaltenen Ergebnisse wurden zusammengefasst um drei Forschungsfragen zu beantworten und die Verwendung von K-Feldspat als Bettmaterial voranzutreiben. Erstens wurde die Eignung von K-Feldspat als Alternative zu Olivin evaluiert. Zweitens wurde der Mechanismus hinter dem Schichtwachstum mit P-armen und P-reichen Brennstoffen ermittelt. Drittens wurde die katalytische Aktivität von Ascheschichten auf K-Feldspat sowie seine zeitabhängige Aktivierung bezüglich Vergasungsreaktionen, mit einem Fokus auf die Wasser-Gas-Shift Reaktion, beschrieben.

Es war möglich die Anwendbarkeit von K-Feldspat für die Wirbelschichtverbrennung sowie die Zweibettwirbelschichtdampfvergasung zu zeigen. Die auftretenden Probleme mit Agglomeration und Ascheanreicherung wurden gelegentlich beobachtet, konnten aber auf die verwendeten Brennstoffe und die niedrigschmelzenden Eutektika der Brennstoffasche zurückgeführt werden. Die Versuche zeigten daher, dass die Handhabung der Brennstoffasche besonders beachtet werden muss.

Ascheschichten auf K-Feldspat wurden für eine Vielzahl an verschiedenen Brennstoffen untersucht. Während dieser Arbeit war es möglich die bereits vorgeschlagenen Mechanismen des Schichtwachstums mit P-armen Brennstoffen zu bestätigen. Zusätzlich wurde ein erster Mechanismus für P-reiche Brennstoffe vorgestellt. P hemmt die Diffusion von Ca in K-Feldspat was zu dünneren inneren Schichten führt. Aufgrund der verringerten Diffusion von Ca in das Partikel war die Diffusion von K aus dem Partikel hinaus ebenfalls gehemmt. Ebenfalls war es möglich zu zeigen, dass Brennstoffasche zu einer katalytischen Aktivierung von katalytisch inaktiven Bettmaterialien wie K-Feldspat führt. Die Anwendung von K-Feldspat als Bettmaterial in der Zweibettwirbelschichtdampfvergasung in Kombination mit aschereichen Brennstoffen ist daher besonders vielversprechend. Weitere Untersuchungen sowie dezidierte Langzeitversuche werden notwendig sein, damit die Rolle von aschereichen Brennstoffen auf die Aktivierung von K-Feldspat vollständig geklärt werden kann.

Contents

Affidativ	I
Abstract	V
Kurzfassung	VII
List of appended journal papers	XIII
Author’s contribution	XV
Other scientific publications of relevance	XVII
List of supervised and co-supervised theses	XIX
1 Introduction	1
1.1 Unsustainability of Today’s Energy Consumption	1
1.2 Energy Production in a Circular Economy	3
2 Fundamentals	5
2.1 Thermochemical Conversion of Biomass and Waste	5
2.1.1 Gasification Technologies	7
2.2 Dual Fluidised Bed Steam Gasification	9
2.2.1 Current Developments in DFB Steam Gasification	9
2.3 Bed Material-Fuel Ash Interactions	10
2.3.1 Agglomeration	11
2.3.2 Layer Formation	12
2.3.3 Influencing the Product Gas Quality by Bed Material Choice and Fuel Ash Layers	14
2.4 Alternative Biogenic Fuels in Gasification	15

2.4.1	Woody Biomass	15
2.4.2	Agricultural Residues	16
2.4.3	Sewage Sludge and Manures	17
3	Aim of the Work	19
4	Experimental Setup and Methodology	21
4.1	Used Fuels	21
4.2	Used Bed materials	21
4.3	Fluidised Bed Combustion	23
4.4	Dual Fluidised Bed Steam Gasification	24
4.5	Determination of Catalytic Activity	26
4.5.1	Water-Gas-Shift Calculations	28
4.6	Morphological and Elemental Analysis	29
4.6.1	XRF	29
4.6.2	XRD	29
4.6.3	SEM/EDS	29
4.6.4	BET	31
5	Results and Discussion	33
5.1	Fluidised Bed Performance	33
5.1.1	Fluidised Bed Combustion	33
5.1.2	Fluidised Bed Gasification	38
5.1.3	Summary	40
5.2	Layer Formation on K-Feldspar	40
5.2.1	Comparison of Layer Formation during Combustion and Gasification	40
5.2.2	Time-Dependent Layer Formation	43
5.2.3	Layer Thickness	47
5.2.4	Surface Characterisation	51
5.2.5	Detailed Layer Formation Observations	53
5.2.6	Proposed Layer Formation Process on K-Feldspar with P-rich Fuels	55
5.2.7	Differences to Fuel Ash Fractions	57
5.2.8	Comparison to Layer Formation on Quartz and Limestone	59
5.3	Bed Material and Ash Layers Catalytic Activity	62
5.3.1	Catalytic Activity during Gasification	62
5.3.2	Activation of Different Bed Materials during Gasification	65
5.3.3	Time-Dependent Activation of Bed Material by Fuel Ash Layers	66

6	Future Work	69
6.1	K-feldspar as Bed Material in Industrial Plants	69
6.2	Long-term Experiments with Alternative Fuels	70
6.2.1	Sewage Sludge	70
6.3	Further Characterisation of Ash Fractions	71
6.4	Further Development of Micro-Scale Test-Rig	71
7	Conclusions	73
	List of Figures	77
	List of Tables	81
	Nomenclature	83
	Abbreviations and Acronyms	83
	Symbols	84
	Bibliography	85



Die approbierte gedruckte Originalversion dieser Dissertation ist an der TU Wien Bibliothek verfügbar.
The approved original version of this doctoral thesis is available in print at TU Wien Bibliothek.

List of appended journal papers

The work presented in this thesis is based on five published peer-reviewed papers.

- Paper I** Layer formation mechanism of K-feldspar in bubbling fluidized bed combustion of phosphorus-lean and phosphorus-rich residual biomass
Wagner K., Häggström G., Skoglund N., Priscak J., Kuba M., Öhman M., Hofbauer H.
Applied Energy, **2019**, 248, 545-554
<https://doi.org/10.1016/j.apenergy.2019.04.112>
- Paper II** Layer formation on K-feldspar in fluidized bed combustion and gasification of bark and chicken manure
Wagner K., Häggström G., Mauerhofer A. M., Kuba M., Skoglund N., Öhman M., Hofbauer H.
Biomass and Bioenergy, **2019**, 127, 105251
<https://doi.org/10.1016/j.biombioe.2019.05.020>
- Paper III** Impact of residual fuel ash layers on the catalytic activation of K-feldspar regarding the water–gas shift reaction
Fürsatz K., Kuba M., Janisch D., Aziaba K., Hammerl C., Chlebda D., Lojewska J., Hofbauer H.
Biomass Conversion and Biorefinery, **2021**, 11, 3-14
<https://doi.org/10.1007/s13399-020-00645-w>
- Paper IV** Effect of Biomass Fuel Ash and Bed Material on the Product Gas Composition in DFB Steam Gasification
Fürsatz K., Fuchs J., Benedikt F., Kuba M., Hofbauer H.
Energy, **2021**, 219, 119650
<https://doi.org/10.1016/j.energy.2020.119650>

- Paper V** Fate of Phosphorus in Fluidized Bed Cocombustion of Chicken Litter with Wheat Straw and Bark Residues
Hägström G., Fürsatz K., Kuba M., Skoglund N., Öhman M.
Energy Fuels, **2020**, 34, 1822-1829
<https://doi.org/10.1021/acs.energyfuels.9b03652>

Author's contribution

- Paper I** Katharina Fürsatz carried out the majority of the performed experiments and the sampling of bed material samples. Furthermore, Katharina Fürsatz performed all SEM/EDS measurements and all data evaluation. In addition, Katharina Fürsatz wrote the scientific paper and acted as corresponding author.
- Paper II** Katharina Fürsatz carried out all combustion experiments including bed material sampling. During the gasification experiments on the 100 kW pilot plant Katharina Fürsatz was involved in the experimental design. Additionally, Katharina Fürsatz performed all SEM/EDS measurements as well as data evaluation. Furthermore, Katharina Fürsatz wrote the scientific paper and acted as corresponding author.
- Paper III** Katharina Fürsatz designed and supervised the experiments on the micro-scale test-rig and performed the BET analyses. Additionally, Katharina Fürsatz performed all data analysis. Furthermore, Katharina Fürsatz wrote the scientific paper and acted as corresponding author.
- Paper IV** Katharina Fürsatz assisted in the preparation in the gasification experiments and performed all experiments on the micro-scale test-rig. Additionally, Katharina Fürsatz performed all SEM/EDS measurements and all data analysis regarding the experiments on the micro-scale test-rig. Furthermore, Katharina Fürsatz wrote the scientific paper and acted as corresponding author.
- Paper V** Katharina Fürsatz carried out the majority of the performed experiments and bed material and fuel fraction sampling. Furthermore, Katharina Fürsatz critically reviewed the manuscript.



Die approbierte gedruckte Originalversion dieser Dissertation ist an der TU Wien Bibliothek verfügbar.
The approved original version of this doctoral thesis is available in print at TU Wien Bibliothek.

Other scientific publications of relevance

- Paper 1** Influence of Phosphorus on the Layer Formation on K-Feldspar during Fluidized Bed Combustion and Gasification
Wagner K., Kuba M., Häggström G., Skoglund N., Öhman M., Hofbauer H.
European Biomass Conference and Exhibition Proceedings, **2018**, 26th EUBCE, 486-492
<https://doi.org/10.5071/26thEUBCE2018-2BO.6.2>
- Paper 2** Suitability of K-Feldspar as Alternative Bed Material in Dual Fluidized Bed Steam Gasification in Combination with Ash-Rich Feedstocks
Wagner K., Mauerhofer A.M., Kuba M., Hofbauer H.
23rd International Conference on FBC, **2018**, 967-976
- Paper 3** Effect on P-Mineralization in Fluidized Bed Combustion of Chicken Litter with Wheat Straw and Bark Residues
Häggström G., Wagner K., Kuba M., Skoglund N., Öhman M.
27th International Conference of Impacts of Fuel Quality on Power Production and the Environment, 23–28 September, **2018**, Lake Louise, Canada
- Paper 4** Time-Dependent Catalytic Activation of Inactive K-Feldspar by Layer Formation During Fluidized Bed Conversion with Residual Fuels
Wagner K., Hammerl C., Kuba M, Hofbauer H.
European Biomass Conference and Exhibition Proceedings, **2019**, 27th European Biomass Conference and Exhibition, 779-785
<https://doi.org/10.5071/27thEUBCE2019-2CV.2.4>

- Paper 5** Influence of Fuel Ash and Bed Material on the Water-Gas-Shift Equilibrium in DFB Biomass Steam Gasification
Fürsatz K., Fuchs J., Bartik A., Kuba M., Hofbauer H.
Proceedings of the ICPS 19, **2019**, 10-19
ISBN: 978-3-9503671-1-9
<https://doi.org/10.34726/42>
- Paper 6** Investigation of the Formation of Coherent Ash Residues during Fluidized Bed Gasification of Wheat Straw Lignin
Priscak J., Fürsatz K., Kuba M., Skoglund N., Benedikt F., Hofbauer H.
energies, **2020**, 13(15), 3935
<https://doi.org/10.3390/en13153935>
- Paper 7** Surface Characterization of Ash-Layered Olivine from Fluidized Bed Biomass Gasification
Kuba M., Fürsatz K., Janisch D., Aziaba K., Lojewska J., Forsberg F., Umeki K., Hofbauer H.
Biomass Conv. Bioref., **2021**, 11, 29-38
<https://doi.org/10.1007/s13399-020-00863-2>

List of supervised and co-supervised theses

The following Bachelor Master theses were supervised or co-supervised by the author:

- | | |
|----------------------|--|
| Martin, M. | Gasification of alternative biomass feedstock in a dual fluidized bed gasification |
| Hannl, T. | Ash Chemistry Characterization after DFB Steam Gasification of Waste Feedstock Mixtures Using Quartz, Olivine & Lime Bed Materials |
| Foglar, A. | Asche - Bettmaterial - Interaktionen während thermischer Wirbelschichtumwandlungen von Rinde, Gülle und landwirtschaftlichen Abfällen |
| Hammerl, C. | Time-dependent catalytic activity of used K-feldspar for biomass gasification |
| Reichmann, F. | Katalytische Aktivität von Biomasseasche: Vergleich der katalytischen Aktivität von gebrauchtem Bettmaterial mit Mischungen aus Olivin und Kalziumoxid |
| Langer, M. | Suitability of a newly developed fluidized bed reactor for the activation of alternative bed materials |



Die approbierte gedruckte Originalversion dieser Dissertation ist an der TU Wien Bibliothek verfügbar.
The approved original version of this doctoral thesis is available in print at TU Wien Bibliothek.

Chapter 1

Introduction

1.1 Unsustainability of Today's Energy Consumption

The wealth of today's society is mainly based on the exploitation of natural resources in an unsustainable way. Several control variables summarised as planetary boundaries scurrently exceed their threshold or are in a zone of uncertainty (see Figure 1.1). Climate change is only one prominent example of a planetary boundary in a zone of uncertainty. There are several international efforts combating climate change, with the Paris Agreement being one of the

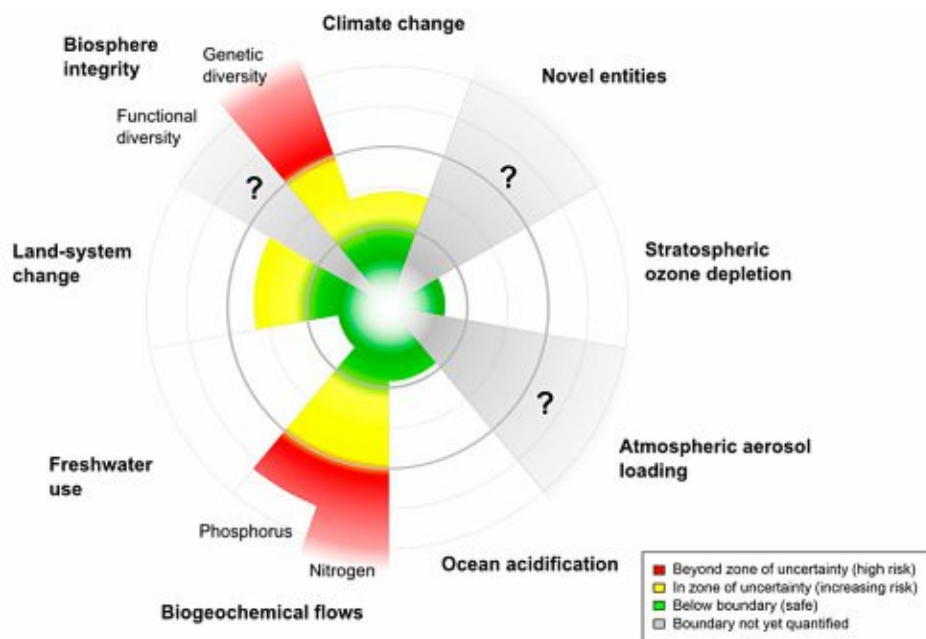


Figure 1.1: Current status of seven from nine planetary boundaries as defined by Steffen et al. [1].

most recent ones. The Paris Agreement is a worldwide agreement within the United Nations Framework Convention on Climate Change. Parties that ratified the Paris Agreement accord to hold the rise in global temperature below 2 °C compared to pre-industrial levels and aim to limit the increase in global temperature to 1.5 °C [2]. Currently 188 of the 197 Parties of the Convention have ratified the Paris Agreement [3].

Climate change is caused by man-made emissions of CO₂ and other greenhouse gases. CO₂ emissions rose from 280 ppm in pre-industrial times [4] to 414 ppm in April 2020 [5]. Figure 1.2 (top) depicts the worldwide CO₂ emissions by sector. The highest emissions can be attributed to electricity and heat production and the highest proportionate increase in emissions was observed for industry.

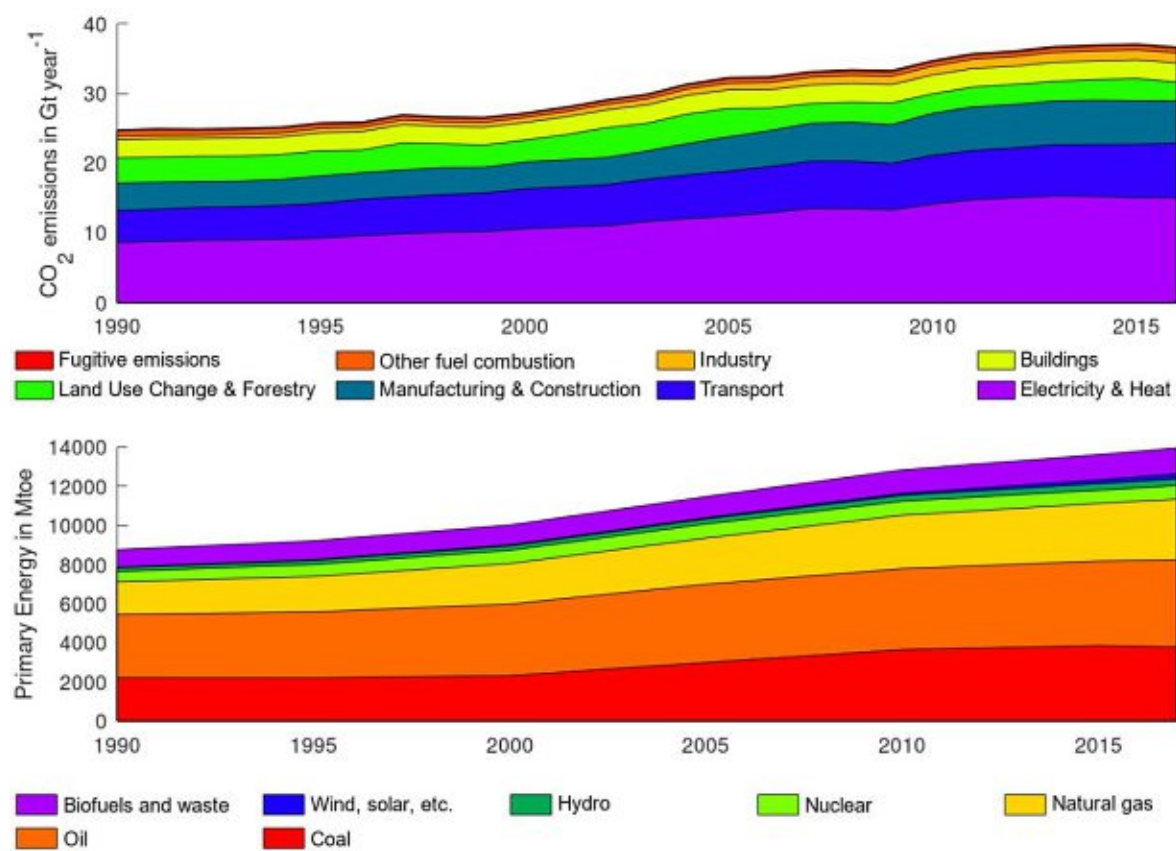


Figure 1.2: Top: CO₂ emissions worldwide by sector in the years 1990 to 2016. Adapted from [6]. Bottom: Primary Energy consumption in million tonnes oil equivalent worldwide in the years 1990 to 2017. Adapted from [7].

The increase in CO₂ emissions observed for electricity and heat production can be further explained with the increase in primary energy consumption (see Figure 1.2 bottom). The majority of primary energy is currently produced from fossil resources and its share on total primary energy consumption stayed constant in the years 1990 to 2017 at around 81 %.

1.2 Energy Production in a Circular Economy

Today's linear economy with one-time use of resources is one of the causes for exceeding several of the planetary boundaries. A linear economy leads to a depletion of natural resources and accumulation of unused waste deposited in landfills or polluting the oceans. Switching to a more sustainable economy is necessary to reduce humanities' impact on the environment.

A possible approach to reduce the use of resources can be summarised under the term circular economy. Geissdoerfer et al. [8] defined circular economy in the following way:

Circular economy is a regenerative system in which resource input and waste, emission, and energy leakage are minimised by slowing, closing, and narrowing material and energy loops. This can be achieved through long-lasting design, maintenance, repair, reuse, remanufacturing, refurbishing, and recycling.

Pursuing a Circular Economy leads to a more sustainable economy and helps in reducing CO₂ emissions. The European Green Deal is an ambitious goal set by the European Commission for zero net emissions of greenhouse gases in the European Union by 2050 [9]. Additional goals of the Green Deal are the transition to a clean, circular economy by an efficient use of resources and the restoration of biodiversity.

An increase in renewable energy is one piece in transitioning to a more sustainable economy by reducing the one-time use of fossil resources for energy production. An especially appealing approach is gasification of waste. This way waste is not deposited on landfills but further utilised. By choosing waste gasification it is not only possible to provide power and heat but also valuable gases that can be used for synthesis of chemicals and liquid fuels. More details will be provided in the following chapter.

Wastes often contain a notable amount of inorganic components that remain as so-called ash after gasification. Some waste materials, like manures, contain considerable amounts of valuable nutrients like P. Utilizing these waste streams in gasification is one way to concentrate these nutrients and making it easier to recover them. Phosphorus (P) is an important nutrient necessary for all life to flourish. The European Food Safety Agency recommends a P uptake of 700 mg d⁻¹ [10]. Currently P is mainly produced from phoshate rock, which is a finite ressource [11]. In a report from 2017 the European Union recognises P as critical raw material [12]. P was also identified as one of nine planetary boundaries for a sustainable society and P depletion is an even greater risk to the planet than climate change [1] (Figure 1.1).

Manures are one possible source for P recycling. Manures can be used as fertiliser directly,

but this is infeasible in areas where not enough agriculture is close to animal farms. Combustion of manures facilitates the organic compounds for energy production while the resulting ash is enriched in P and other nutrients. Pig manure ash after combustion contains 18.8 % of P_2O_5 , chicken manure ash contains 15.3 % and kitchen waste typically contains 18.8 % [10]. The resulting ash can be used for P recovery or might already be suitable as fertiliser as it is.

During combustion P can be precipitated in a variety of compounds. Apatite is a mineral unavailable for plants for nutrient uptake while whitlockites incorporating K into their crystal structure have shown positive leaching properties for plant uptake [13]. Schiemenz and Eichler-Löbermann [14] tested three different biomass ashes (rape meal, straw and cereal ash) for their suitability as P fertiliser. Overall, the results showed a similar fertilization effect compared to triple superphosphate, a highly soluble P source. Codling et al. [15] studied the effect of poultry manure ash as a source for P comparing to another commercial fertiliser, namely potassium phosphate. The tests did not show any differences between the poultry manure ash and the commercial fertiliser, suggesting that poultry manure ash is a suitable fertiliser.

Chapter 2

Fundamentals

2.1 Thermochemical Conversion of Biomass and Waste

Biomass is a renewable energy source originally gaining its energy content from solar irradiation via photosynthesis [16]. Compared to other energy forms originating from the sun (e.g. photovoltaics, wind energy) biomass stores solar energy and is independent of the current weather [16]. Biomass can be converted into energy by physico-chemical, bio-chemical or thermo-chemical conversion processes. A physico-chemical conversion process is the extraction of plant oil from oil-rich biomass by pressing. Anaerobic digestion to biogas and fermentation are examples for bio-chemical conversion processes. Thermo-chemical conversion processes include combustion, pyrolysis and gasification [16, 17].

During thermochemical conversion biomass passes several stages. During heating and drying, water is removed from the biomass matrix. Drying can take place up to temperatures of 200 °C [16].

Pyrolysis is the next step occurring after drying. At temperatures of around 150 °C–220 °C the destruction of macromolecules inside the biomass starts. This process occurs until a temperature of around 500 °C. The macromolecules (cellulose, hemicellulose, lignin) are mainly converted to H₂O, CO₂, CO and methanol as well as solid residues, also referred to as coke [16]. Pyrolysis reactions take place without O₂, even if O₂ would be available. The vast amount of gaseous products forming during pyrolysis are released from inside the particle and hinder the access of O₂ to the biomass [16].

The coke produced during pyrolysis is further decomposed if oxygen is available, marking the so-called gasification step. The carbonaceous material is transformed into a gas mixture of CO, CO₂, H₂, H₂O and CH₄. Depending on the gasification method the resulting gas additionally contains N₂, tars, soot and other higher hydrocarbons [18].

A wide variety of reactions occur during gasification, the most important ones are given in Equations (2.1)–(2.8). Equations (2.1) and (2.2) display the exothermal (partial) oxidation of C and occur when O₂ is available in the gasification agent. The C-matrix can also be gasified by H₂O (water-gas reaction), CO₂ (boudouard reaction) and H₂ (hydrogasification), shown in Equations (2.3)–(2.5).

- Oxidation:



- Partial oxidation:



- Heterogeneous water-gas reaction:



- Boudouard reaction:



- Hydrogasification:



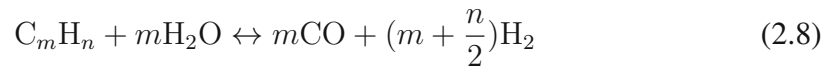
- Water-gas-shift reaction:



- Steam reforming of methane:



- Steam reforming of hydrocarbons:



Apart from heterogeneous reactions between the solid C-matrix and the fluidisation medium a variety of homogeneous gas phase reactions occur. Equations (2.6)–(2.8) show a selection of homogeneous gas phase reactions occurring in the presence of steam. The Water-Gas-Shift (WGS) reaction is one of the major reactions in controlling the H₂:CO ratio in the gas produced during gasification.

Combustion is the last step of thermochemical conversion. It describes the complete conversion of carbonaceous matter to CO₂ and H₂O. The heat produced during combustion can be either used directly as heat source or further converted to power [16]. Enough O₂ has to be available for complete oxidation to occur. The relation of available oxygen to the minimal necessary oxygen for complete oxidation is the air excess number λ (see Equation (2.9)).

$$\lambda = \frac{\text{available oxygen}}{\text{stoichiometric O}_2} \quad (2.9)$$

2.1.1 Gasification Technologies

Thermochemical gasification of biogenic fuels produces a gas rich in CO, CO₂, H₂, H₂O and CH₄, the so-called product gas [16]. Gasification is a promising option to advance the eco-friendly and efficient production of secondary energy carriers as well as heat and power generation from this product gas. It can additionally be used as reactant for various syntheses, like Fischer-Tropsch [19, 20], natural gas [21, 22], and mixed alcohol synthesis [23]. Additionally it is possible to separate H₂ from the gas stream for renewable H₂ generation [24].

Gasification can be performed in a variety of different reactors. All of these designs have different advantages and disadvantages, which will be further described in the following section. Especially the plant size is one criterion when choosing the appropriate gasification technology. The smallest plants can be realised as fixed bed gasifiers with a size of 10 kW–10 MW. Fluidised beds cover the medium range of applicability with a size of 2 MW–100 MW and entrained flow gasifiers are most optimal at power ranges of 40 MW–1 GW [18].

Fixed Bed Gasification

In fixed bed gasifiers the fuel forms a fixed bed (i.e. the gas velocity is too low to move the fuel). The fuel is fed from the top and undergoes all steps of thermochemical conversion at different heights of the reactor while moving downwards leaving behind ash at the bottom of the reactor. The most common fixed bed gasifiers are the co-current and counter-current fixed bed gasifiers. The terms co-current and counter-current describe the relation of flow directions of the fuel (always downward) and the gas (downwards for co-current and upwards for counter-current gasification). This design is especially suitable for small scale applications due to its simple design.

Fluidised Bed Gasification

Fluidised bed reactors consist of a bed material which is held in suspension by the gas stream. The bed material consists of solid particles, typically with a size of 0.5 mm–1 mm, and it can be inert or act as a catalyst [16]. The use of a fluidised bed ensures good gas-solid mixing and a uniform temperature throughout the bed making it possible to use a variety of fuels of different qualities [25] (e.g. possible fuel water contents of 0.05 kg kg⁻¹–0.6 kg kg⁻¹ dry fuel [16]). Fluidised bed gasification can be performed in bubbling fluidised beds or circulating fluidised beds which vary in the applied gas velocities. A special form of fluidised bed gasifiers are dual fluidised beds (DFBs). DFBs consist of two reactors, with one reactor being dedicated to gasification and the second being dedicated to combustion to supply heat for endothermic gasification reactions.

Entrained Flow Gasification

For entrained flow gasification the fuel is finely ground, which is especially challenging for biomass since grinding of fibrous materials is energy intensive [18]. The fuel is then gasified at 1200 °C in co-current flow with air or oxygen [16]. The small particle size of the fuel leads to complete gasification after a few seconds. Due to the high temperatures occurring the fuel ash normally melts and can be collected as slag. Therefore, entrained flow gasification is especially suitable for fuels with low ash-melting behaviour which cannot be used easily in other gasification technologies. The high temperatures also lead to a low tar content and low methane content which are especially advantageous for synthesis applications [18].

2.2 Dual Fluidised Bed Steam Gasification

DFB steam gasification employs steam as a gasification agent, leading to a N_2 -free product gas [26–28] with a heating value of around 10 MJ m^{-3} – 16 MJ m^{-3} [29].

The basic principle of DFB steam gasification is shown in Figure 2.1. This process is based on the separation of endothermic gasification and exothermic combustion. Heat, which is necessary for the endothermic gasification, is provided by a circulating bed material from the combustion reactor (CR) to the gasification reactor (GR). Steam is used as the gasification agent for the bubbling bed in the GR. A part of the produced char is transported to the CR with the bed material and combusted to provide the heat necessary for gasification [30, 31]. Apart from heat transfer the bed material additionally works as a catalyst regarding tar reduction and the WGS reaction [32–34]. Due to its attrition resistance and catalytic activity towards tar reforming olivine was originally chosen as a suitable mineral for this application [35].

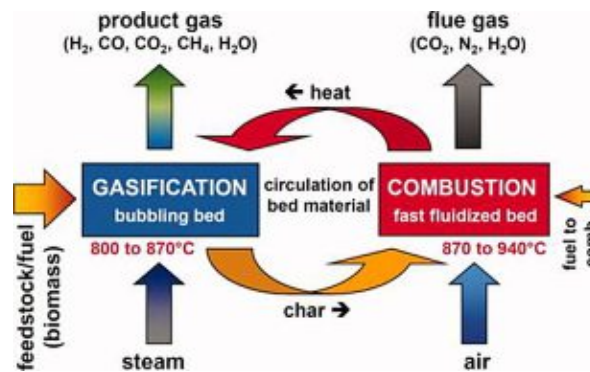


Figure 2.1: Basic principle of DFB steam gasification [30].

Based on this concept, the first industrial application using wood as fuel was commissioned in the early 2000s with the combined heat and power plant Güssing in Austria (8 MW thermal input fuel capacity). Further plants went into operation in Oberwart, Austria (9 MW thermal input fuel capacity), Villach, Austria (15 MW thermal input fuel capacity), Senden, Germany (15 MW thermal input fuel capacity), and Göteborg, Sweden (32 MW thermal input fuel capacity) [29, 36].

2.2.1 Current Developments in DFB Steam Gasification

Due to economic problems most of the DFB steam gasification plants erected until now are currently not in operation [37]. In Austria the plants in Güssing and Oberwart were shut down after the expiration of the "Ökostromförderung" for the plants making them econom-

ically infeasible. An economically infeasible operation also led to shut downs of plants in Germany and Sweden.

Recent research in the field of DFB steam gasification is focussing on improving economics and process performance in a variety of ways. Considerable research is focussed on alternative fuels with lower costs compared to softwood. Further information regarding alternative fuels is summarised in Section 2.4.

Also the bed material is subject to continuous research in DFB steam gasification. The olivine used until now contains considerable amounts of heavy metals like Ni and Cr making it necessary to deposit the ash, which contains fractions of olivine due to attrition [38]. By changing to a heavy metal-free alternative the deposition costs can be saved. The research on alternative bed materials and their performance regarding layer formation and catalytic activity are summarised in Section 2.3. Additionally, it may be possible to further utilise the ash to generate additional revenue. This is especially interesting when using ash- and nutrient-rich fuels. Preliminary research on the fertilisation potential of P-rich fuel ashes showed promising results, as was already described in Subsection 1.2.

The products strived for are also developing to more high value outputs. Instead of providing a gas suitable for heat and power production, as was the case for most of the previous commercial plants, the product gas is now optimised for downstream syntheses. Ways to influence the $H_2:CO$ ratio are investigated to achieve a ratio suitable for syntheses (2:1 for Fischer Tropsch synthesis [39] and mixed alcohol synthesis [23], 3:1 for methanation [40]). This and reduced tar contents, reducing gas cleaning complexity, are mainly achieved by using catalytically active bed materials and optimised process conditions.

A demonstration plant of 1 MW is currently being erected in Vienna with a focus on waste and especially sewage sludge gasification. The differences to wood gasification will be studied in campaigns of several weeks as a last step before commercialisation. Syntheses (e.g Fischer-Tropsch) will also be performed downstream to represent the entire process chain.

2.3 Bed Material-Fuel Ash Interactions

The interactions between fuel ash, which is produced during thermo-chemical conversion, and bed material can have several positive as well as negative effects on the operation of fluidised beds. Agglomeration of the bed material can lead to defluidization and unplanned plant shut-downs. On the other hand, layer formation is increasing the catalytic activity of bed materials for gasification reactions.

2.3.1 Agglomeration

Agglomeration occurs when several bed material particles stick together to form an agglomerate of particles, which cannot be fluidised with the same fluidisation velocity, leading to defluidisation. Most literature regarding agglomeration is focused on quartz, the most common bed material used for fluidised bed combustion applications. Two types of agglomeration are described in literature, namely coating-induced and melt-induced agglomeration [41]. Figure 2.2 depicts both agglomeration types.

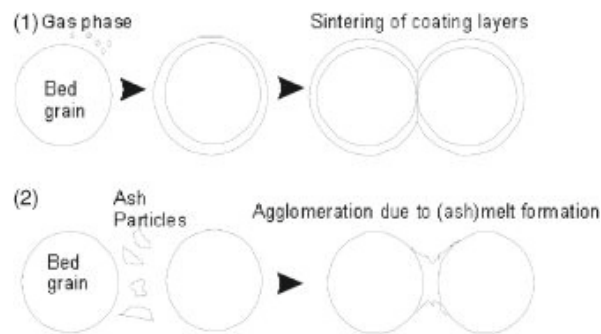


Figure 2.2: Agglomeration types. (1) Coating-induced agglomeration, (2) Melt-induced agglomeration [41].

Coating-induced agglomeration is caused by the formation of alkali silicate melts on the bed material surface. These alkali silicates are normally potassium silicates due to the higher concentration of K compared to Na in most of the fuels [42]. An inner layer forms via interaction of alkali from the fuel ash with the Si from the bed material. When bed material particles collide, agglomeration might occur by the formation of a potassium silicate neck connecting the particles at critical conditions. Higher temperatures and thicker layers were identified as conditions promoting agglomeration [41].

Melt-induced agglomeration is caused by the collision of molten ash particles with bed material particles [42]. Agglomerates resulting from melt-induced agglomeration normally show more melt and agglomerate formation compared to coating-induced agglomeration. In this case the melt phase approximately mirrors the fuel ash composition [41].

Reduction of ash related problems by additives

Kaolin ($\text{Al}_2\text{Si}_2\text{O}_5(\text{OH})_4$) is a possible additive that can be used to increase the ash melting temperature in fluidised beds [42–44]. Öhman and Nordin [45] were able to increase the agglomeration temperature of wheat straw in a quartz bed from 739 °C to 886 °C.

Vuthaluru et al. [46, 47] tested the potential of calcite and magnesite to reduce ash-related problems during the combustion of low-rank coals. While the presence of Mg made it

possible to contain ash-related problems it was only possible to delay and reduce the severity of ash-related problems with Ca-containing minerals. Zhou et al. [48] correlated the higher stability of dolomite against agglomeration compared to magnesite to its Ca-content. The Ca in dolomite binds the Si from the ash so it is not available for reactions with K to form low-melting eutectics.

2.3.2 Layer Formation

Quartz

Quartz (SiO_2) is one of the most abundant minerals in the continental crust and is the most commonly used bed material in fluidised bed combustion. It has a Mohs' hardness of 7 and a density of 2.65 g cm^{-3} [49].

Öhman et al. [50] performed combustion and gasification experiments with various fuels in a quartz bed. They observed two layers on the quartz bed material particles, a homogeneous inner layer rich in K-Ca-silicates and an ash particle-rich outer layer. Apart from the fuel Lucerne, an S-rich fuel, no difference in layer formation was determined between combustion and gasification. Similar observations were made by Brus et al. [51]. The inner layer grew inwards the particle forming Ca-rich silicates. For fuels rich in K and Na, a layer rich in alkali silicates developed. The outer layer originated from an adhesion of ash particles.

Grimm et al. [52] observed a change in layer formation mechanisms with P-rich fuels. As soon as P is available, alkali and alkaline earth metals first react with P before reacting with Si [53] leading to the changes in layer formation.

Feldspars

Feldspars are a group of minerals consisting of K-feldspar (KAlSi_3O_8), Na-feldspar ($\text{NaAlSi}_3\text{O}_8$) and Ca-feldspar ($\text{CaAl}_2\text{Si}_2\text{O}_8$) as its end members. Feldspars are the most common mineral in the Earth's crust, making up around $0.51 \text{ m}^3 \text{ m}^{-3}$ [49]. Feldspars have a Mohs' hardness of 6 and a density of 2.6 g m^{-3} – 2.7 g m^{-3} [49].

Kuba et al. [38] observed layers on K-feldspar particles from a DFB gasification process in Senden, Germany. The K-feldspar particles were introduced into the olivine bed as impurities, probably from the woody biomass used as fuel. The Ca-content inside the layers increased towards the particle surface, while K was depleted. This indicates a substitution of K^+ by Ca^{2+} . The increase in Ca towards the surface also decreases the amount of melt predicted through thermochemical calculations, indicating a reduced agglomeration

tendency of the layers. He et al. [54] also observed a substitution of K with Ca in K-feldspar layers indicating that the diffusion of Ca into the particle plays a major role in layer formation.

Berguerand and Berdugo Vilches [55] used an alkali-feldspar (0.48 kg kg^{-1} K-feldspar, 0.4 kg kg^{-1} Na-feldspar, 0.06 kg kg^{-1} Ca-feldspar, 0.06 kg kg^{-1} quartz) as bed material in a DFB steam gasification plant. Layers rich in Ca, K, Mg and Na were observed. Faust et al. [56] and Hannl et al. [57] further studied alkali feldspars in a two part study and compared the layer formation on K- and Na-feldspars. They observed that Na-feldspar undergoes an additional reaction step by forming K-rich layers with K from the fuel ash. Due to this additional reaction layer they concluded that Na-feldspar is a less stable bed material compared to K-feldspar. During the formation of this K-rich layer Si and Na are expelled from the Na-feldspar particle which can cause an increase in ash melting and agglomeration.

Olivine

Olivine ($(\text{Mg, Fe, Mn})_2\text{SiO}_4$) is the most commonly used bed material in commercial DFB steam gasification plants. It has a Mohs' hardness of 6.5–7 and a density between 3.2 g cm^{-3} (Mg_2SiO_4) and 4.3 g cm^{-3} (Fe_2SiO_4) [49].

De Geyter et al. [58] observed layer formation on olivine during bark, olive residue and wheat straw combustion. The inner layers that formed during these experiments were rich in Mg, Si, Ca and K. Davidsson et al. [44] performed combustion experiments with olivine and wood pellets co-fired with straw pellets. Layers rich in Ca could be observed. No K and only little Si-enrichment could be observed in the layers. Ca-rich layers were also observed by Kirnbauer and Hofbauer [59]. They studied bed materials from the DFB steam gasification plant located in Güssing, Austria. The missing K in the inner layers formed on olivine is in accordance with chemical equilibrium calculations [60].

Kuba et al. [34] proposed a mechanism for layer formation based on long-term operation at the DFB steam gasification plant in Senden, Germany and thermochemical calculations with the tool FactSage. They described several phases of layer formation. The first phase is a solid-solid reaction between Ca^{2+} and olivine. The continuous addition of Ca by fuel ash slowly substitutes Fe and Mg from the olivine structure, starting with Fe. Several Ca-Mg-silicates are formed as intermediates before the substitution ends with Ca_2SiO_4 . The Mg expelled from the inner layer is trapped between inner layer and outer ash-rich layer, leading to an Mg-rich part in the inner layer. The changes in bond length due to the substitution reactions lead to tensions inside the particle and subsequently to cracks in the layers and fragmentations of the layer. The findings reported by Faust et al. [61] support the proposed

mechanism. They observed two layers, a porous outer layer which was rich in MgO and an inner layer rich in Ca-Mg-silicates.

2.3.3 Influencing the Product Gas Quality by Bed Material Choice and Fuel Ash Layers

While fresh K-feldspar showed no catalytic activity towards tar reforming [62], a recognisable catalytic activity was observed for alkali feldspar [55, 63]. The used alkali feldspar consisted of 0.48 kg kg⁻¹ K-feldspar, 0.4 kg kg⁻¹ Na-feldspar, 0.06 kg kg⁻¹ Ca-feldspar and 0.06 kg kg⁻¹ quartz [63]. The literature indicates that K-feldspar and quartz are inactive components in the alkali feldspar [62, 64], but no information is available for pure Na-feldspar and Ca-feldspar in literature.

At the elevated temperatures used for DFB steam gasification, calcite is calcined to CaO. Calcite, resp. CaO, has been occasionally tested as bed material for DFB steam gasification [65, 66]. The use of calcite leads to elevated contents of H₂ and reduced tar contents. Only the dust content in the product gas is increased due to abrasion caused by the low hardness of calcite. Another application of calcite is sorption enhanced reforming (SER), using the same reactor setup as DFB steam gasification [67]. SER takes advantage of the calcination of CaCO₃ to CaO. The gasification takes place at comparably low temperatures of around 650 °C where CaCO₃ is still stable. The bed material is then transported to the combustion reactor, reaching around 900 °C calcinating the CaCO₃ to CaO and releasing CO₂ with the flue gas. The bed material is transported back to the gasifier where it is carbonated back to CaCO₃. With the aid of calcination and carbonation it is possible to produce a product gas enriched in H₂ and a CO₂-rich flue gas.

Delgado et al. [68] compared the catalytic activity for calcite, magnesite and dolomite during gasification and concluded that dolomite is the most active mineral, followed by magnesite and calcite. They speculated that the presence of both Ca and Mg distorts the crystal lattice, resulting in more active sites for reactions to take place. Hervy et al. [69] detected a deactivation of dolomite of around 24 % during air-blown biomass fluidised bed gasification caused by accumulation of Si and coke on the surface.

An extensive study compared the activation potential of several bed materials [70]. Quartz, ilmenite, bauxite and olivine were used as bed material in the DFB steam gasification plant at Chalmers University of Technology, Sweden for one week each. It was possible to observe an approximation towards the WGS equilibrium over time for all tested bed materials. A reduction in tar content was also observed. The highest catalytic activity was observed for bauxite and the lowest activation was observed for quartz.

The influence of fuel ash layers on olivine on the catalytic activity was studied by Kirnbauer et al. [71]. They saw a decrease in tar content (up to 80 % GCMS tars reduction) in the product gas produced at the DFB plant Güssing, Austria. An influence on the WGS reaction was observed by Kuba et al. [64] for layers formed on olivine from the DFB power plant in Senden, Germany and layers on quartz from a bubbling fluidized bed (BFB) combustion plant in Austria. Marinkovic et al. [72] also detected an increase in catalytic activity for olivine over time. They also measured a positive impact of elemental S, which was added to the boiler. The positive impact of S was explained by its potential to bond K. Gaseous K is attributed with a positive impact on tar reduction as well [72]. The addition of silica sand to the olivine bed led to increased tar concentrations in the product gas. Berdugo Vilches et al. [73] activated olivine with K and S and studied its potential for char gasification with steam. They described the transfer of K and S from the outer olivine layer into the char particle, which enhanced the gasification of the char particle. Faust et al. [74] detected MgO in olivine layers and linked the increase of catalytic activity to its enrichment on the surface instead of K-enrichment.

Layers on feldspars have also been linked to an increased catalytic activity. Berguerand and Berdugo Vilches observed a decrease in tars of 47 % in the first 4 d of operation with alkali feldspar [55]. After 7 d of operation they observed an oxygen-carrying capability of the alkali-feldspar. This means that oxygen was transported from the combustion reactor to the gasification reactor by the bed material further oxidizing the product gas, leading to higher levels of CO₂ and lower levels of H₂.

2.4 Alternative Biogenic Fuels in Gasification

A wide variety of fuels other than wood are possible candidates for combustion and gasification applications. Alternative fuels often have higher ash contents, making it necessary to give additional attention to ash removal and ash melting as well as other ash related influences.

2.4.1 Woody Biomass

Logging residues and bark are already regularly used in combustion plants as well as occasionally in gasification plants due to their lower price or abundant availability. Woody biomass ash is rich in Ca which is advantageous for bed material activation. Nilsson et al. [75] performed air gasification experiments with olive tree prunings in laboratory scale. Based on the experiments they calculated a cold gas efficiency up to 70 % and a carbon con-

version over 95 % for commercial scale.

The DFB steam gasification plant GoBiGas in Göteborg was operated with bark for 12 000 h in the years 2014 to 2018 [76]. Extrapolating the obtained bark gasification data to a fuel input of dried bark showed that a comparable gasification performance could be achieved compared to wood pellets. They also did not observe any agglomeration problems during operation with bark. It was also possible to show a cost reduction for biofuel production from bark gasification of around 40 % compared to wood pellet gasification.

Andritz operates two circulation fluidised bed gasification plants, one in Finland (48 MW) and one in China (65 MW) [77], with bark and chip screening fines and replace fossil fuels in the lime kiln of pulp mills. In the plant in Finland it was possible to replace 95 % of natural gas on a yearly basis.

2.4.2 Agricultural Residues

Many agricultural residuals contain high amounts of Si or other elements which reduce the ash melting point. He et al. [78] tested grape marc, wheat straw and cotton stalks in fluidised beds in combustion and steam gasification atmosphere. They observed different mechanisms for agglomeration for the different fuels. For grape marc and cotton stalk a layer induced agglomeration was observed, while wheat straw showed a melt induced agglomeration. The steam available during steam gasification lowers the melting point of alkali carbonates. This leads to more alkali silicates forming larger agglomerates, which was best observed for grape marc. During the conversion of grape marc and cotton stalk a difference in S distribution over the reactor could be observed as well. In a combustion atmosphere S stays in the ash and binds alkali and earth alkali metals. In a steam gasification atmosphere the S is released into the gas phase leaving more alkali metals free to react with Si to form low melting silicates, enhancing the agglomeration tendency.

Fryda et al. [79] studied the agglomeration tendency of giant reed, sweet sorghum bagasse and olive bagasse during fluidised bed gasification. The first two agglomerated at low temperatures (785 °C to 812 °C) due to the formation of silicate ash melts. Olive bagasse defluidised at higher temperatures (830 °C in a quartz bed, <850 °C in an olivine bed) as was predicted by thermodynamic calculations.

To mitigate the problems associated with low ash melting behaviour blending of agricultural residues with other fuels was studied. Valin et al. [80] gasified two mixtures of wheat straw with oak bark (50:50 and 15:85 weight %) modelling dual fluidised bed gasification by first gasifying and then switching to combustion of the char in the same reactor. They observed initial agglomeration formation for the 50:50 mixture but did not observe any problems

with the lower straw admixture. The gasification with the 15:85 mixture seemed overall promising with a cold gas efficiency of 80 %.

2.4.3 Sewage Sludge and Manures

Manures and sewage sludge are rich in various nutrients like P. Their high ash and water content makes using them more challenging than wood. Skoglund et al. [81] combusted pelletised sewage sludge in a bench-scale fluidised bed. The burnt-out fuel formed so-called "ash pellets", meaning that the fuel ash basically kept the shape of the pellets during burn-out. Due to these ash pellets most of the fuel ash remained inside the fluidised bed, making it especially interesting for further utilization as e.g. fertiliser.

Poultry manure has been tested in gasification applications several times [82–84]. Ng et al. [82] co-gasified chicken manure with 70 % wood waste and obtained a comparable lower heating value to the gasification of pure wood waste. Pandey et al. [84] and Horvat et al. [83] studied the gasification of poultry manure in fluidised beds. During the experiments limestone addition was necessary due to agglomerations occurring in the bed without added limestone [84]. The high ash content of poultry manure increased the catalytic activity in the reactor and led to comparably low tar contents in the product gas. The high N content of poultry manure also changes the range of tars observed during poultry gasification leading to a variety of N-containing tars in the product gas [83].



Die approbierte gedruckte Originalversion dieser Dissertation ist an der TU Wien Bibliothek verfügbar.
The approved original version of this doctoral thesis is available in print at TU Wien Bibliothek.

Chapter 3

Aim of the Work

The main aim of this work is to increase the sustainability of DFB steam gasification. K-feldspar was studied as alternative, heavy metal-free bed material to substitute olivine in future DFB steam gasification applications. It was chosen since it is a mineral abundant in the earth's crust worldwide, making it a possible candidate to be an alternative bed material globally. Apart from the bed material also different waste fuels were investigated to increase the sustainability of the system. The waste streams studied were bark, straw and chicken manure. This way a wide array of different fuel types and their suitability for DFB steam gasification were identified. Especially the use of chicken manure influenced the layers occurring on K-feldspar compared to the layers described in literature for woody biomass. Further understanding the mechanisms behind layer formation is of major importance to be able to better predict agglomeration of the bed material. Since agglomeration can lead to costly plant shut-downs, being able to better predict and hinder agglomeration further improves the efficiency of DFB steam gasification plants. The effect of fuel ash and layer formation is of importance regarding catalytic activation. The possibilities of fuel ash to activate catalytically inactive K-feldspar are of major interest to optimise DFB steam gasification performance. Especially the initial activation is relevant since it shows the time-span at which a noticeable enhancement of the product gas composition can be expected.

Additionally, an outlook on the next steps necessary to further develop K-feldspar as bed material and the use of alternative fuels in DFB steam gasification will be given.

Throughout this thesis the following research questions will be addressed and answered:

1. *Can K-feldspar be used as alternative bed material in DFB steam gasification to replace olivine?*

2. *What are the mechanisms behind fuel ash layer formation on K-feldspar?*
3. *How is the catalytic activity and time-dependent activation of fuel ash layers influenced by different fuels?*

Chapter 4

Experimental Setup and Methodology

4.1 Used Fuels

A wide variety of fuels were used throughout this thesis. A summary of fuel properties is given in Table 4.1 and the fuel ash composition is depicted in Figure 4.1. The used fuels cover a wide range regarding their ash content and ash composition. Therefore, the content of ash-forming elements varies in a range of several magnitudes. While softwood (SW) is an ash-lean fuel, chicken manure (CM) contains a considerable amount of ash, mentionable are the high contents of Ca and P which are relevant elements in layer formation processes.

If necessary, fuels were pre-dried in a first step. Each fuel was then milled and pelletised to pellets with a diameter of 6 mm. For preparation of the fuel mixtures the fuels were mixed before milling, to ensure a homogeneous mixture. All fuel mixtures (given in Table 4.1) are based on a dry mass basis (db). SW and CM pellets were the only fuels not milled and pelletised since they were already available as 6 mm pellets.

4.2 Used Bed materials

Several bed materials were used throughout this work to study their behaviour during DFB steam gasification (see Table 4.2). K-feldspar is the focus of this thesis as a new bed material candidate for DFB steam gasification. Olivine was tested since it is the bed material currently utilised in commercial plants. Two types of olivine were studied throughout this work, a fresh, calcined olivine and a used olivine from the DFB steam gasification plant in Senden, Germany. Limestone was taken for mixtures with K-feldspar to model activated bed material. Pure limestone was also applied as bed material as benchmark for a catalytically active bed material.

Table 4.1: Summary of properties of the fuels used throughout this thesis.

fuel (mixtures)	abbr.	ash content	LHV	volatile matter	ash deformation temperature
fuel mixtures in weight-% db		kg kg ⁻¹ db	kJ kg ⁻¹ db	in kg kg ⁻¹ db	°C
softwood bark	SW	0.002	18 943	0.854	1180
wheat straw	BA	0.081	18 180	0.722	1160
chicken manure	WS	0.075	16 860	0.747	830
90 % BA, 10 % CM	CM	0.254	13 900	0.677	n.o.
70 % BA, 30 % CM	B9C1	0.095	17 500	0.702	1230
90 % WS, 10 % CM	B7C3	0.135	16 430	0.687	n.o.
70 % WS, 30 % CM	S9C1	0.090	16 900	0.742	880
70 % WS, 30 % CM	S7C3	0.130	16 010	0.718	1170
59.5 % BA, 15 % WS, 25.5 % CM	BSC	0.125	16 780	0.699	1335

db dry mass basis

n.o. not observed

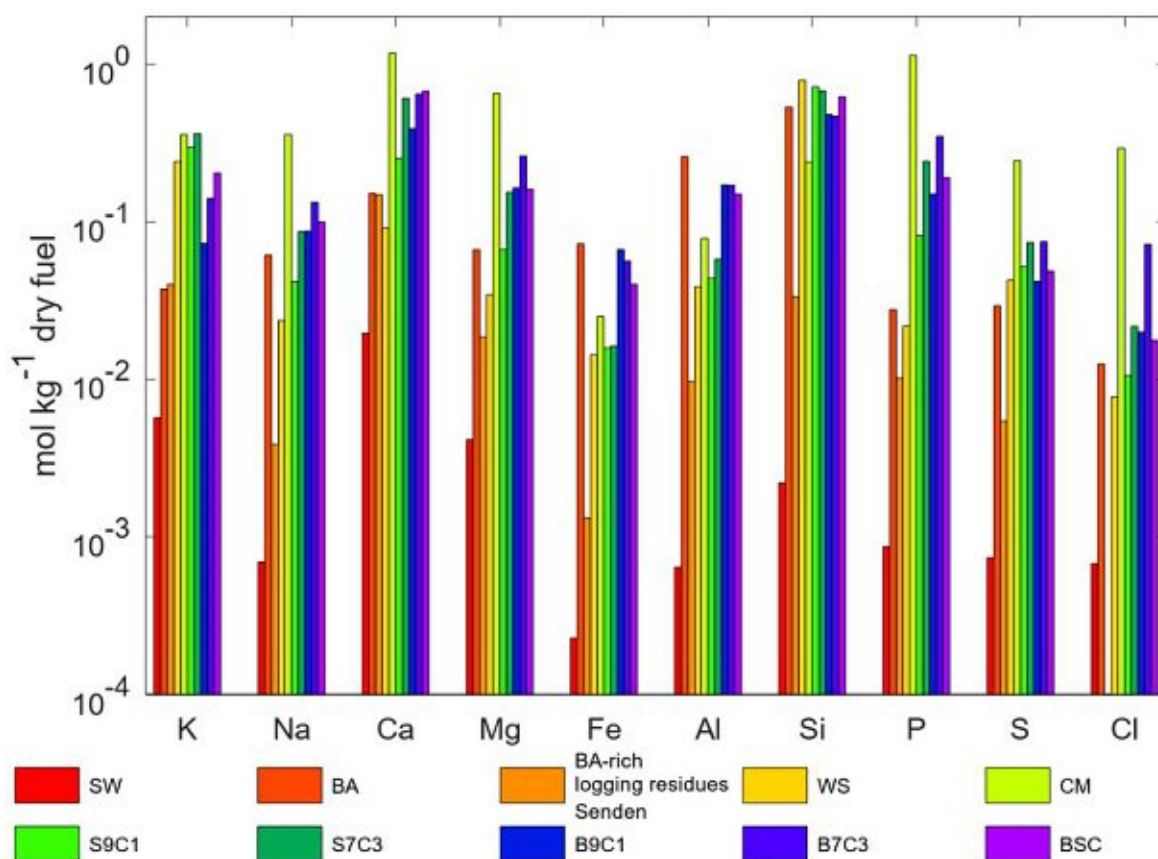


Figure 4.1: Fuel ash composition of the fuels used throughout this thesis.

Table 4.2: Sauter diameter, density as well as hardness of the used bed materials.

Bed material	Sauter diameter μm	particle density kg m^{-3}	bulk density kg m^{-3}	Moh's hardness -
K-feldspar	287	2600	1250	6
Limestone	480	2650 (1500*)	1400 (800*)	3
fresh olivine	250	2850	1500	6
used olivine	329	n.d.	n.d.	n.d.

* after calcination

n.d. not determined

K-feldspar was also used as bed material for combustion experiments. For these experiments it was sieved to a size of $200\ \mu\text{m}$ – $250\ \mu\text{m}$.

4.3 Fluidised Bed Combustion

The 5 kW fluidised bed combustion plant at Umeå University was used for an experimental campaign with a focus on the formation of ash layers on K-feldspar. A detailed scheme of the plant is depicted in Figure 4.2. The fluidised bed has a height of 2 m, an inner diameter of 100 mm in the fluidised bed and a diameter of 200 mm in the freeboard section. A primary air flow of $50\ \text{L min}^{-1}$ and a secondary air flow of $30\ \text{L min}^{-1}$ were used during the experiments. External heating was applied to ensure a homogeneous temperature along the reactor height. Temperatures, differential pressures and the flue gas composition were monitored continuously. The cyclone removed all particles bigger than $10\ \mu\text{m}$ from the flue gas. The flue gas was then further cleaned in a water scrubber (not depicted in Figure 4.2). A more detailed description of the plant was published by Öhman and Nordin [85].

540 g of sieved K-feldspar ($200\ \mu\text{m}$ – $250\ \mu\text{m}$) was filled into the reactor for each experiment. The reactor was heated up to the operational temperature ($730\ ^\circ\text{C}$ – $830\ ^\circ\text{C}$) before starting with the fuel feed. The lower end of the range was used for wheat straw (WS) and WS mixtures, due to WS's lower ash melting point (see Table 4.1). The fuels were fed with a rate of around $0.7\ \text{kg h}^{-1}$ for 40 h or until the bed collapsed. Bed material samples were taken after 2 h, 4 h, 8 h, 16 h, 24 h, 32 h and 40 h or until possible. To ensure a combustion atmosphere the O_2 concentration was maintained above 6 %.

Cyclone ash samples were taken out after the experiments. During operation, additional ash samples were collected after the cyclone in a 13-stage low-pressure cascade impactor from Dekati Ltd. (DLPI), which classifies the size of ash particles according to the aerodynamic diameter in the range of $0.03\ \mu\text{m}$ – $10\ \mu\text{m}$. Aluminium foils were used as substrates, and

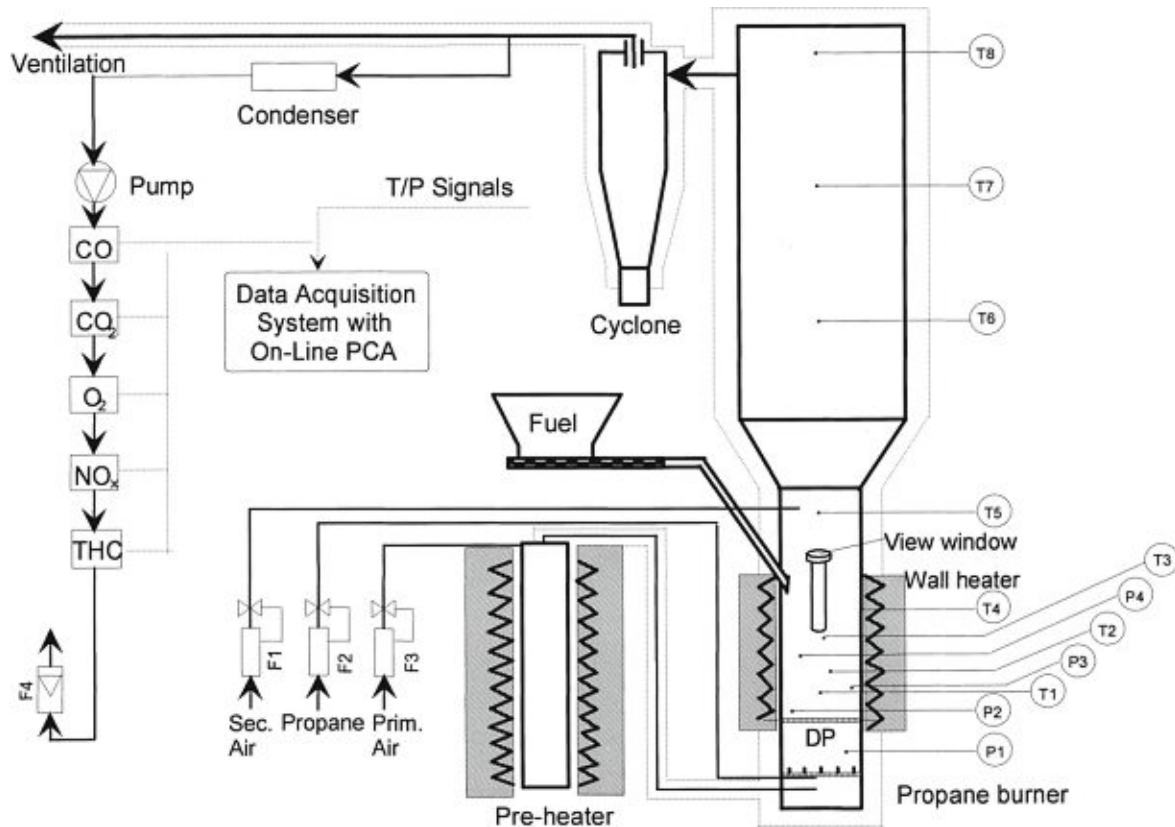


Figure 4.2: Scheme of the fluidised bed combustion plant in Umeå [85].

the impactor was heated to prevent water condensation during sampling. The 13 stages were further consolidated into fine (stage 1–7, $<1 \mu\text{m}$) and coarse (stage 8–13, $1 \mu\text{m}$ – $10 \mu\text{m}$) fractions.

4.4 Dual Fluidised Bed Steam Gasification

DFB steam gasification experiments were performed on the 100 kW (thermal fuel input capacity) pilot plant. Figure 4.3 shows the new reactor concept of the DFB steam gasification process in detail. Due to ongoing research, an advanced design of the DFB steam gasification plant was designed and went in operation for experiments in 2014 at TU Wien [86]. The main improvement focus refers to the design of the GR. The reworked GR is divided into two parts: the lower part is designed as bubbling bed and the upper part consists of turbulent fluidised bed zones. The upper part works as a counter-current flow column of the bed material and the product gas. For realization of this design, the upper GR is equipped with constrictions, which lead to an increased hold-up of bed material particles over the

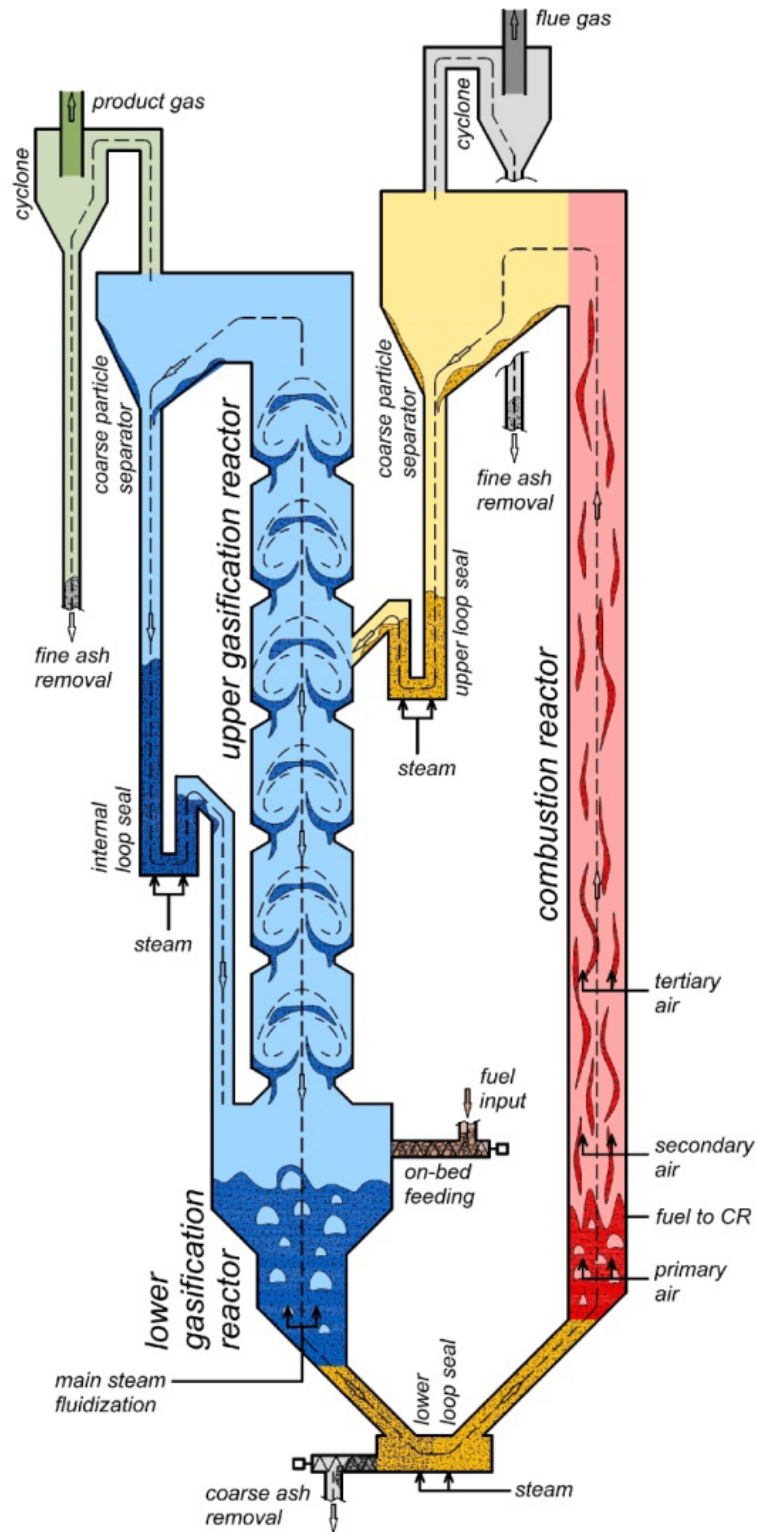


Figure 4.3: Advanced design of the DFB steam gasification plant built at TU Wien [86].

Table 4.3: DFB steam gasification experiments performed throughout the course of this thesis

Fuel (blend)	Bed material (blend) (bed material ratios are given in mass fractions)
SW	K-feldspar
BSC	K-feldspar
SW	K-feldspar (0.90), limestone (0.10)
B7C3	K-feldspar (0.90), limestone (0.10)
CM	K-feldspar (0.90), limestone (0.10)
SW	K-feldspar (0.50), limestone (0.50)
SW	limestone
SW	fresh olivine
SW	activated olivine
B7C3	activated olivine
CM	activated olivine

height of the GR. Thus, an increased residence time as well as an improved gas-solid contact of downward flowing hot bed material particles with upwards flowing product gas can be realised. Therefore, improved conversion efficiencies can be obtained. Additionally, the relatively high temperatures in the counter-current column of the GR influence tar reduction in a positive way [87]. In the advanced design of the DFB steam gasification system another optimization step, which relates to the separation system on top of the reactors, is implemented. In order to enable the use of soft bed materials like limestone, the cyclones are replaced by gravity separators to compensate the low abrasion resistance. Fines, which occur after the gravity separators, are removed by cyclones [66].

For the gasification test runs the DFB steam gasifier was first heated up with electrical trace heating and later on additionally by combusting SW pellets until the desired temperatures were reached. At that point fluidization was changed to steam in the GR and several parameters were varied until stable gasification operation was achieved. This procedure was applied for all fuels tested.

Table 4.3 gives an overview of the DFB steam gasification experiments performed throughout this thesis. SW was used with all bed materials and bed material mixtures as benchmark. Additionally, ash-rich fuels were used with every bed material (mixture).

4.5 Determination of Catalytic Activity

Figure 4.4 shows the flow sheet of the used micro-scale test-rig for testing catalytic activity of bed materials. Gases were supplied from gas bottles and flows were set with mass flow

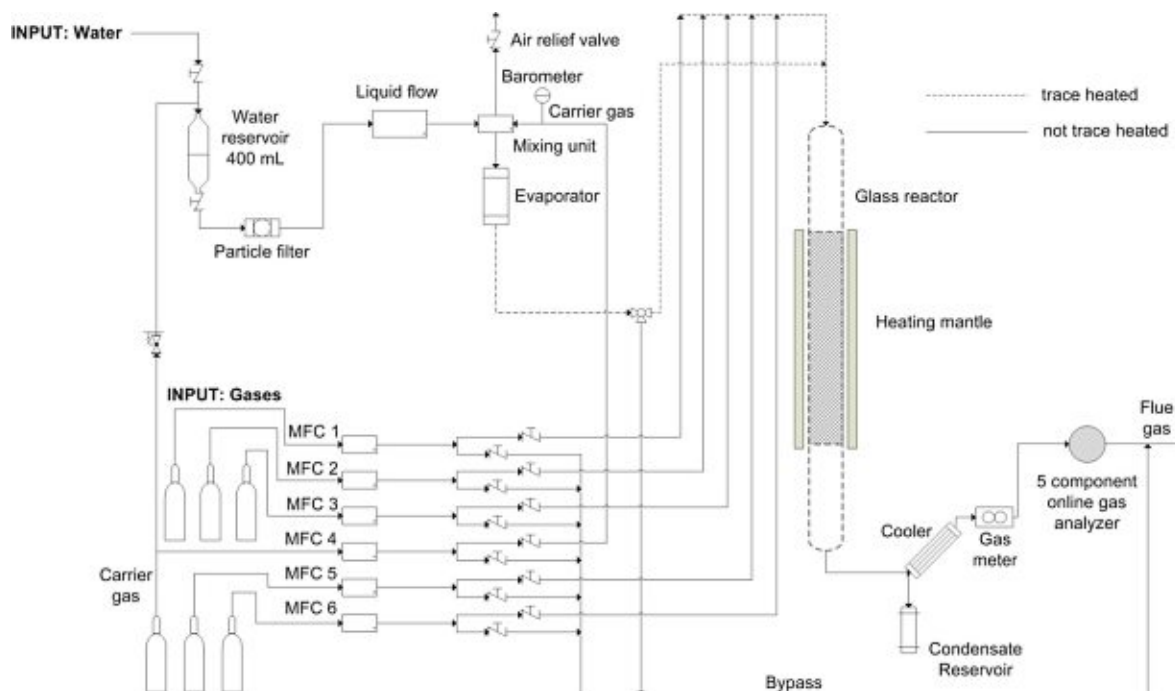


Figure 4.4: Detailed flow sheet of the used micro-scale test-rig

controllers (MFCs). The gas mixture was preheated to 130 °C. Demineralised water was stored in a reservoir and was pressed out with pressurised N₂. The water passed a particle filter; the flow was set with a liquid MFC and the water was then evaporated in a controlled evaporator mixer from Bronkhorst, which was heated to 140 °C. Steam was mixed with carrier gas and transported into the reactor. In this case N₂ was used as carrier gas since it does not react with the other gases and only dilutes the gas stream. Steam was mixed with the other preheated gases and led into a quartz glass reactor with an inner diameter of 4 mm. Quartz wool was used to hold the bed material inside the quartz glass reactor. Therefore quartz wool was positioned inside the quartz glass reactor, the bed material was filled in on top of it and another layer of quartz wool was used at the upper end of the bed. In these experiments the bed height was 5 cm. Thermocouples were positioned at the top and bottom of the fixed bed to measure the bed material temperature. The reactor was positioned inside a heating furnace which was able to heat the system up to 850 °C. The exiting gas was cooled in a cooler to condense all water.

During this thesis two experimental campaigns (one with combustion samples, one with gasification samples) were performed. The set gas flows as well as the used analysis equipment are summarised in Table 4.4. The experimental parameters were chosen in a way to lead to low conversions so it is possible to more easily quantify the catalytic activity of different samples.

Table 4.4: Set gas flows as well as used analysis equipment used during the experimental campaigns.

	Combustion Samples	Gasification samples
N ₂	101 h ⁻¹	251 h ⁻¹
CO	101 h ⁻¹	201 h ⁻¹
H ₂ O	8 g h ⁻¹	16 g h ⁻¹
analysis equipment	Rosemount NGA 2000 five-component online gas analyzer	two EasyLine Continuous Gas Analyzers by ABB (EL3020)

4.5.1 Water-Gas-Shift Calculations

The catalytic activity during gasification and the micro-scale experiments was quantified by the deviation from the WGS equilibrium. At the temperatures present during DFB steam gasification (around 800 °C) the WGS equilibrium can only be reached with the aid of a catalyst [18], making the deviation from WGS equilibrium a good indicator for catalytic activity. The deviation of the WGS equilibrium makes it also possible to directly compare experiments performed at different temperatures which is not possible by comparing the gas composition alone.

Equation (4.1) was used for the calculation of the deviation and is based on the equation established by Fuchs et al. [88].

$$p\delta_{eq,WGS}(p_i, T) = \log_{10} \left[\frac{\prod_i p_i^{\nu_i}}{K_p(T)} \right] \quad (4.1)$$

The deviation from the WGS equilibrium is negative when less CO₂ and H₂ are present than the equilibrium concentration at the current temperature dictates. A positive value means that more CO₂ and H₂ were produced than the equilibrium dictates and the reaction direction switches from the direction shown in Equation (2.6). The deviation is zero at equilibrium concentration. The software HSC 6 was used to obtain necessary reaction data [89].

The WGS reaction is an important gas phase reaction occurring during gasification [18] (especially steam gasification) and was therefore chosen to quantify the catalytic activity. The WGS reaction is also one of the main reactions for setting the right H₂:CO ratio which is an important index for downstream synthesis.

Another reaction influencing the H₂ contents in the product gas is the reforming of tars (Equation (2.8)) though it was shown in literature that bed material (layers) that are catalytically active regarding the WGS reaction also catalyse tar reforming [32, 62].

4.6 Morphological and Elemental Analysis

4.6.1 XRF

The fuel ash composition was determined with a Panalytical Axios X-ray tube via X-ray fluorescence (XRF). Therefore, 1 g of fuel ash is mixed with 9 g $\text{Li}_2\text{B}_4\text{O}_7$ and melted in a Pt crucible at 1050 °C under air atmosphere. The mixture is cast to a tablet and measured under vacuum. The excitation voltage was 50 kV and the tube current was 50 mA. Evaluation was done with standards provided by Panalytical.

4.6.2 XRD

X-ray diffraction (XRD) data for bed material samples were collected using a PANalytical Xpert Pro Diffractometer equipped with monochromatised $\text{Cu K}\alpha$ -radiation ($\lambda = 1.54 \text{ \AA}$). The analysis was carried out in the scan range from 5°–65° 2θ with a scanning step of 0.02° 2θ . The samples were measured without further preparation as grains. XRD analysis software HighScore by Malvern PANalytical was used for peak assignment [90].

The bed ash (including some bed material) and cyclone ash were subjected to powder XRD analysis using a PANalytical Empyrean diffractometer, employing $\text{Cu K}\alpha$ -radiation and a Pixel3D array detector. The samples were lightly crushed to a size of approximately 10 μm . Data collection was made with a rotating sample for a total acquisition time of 1 h for each sample. Data collection was performed at a 2θ between 10° to 70° with a scan interval of 0.007°. PANalytical HighScore Plus 4.8 [90] together with ICDD PDF-4 [91] database was used for identification and quantification of the main crystalline phases. Quantification was performed with Rietveld analysis coupled with the K-factor method to estimate the amount of amorphous material [92]. Pure crystalline Si was used as the external standard to measure the K-factor at the time of measurements.

4.6.3 SEM/EDS

Bed material samples were positioned on a sample holder and investigated using scanning electron microscopy (SEM) analysis. The analysis was used to determine the morphology of the bed particle surface. The surface morphology assessment was carried out with a FEI Quanta 200. Prior to analysis, the samples were applied onto a graphite band and degassed at 10 mA and 0.1 mbar for about 30 s. The acceleration voltage ranged between 0.2 kV–30 kV but was typically set to 20 kV as those settings yielded the best image quality. Measurements were operated in “low vacuum mode” at 80 Pa. Secondary electron images were taken by

the installed Large Field Detector, and backscattered electron images were taken by a Solid State Backscattered Electron Detector.

Collected bed samples were additionally embedded in an epoxy-based resin. The epoxy disc was subsequently polished to obtain cross-sections of bed particles, which consist of both ash and bed material, which could be used for determination of layer growth and composition. Elemental analyses of the bed material layers and ash particles were carried out with a Carl Zeiss Evo LS15 SEM equipped with Energy-dispersive X-ray spectroscopy (EDS) X-Max 80 by Oxford. The measurements conducted were line scans over the layers and area analysis (mappings) to obtain a distribution of elements. For each sample, at least three typical K-feldspar bed material particles were chosen randomly, and EDS line analysis was done across the layers on three evenly spaced locations on each particle. Layers were analysed similar to the procedure described by Faust et al. [56] and Hannl et al. [57]. Start and end of the layers were selected (approximately in the middle of the transition area of concentrations). The elemental concentrations were determined for constant sections inside the selected layers. If applicable, several layers were selected on a single line scan. To objectively sort the obtained layers into categories a clustering algorithm was used. The chosen clustering algorithm was DBSCAN (Density-Based Spatial Clustering of Applications with Noise) which grouped the layers according to similar concentrations [93]. This approach is dependent on a visible difference in elemental concentration in EDS line scans to be able to select an area. Selected layers were also studied with custom area analyses. These custom area analyses were performed post-analysis from area mappings. By manually selecting an area of interest, e.g. a layer section, the composition of this layer can be obtained. All elemental compositions are given on a C- and O-free basis to exclude the influence of the epoxy-based resin used for mounting.

EDS mappings are presented when layers were not yet thick enough to sufficiently quantify changes in line scans. The brightness in an EDS mapping gives the concentration distribution of the shown element; brighter areas show a higher concentration of the element while darker areas indicate a lower concentration. The brightness is only an indirect measure of concentration and only gives the distribution of an element in the specific mapping. The same brightness can correspond to very different concentrations for different elements in the same mapping but also for the same element for different mappings.

For the ash samples a Zeiss Evo LS-15 and JEOL JSM-IT300 were used for SEM analysis in backscattered mode together with EDS to perform elemental analysis. The ash particles found in the bed and cyclone fractions were analysed for both morphology and elemental composition through mapping, point, and area analyses. The analyses were made on both epoxy-encased particle cross sections and crushed particles mounted on carbon tapes. Partic-

ulate matter collected from the impactor was also analysed for elemental composition. The stages 5 and 13, corresponding to the main peaks of fine and coarse modes of particulate matter were analysed. EDS analyses were made using a combination of elemental mapping, point, and area analyses. The elements included were K, Na, Ca, Mg, Fe, Al, Si, P, S and Cl. The elements C and O were excluded as they are present in the epoxy resin and carbon tapes used for sample mounting.

Samples from gasification experiments including limestone particles were studied with a FEI Quanta 250 field emission gun. Sample preparation was the same as for the other samples though the samples were also coated with a AuPd-coating before being analysed.

4.6.4 BET

Brunauer-Emmet-Teller (BET) measurements were conducted with a Micromeritics ASAP 2020 V4.00 and N₂ sorption at 77 K. Prior to analysis, the samples were degassed under vacuum at 350 °C for 8 h. Analyzed sample weights amounted to around 1000 mg.



Die approbierte gedruckte Originalversion dieser Dissertation ist an der TU Wien Bibliothek verfügbar.
The approved original version of this doctoral thesis is available in print at TU Wien Bibliothek.

Chapter 5

Results and Discussion

5.1 Fluidised Bed Performance

This section is based on Papers I and IV. Additional data was included for more insights.

5.1.1 Fluidised Bed Combustion

To further study the layer formation on K-feldspar a variety of combustion experiments with different ash-rich fuels were performed. Apart from fuel ash layer characterisation, a major focus lay on the study of catalytic activation by fuel ash layers. To facilitate faster fuel ash-bed material interactions, the experiments were performed in a 5 kW bubbling fluidised bed with a comparably low amount of bed material. During the combustion of the fuels a significant amount of ash was produced, in total between $\frac{1}{4}$ and more than 7 times the amount of bed material.

Table 5.1 gives a summary of the experiments performed in the combustion plant at Umeå University. The table gives an overview of the available bed samples, the average bed temperature, when and if the bed defluidised and the amount of ash produced in the fluidised bed during combustion. It can be seen that the experiment with WS defluidised after a relatively short time of 5.5 h. This was caused by agglomerates forming due to the ash melting behaviour of WS (see Table 4.1). The addition of CM allowed for a prolonged operation time of 9.6 h for S7C3. The experiment with pure CM had to be stopped prematurely due to the accumulation of fuel ash in the reactor. An adapted bed ash removal would be necessary to be able to run CM for longer times. The experiment with bark (BA) defluidised as well after 36.5 h. No agglomerates could be found in the bed ash afterwards allowing for the assumption that the fluidization problems observed were not caused by the ash. The only fuels not leading to problems during operation were B9C1 and B7C3. It was

Table 5.1: Experimental results of the combustion experiments. An X in the hour columns indicates an existing bed sample, - indicates that no sample could be taken due to stopped operation beforehand.

	bed material sample time in h							T _{bed} in °C	t _{def} in h	ash created by fuel combustion in g
	2	4	8	16	24	32	40			
BA	X	X	X	X	X	X	-	826 ± 8	36.52	1501
WS	X	X	-	-	-	-	-	735 ± 21	5.52	231
CM	X	X	X	-	-	-	-	804 ± 4	10.83	2039
B9C1	X	X	X	X	X	X	X	798 ± 3	-	2558
B7C3	X	X	X	X	X	X	X	795 ± 4	-	4027
S9C1 - high T	X	-	-	-	-	-	-	778 ± 7	2.23	127
S9C1 - low T	X	X	-	-	-	-	-	753 ± 11	5.48	287
S7C3	X	X	X	-	-	-	-	790 ± 10	9.55	828

possible to operate the test plant with both fuels for the planned 40 h.

To better understand the influence of operating temperature on the defluidisation time, the combustion experiment with 0.9 kg kg⁻¹ straw and 0.1 kg kg⁻¹ chicken manure on a dry basis (S9C1) was performed at two different temperatures, labeled "high T" and "low T" in Table 5.1. The reduction of the combustion temperature to 750 °C more than doubled the time until defluidisation to 5.5 h highlighting the influence of temperature on agglomeration tendencies. Additionally, an agglomeration test was performed with 0.7 kg kg⁻¹ bark and 0.3 kg kg⁻¹ chicken manure on a dry basis (B7C3), since it did not agglomerate during normal operation. After the experiment the reactor was heated up to 970 °C and still no agglomeration could be observed.

Bed Material Characterisation

A variety of large scale SEM images were obtained for the samples after the combustion experiments (Figures 5.1–5.6). Figure 5.1 shows the sample obtained after the combustion of BA. Layers forming on quartz particles (▲) and, to a lesser extent, on K-feldspar (■) can be discerned. Fe particles (●) most likely originating from the reactor walls can also be seen in this image as bright white particles. More Fe from the reactor walls was released due to the more rigorous cleaning before the experiment compared to the other experiments performed in this study. It is assumed that these Fe particles are the cause for the defluidization of the experiment with BA. De Geyter et al. [58] previously performed the combustion of BA with K-feldspar for the full 40 h without observing problems or these Fe particles. In the subsequent agglomeration tests they determined a defluidisation

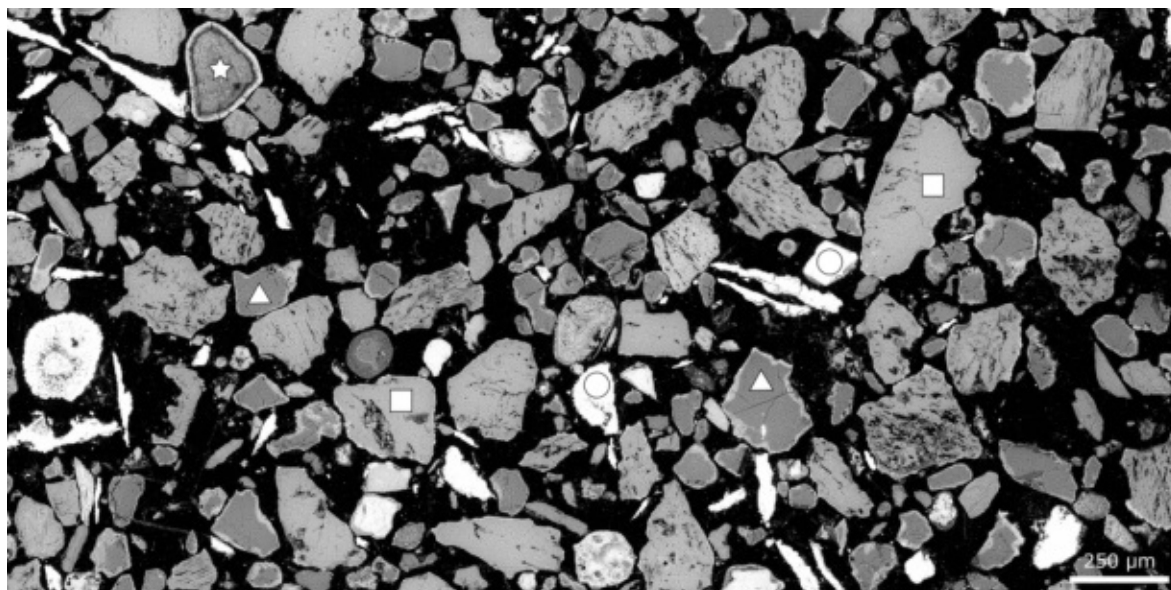


Figure 5.1: SEM stitching showing a big section of the K-feldspar bed material sample obtained after BA combustion. Several particle types are marked throughout the image: ■ K-feldspar, ▲ quartz, ★ porous ash particle, ● Fe particles. Layers can be seen on K-feldspar and quartz particles, as well as on the porous ash particle.

temperature of 865 °C–875 °C which is also higher than the temperature the fluidised bed was operated at here. Apart from layers developing on K-feldspar and quartz, layer development can also be identified on ash particles (★).

Figure 5.2 clearly shows the reason why the experiment with WS defluidised. Big ash melt particles (+) can be seen, partially also sticking to bed material particles. The ash melt particles are enriched in Si and K. The high contents of these elements led to a low ash melting point, explaining the ash melt formation. Apart from melt formation, initial layer formation can be seen for some quartz particles.

Figure 5.3 shows a section of the K-feldspar bed material sample obtained after CM combustion. It can be seen that, compared to the other samples, the bed sample contains a higher fraction of ash particles(★ and +). This increased amount of ash particles correlates to the observed increase of fluidised bed height, which led to the stop of the combustion with CM. Two different types of ash can be distinguished, ash melt particles similar to the ones seen for WS and big circular porous particles. The porous particles mainly consist of Ca and are assumed to originate from Ca-additives typically added to chicken feed. Layer formation can be seen on both K-feldspar and quartz.

The samples from B9C1 (Figure 5.5) and B7C3 (Figure 5.6) combustion show layers forming on bed material and ash particles. Unlike to the other samples the bed material here shows small bumps in the layer surface giving the particle a more irregular shape. It can

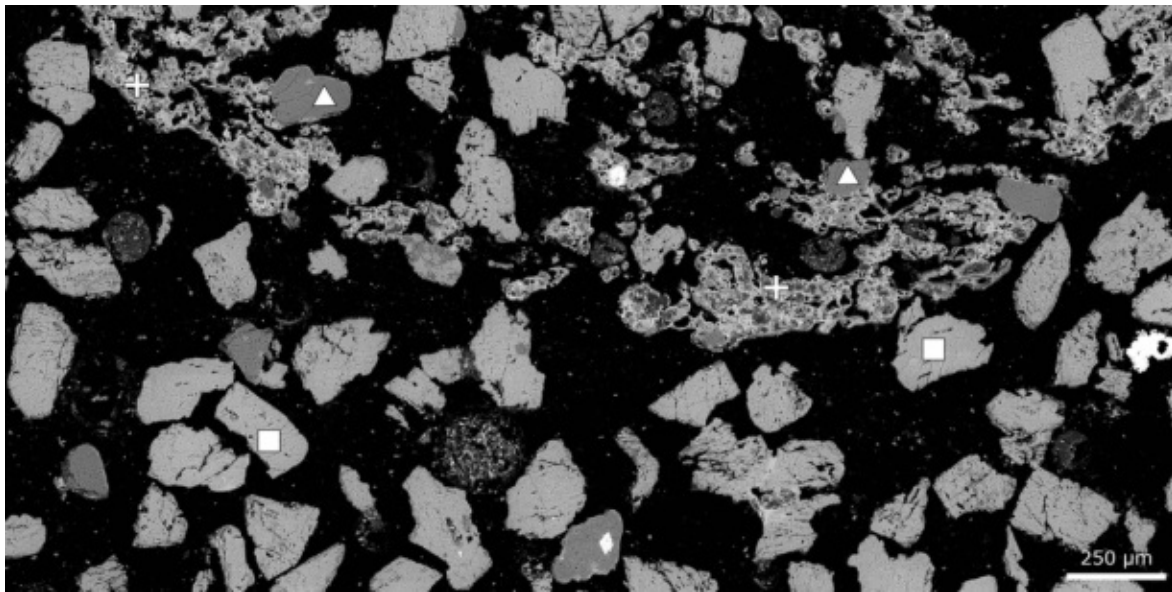


Figure 5.2: SEM stitching showing a big section of the K-feldspar bed material sample obtained after WS combustion. Several particle types are marked throughout the image: ■ K-feldspar, ▲ quartz, + ash melt. A considerable share of quartz particles are involved in agglomeration formation with the ash melt.

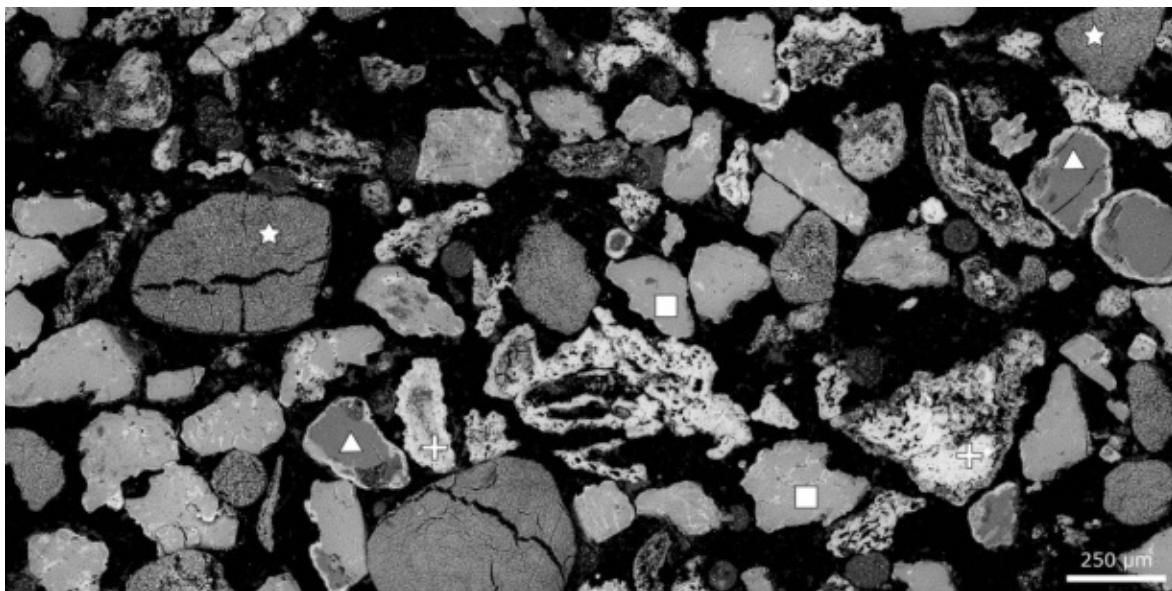


Figure 5.3: SEM stitching showing a big section of the K-feldspar bed material sample obtained after CM combustion. Several particle types are marked throughout the image: ■ K-feldspar, ▲ quartz, ★ porous ash particle, + ash melt. The ash melt and porous ash particles show the reason why the experiment had to be stopped prematurely.

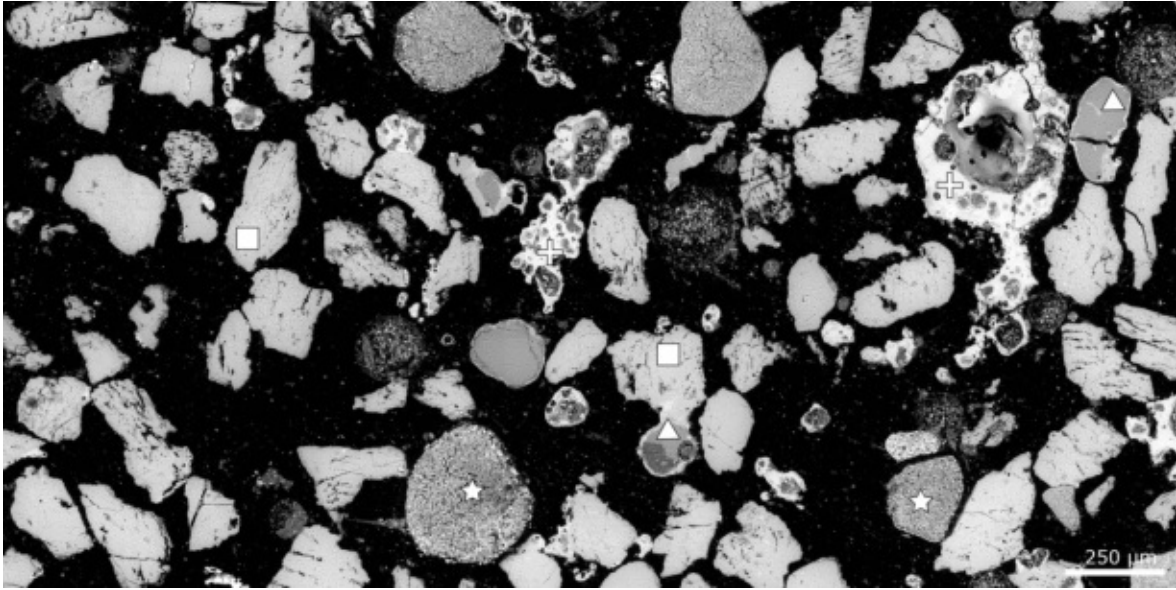


Figure 5.4: SEM stitching showing a big section of the K-feldspar bed material sample obtained after 0.7 kg kg^{-1} straw and 0.3 kg kg^{-1} chicken manure on a dry basis (S7C3) combustion. Several particle types are marked throughout the image: ■ K-feldspar, ▲ quartz, ★ porous ash particle, + ash melt. Big ash melt particles formed, causing the observed defluidisation.

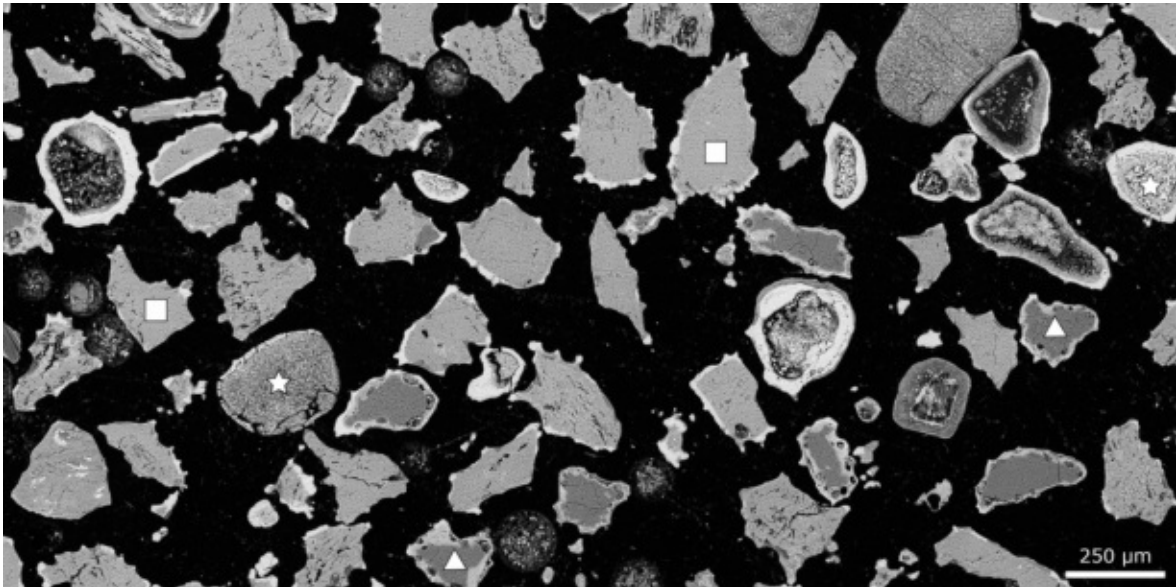


Figure 5.5: SEM stitching showing a big section of the K-feldspar bed material sample obtained after 0.9 kg kg^{-1} bark and 0.1 kg kg^{-1} chicken manure on a dry basis (B9C1) combustion. Several particle types are marked throughout the image: ■ K-feldspar, ▲ quartz, ★ porous ash particle. Bumps formed on the surface of K-feldspar particles giving the particles an irregular surface.

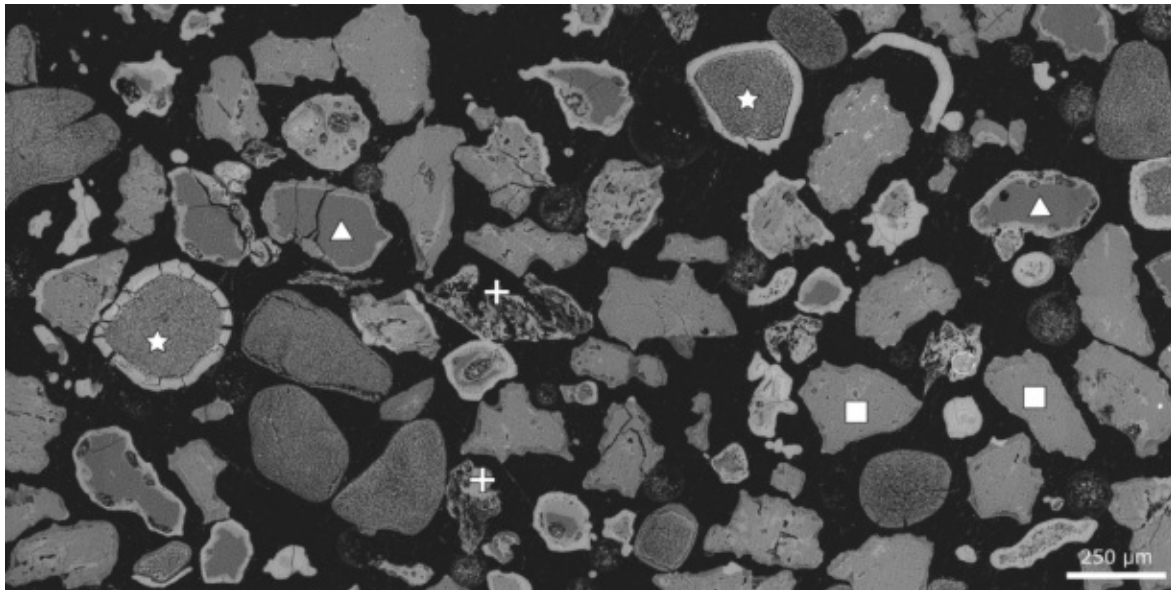


Figure 5.6: SEM stitching showing a big section of the K-feldspar bed material sample obtained after B7C3 combustion. Several particle types are marked throughout the image: ■ K-feldspar, ▲ quartz, ★ porous ash particle, + ash melt.

be assumed that these bumps originate from ash adhering to the particle at certain positions promoting layer formation at these regions. The samples also contain the Ca-rich particles observed for CM combustion, highlighting the high fraction of CM ash in the used fuels. Different to the Ca-rich particles observed for CM combustion, these particles also show a layer forming on them. These layers are rich in K, S, P, Si and Mg apart from the Ca forming the particles.

No layer formation could be observed on K-feldspar bed material samples for S7C3 combustion, see Figure 5.4. However, the adhesion of ash melt onto bed material particles can be identified, which led to a bigger particle size. The increase in particle size is also the cause for the defluidisation observed during S7C3 combustion. It can also be seen that the quartz impurities in the bed material are affected by ash melts to a higher degree compared to K-feldspar. The agglomerates formed during S7C3 combustion also vary from the agglomerates formed during WS combustion by their appearance.

5.1.2 Fluidised Bed Gasification

A wide range of gasification experiments were executed in the 100 kW DFB steam gasification pilot plant at TU Wien for this thesis. Several admixture ratios of limestone to K-feldspar were studied for their influence on gasification performance. For comparison experiments

were also carried out with fresh and activated olivine. DFB steam gasification was operated without problems for most experiments. Fluidization problems were observed for the experiment with BSC and K-feldspar as bed material as well as the experiment with CM and activated olivine as bed material. It was not possible to obtain a stable operation with CM with activated olivine. The cause for fluidisation problems is not entirely clear but it is assumed that the high ash content is the main cause since the plant is not equipped with any bed ash removal possibilities.

Table 5.2 summarises the obtained product gas yield, the overall cold gas efficiency as well as the observed temperatures in the gasification reactor for all experiments except CM with activated olivine as bed material since it was not possible to obtain stable operation for this experiment. Most of the experiments were performed at around 770 °C in the gasifier bubbling bed, with only some experiments having temperatures above 800 °C in the bubbling bed. The overall cold gas efficiency is in a similar range for all experiments but no trend can be discerned regarding bed material or fuel. An increase in product gas yield can be seen for more active bed materials as well as ash-rich fuels. The higher product gas yield observed for activated olivine can also be linked to an increased gasification temperature which is attributed with higher product gas yields [94].

Table 5.2: Experimental results of the gasification experiments. The experiment with CM and activated olivine did not achieve stable operation. Already published data was adapted from Mauerhofer et al. [65].

Fuel	Bed material	product gas yield in $\text{m}^3_{\text{stp,db}} \text{kg}_{\text{fuel,daf}}^{-1}$	overall cold gas efficiency -	T_{mean} in GR_{lower} in °C	T in GR_{upper} in °C	T at $\text{CR}_{\text{outlet}}$ in °C
SW	K-feldspar	1.17	0.71	772	934	923
BSC	K-feldspar	1.34	0.78	761	961	949
SW	K-feldspar (90), limestone (10)	1.36	0.72	771	933	942
B7C3	K-feldspar (90), limestone (10)	1.4	0.74	777	964	973
CM	K-feldspar (90), limestone (10)	1.5	0.7	766	933	939
SW	K-feldspar (50), limestone (50)	1.44	0.71	797	967	977
SW	limestone	1.43	0.73	769	991	1010
SW	fresh olivine	1.35	0.71	836	951	954
SW	activated olivine	1.46	0.72	810	905	916
B7C3	activated olivine	1.68	0.69	821	920	932
CM	activated olivine	-	-	-	-	-

5.1.3 Summary

In summary, the experiments with K-feldspar showed that it is a possible candidate to be used as bed material in thermochemical fluidised bed applications. Problems could be observed when the fuels CM and WS were used. Due to the high ash content of CM both the operation of the fluidised bed combustion and the DFB steam gasification pilot plant showed problems due to ash accumulation in the system. The experiments with WS (and WS mixtures) showed problems due to low melting eutectica. It is therefore of major importance to further study alternative fuels and their impact on fluidised bed applications.

5.2 Layer Formation on K-Feldspar

This section is based on Papers I-V, supervised Master Theses as well as unpublished data.

5.2.1 Comparison of Layer Formation during Combustion and Gasification

Figure 5.7 compares several SEM images and EDS mappings for combustion and gasification experiments as well as a sample from the industrial plant Senden. The K-feldspar particle depicted is an impurity in the used olivine bed material from the Senden plant [38]. Layers can be seen for all experiments. For all samples layers rich in Ca formed. P was also incorporated into the layers if P was available from the fuel ash. For the combustion experiments with B7C3 and CM it was also possible to detect S discontinuously in the layers.

Exemplary line scans corresponding to the experiments shown in Figure 5.7 are depicted in Figure 5.8. Some of the particles show both inner and outer layers, which is mainly dependant on the interaction time between fuel ash and bed material. Though, the composition of these layers is independent of layer thickness and interaction time [54] but outer layers are only formed after a minimal operation time. As soon as sufficiently thick layers formed it is therefore possible to compare different experiments. The layers shown in Figure 5.8 all exceed this minimal needed layer thickness and are therefore comparable.

For the line scan for BA combustion it can be observed that the concentration of Ca increases towards the surface while K is depleted. This can be seen from the deviation of the inherent K-feldspar K:Al ratio from 1 to 0.33 in the layers formed. Since Al in the K-feldspar (KAlSi_3O_8) does not participate in layer formation processes it is possible to describe a change in K concentration in the K-feldspar matrix by the K:Al ratio [54, 56].

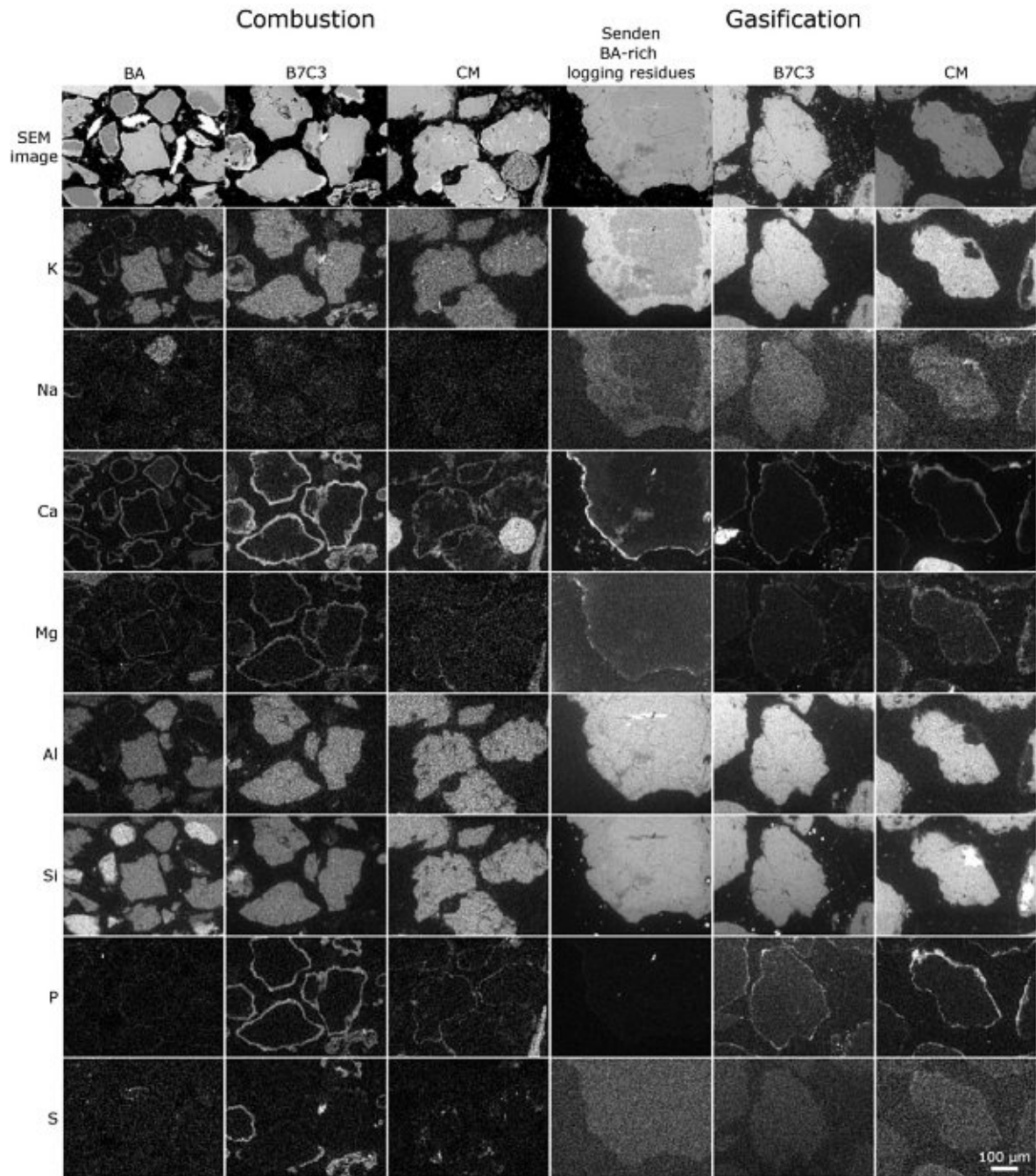


Figure 5.7: SEM and EDS analysis of K-feldspar particles for the experiments with BA, B7C3, and CM in combustion and gasification atmospheres.

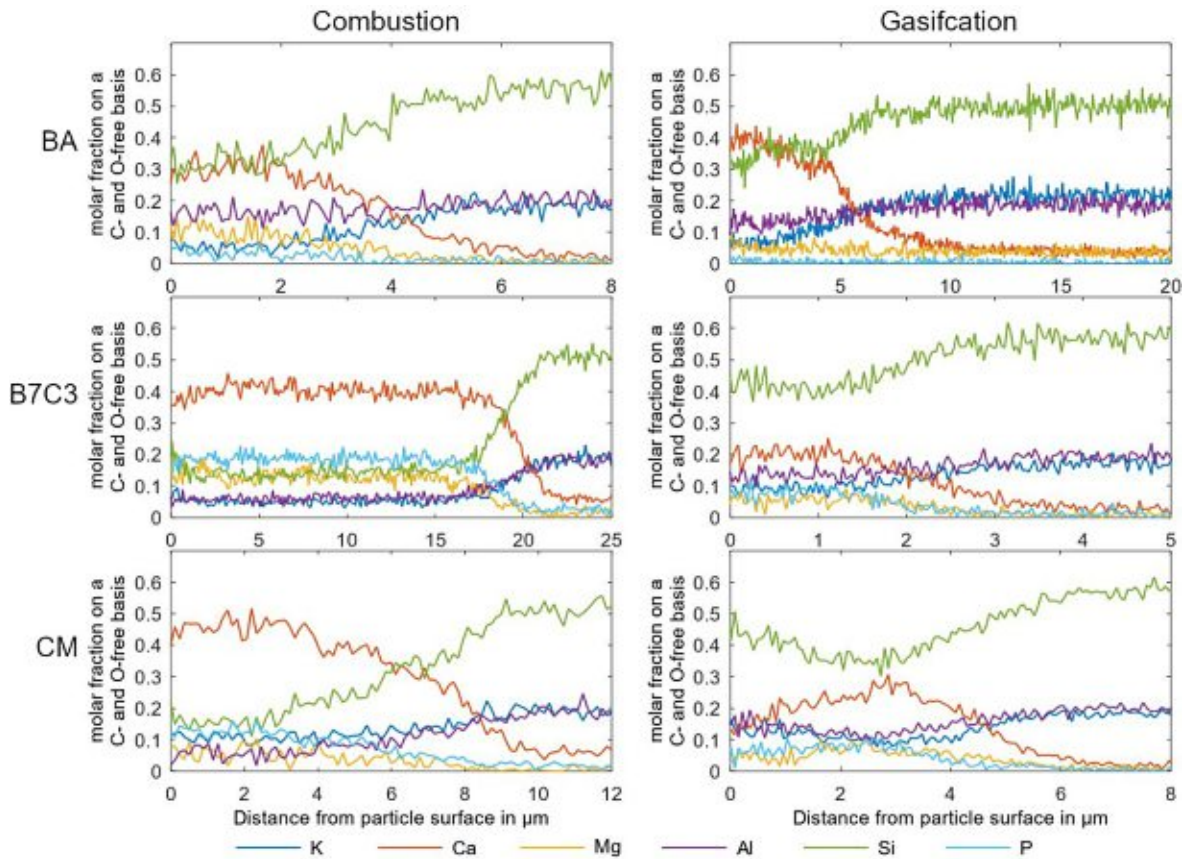


Figure 5.8: Line scans measured on K-feldspar for samples from combustion and gasification of BA, B7C3 and CM. The given distance starts at the outside of the particle and points towards the core. The sample for the gasification of BA originates from a K-feldspar impurity from an olivine bed from Senden where gasification is performed with BA-rich logging residues.

The substitution of K by Ca is typical for woody biomass ash interacting with K-feldspar [38, 54]. Apart from Ca and the elements naturally contained in K-feldspar, only Mg is found in a relevant amount. The line scan measured for K-feldspar in the sample used for the gasification of BA-rich logging residues is shown as well. Similarly to the results observed for the combustion of BA, enrichment with Ca was detected while K was depleted. The depletion can again be characterised by a K:Al ratio of 0.47. In this sample, no Mg was observed in the layer. This can be explained by the lower Mg concentrations in the fuel used for gasification compared to the fuel used for combustion (see Figure 4.1). Since reduced amounts of Mg are available during gasification, a reduced interaction with the bed material is anticipated. Even though K-feldspar was contained only as an “impurity” in the olivine bed used for the gasification of BA-rich logging residues at the CHP in Senden, the same layers formed during combustion when no olivine was present. The impurity K-feldspar particles are also the particles that have been exposed to ash for the longest time in this study.

Though, with the data available it is not possible to state whether initial layer formation is the same for pure beds and impurities but long-term layer formation is comparable. The layer formed during the combustion of B7C3 is mainly dominated by Ca, P, and Mg. Ca seems to be found further inside the K-feldspar compared to Mg and P. The same can be said for the layer formed during the gasification of B7C3. Even though the layer is thinner, Ca is again measured further inside the particle compared to P and Mg. The Ca, P, and Mg levels are considerably lower for the gasification case. This might be due to the electron beam measuring a small area and not a single dot. The influence of surrounding K-feldspar is therefore bigger for thin layers compared to thick layers. Besides Ca, P, and Mg, no other elements could be found in a relevant amount. Additionally, little to no K-depletion (K:Al ratio of 0.85 for combustion and 0.71 for gasification) could be observed for B7C3.

Similar observations can be made for the layers studied after the combustion and gasification of CM. Ca is again found further inside the particle, while P and Mg are enriched in the layer at the same location and no K depletion (K:Al ratio of 1.81 for combustion and 0.90 gasification) is occurring. The K:Al ratio of 1.81 for the combustion of CM even indicates that additional K is deposited on the bed particle. The lower concentration of Ca, P, and Mg in the layers from CM gasification can again be linked to the thinner layers formed. Even though B7C3 and CM were used successively during gasification it is not possible to discern two different layers in the bed material sample for CM gasification. This is either caused by the fact that the layers are too thin to discern them or that the composition of the layers formed is too similar to distinguish them. Since the layers formed during the combustion of B7C3 and CM are similar, it can be concluded that a similarity in layer formation is the cause for only one layer being observable CM gasification.

5.2.2 Time-Dependent Layer Formation

SEM images were obtained for several bed material samples from B7C3 combustion (see Figure 5.9). It can be seen that longer operational times lead to thicker layers. While no layer was observed for 0 h–4 h on K-feldspar particles, initial layer formation can be seen on the quartz particle (darker grey compared to K-feldspar) after 4 h, see Figure 5.9 c). After 8 h, Figure 5.9 d), a continuous layer formed on K-feldspar particles.

A growth in layer thickness was also observed for BA combustion (see 5.10, but, overall, the layers remained thinner compared to B7C3. While a continuous layer on K-feldspar was achieved after 8 h for B7C3 combustion continuous layers were only observable after 16 h for BA combustion. The slower ash layer formation can be explained by the lower ash content

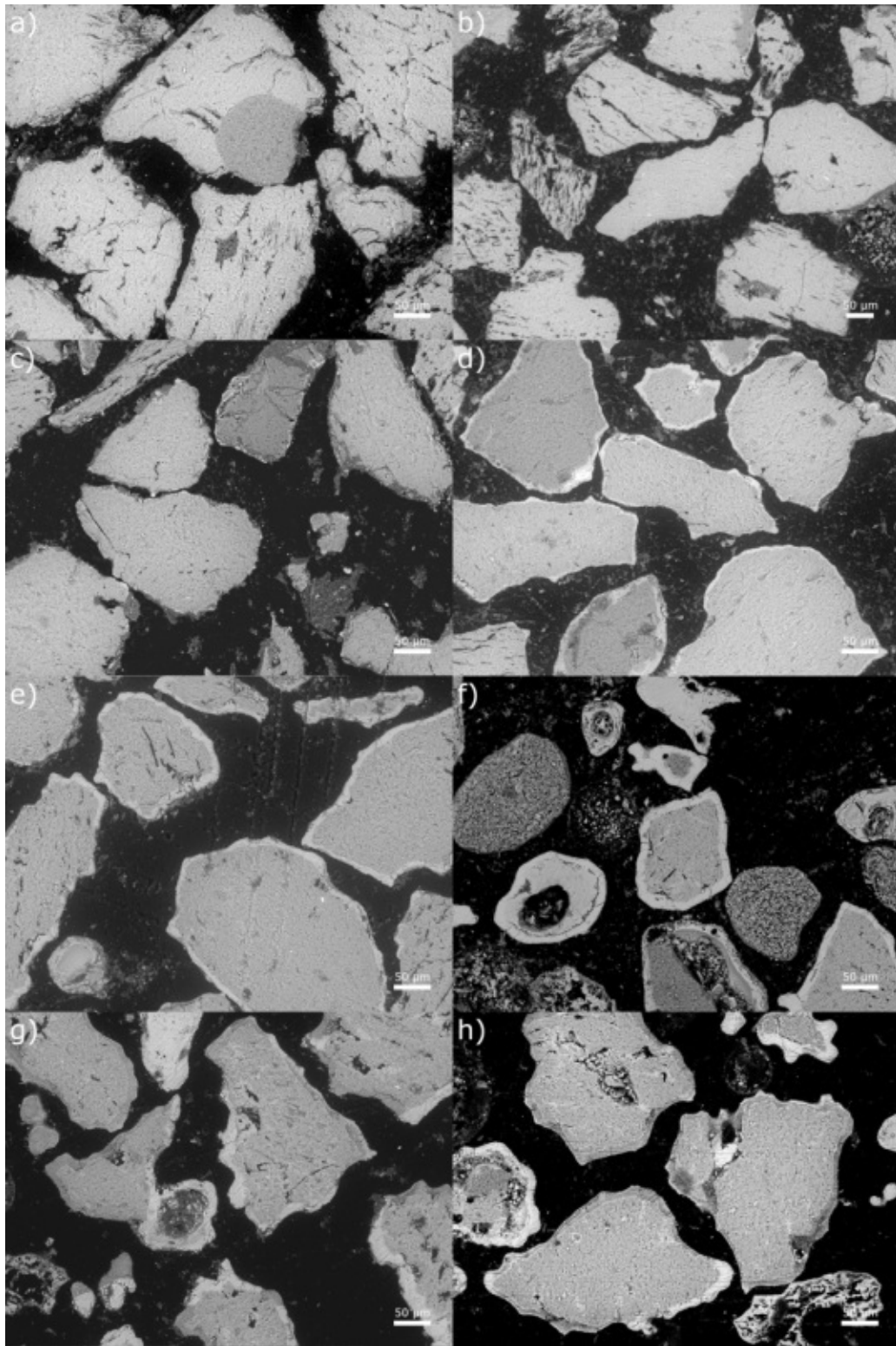


Figure 5.9: SEM images of bed material samples from B7C3 combustion after a) 0 h, b) 2 h, c) 4 h, d) 8 h, e) 16 h, f) 24 h, g) 32 h, h) 40 h

of BA compared to B7C3 (see Table 4.1).

Figure 5.11 depicts the layer formation for CM combustion (Figure 5.11 a-c)) as well as S7C3 combustion (Figure 5.11 d-f)). Initial layer formation can already be seen after 4 h of CM combustion. After 8 h a continuous layer formed around the K-feldspar bed material. For S7C3 combustion initial layers can be observed after 4 h but only for quartz impurities.

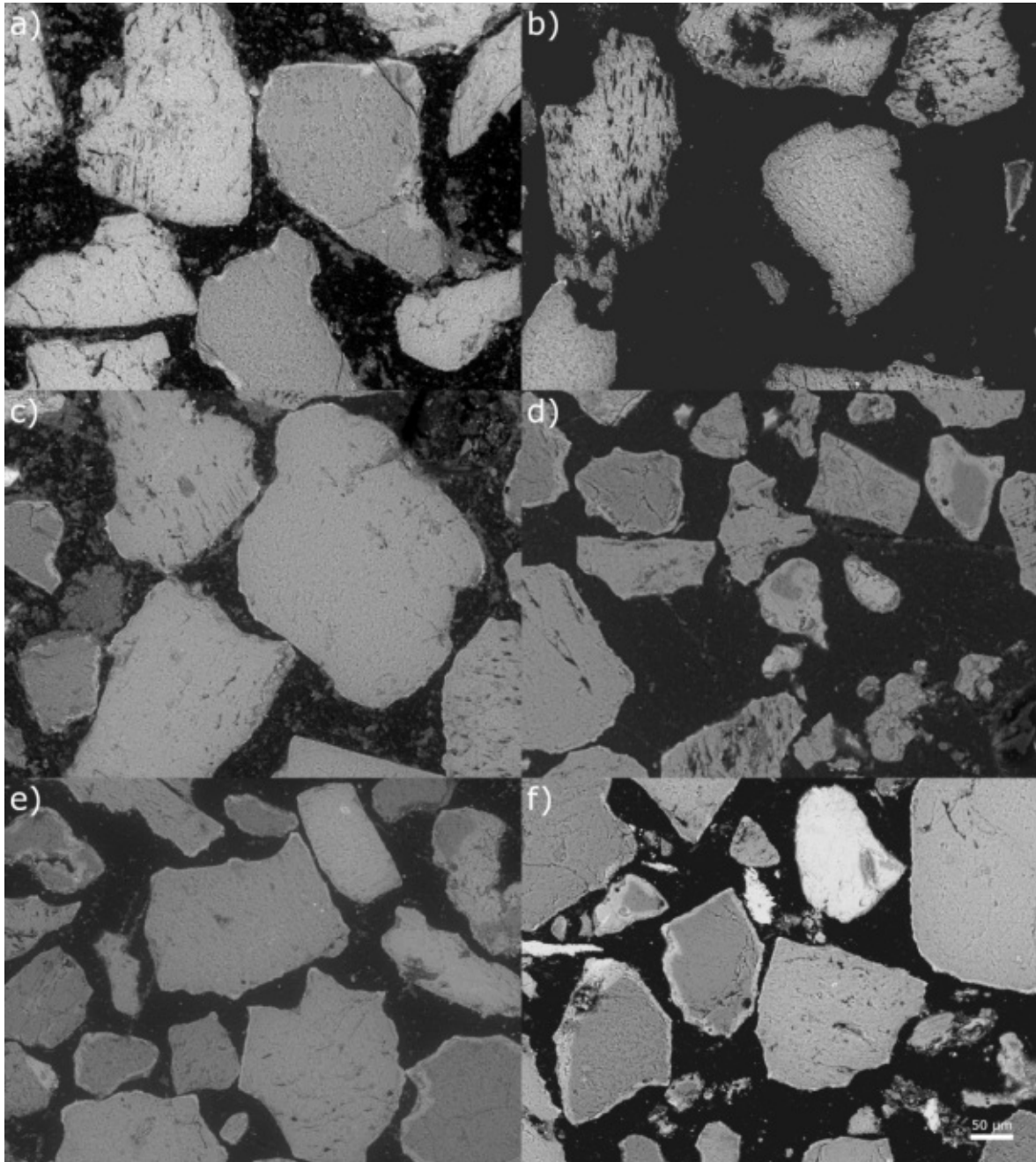


Figure 5.10: SEM images of bed material samples from BA combustion after a) 4 h, b) 8 h, c) 16 h, d) 24 h, e) 32 h, f) 36.5 h

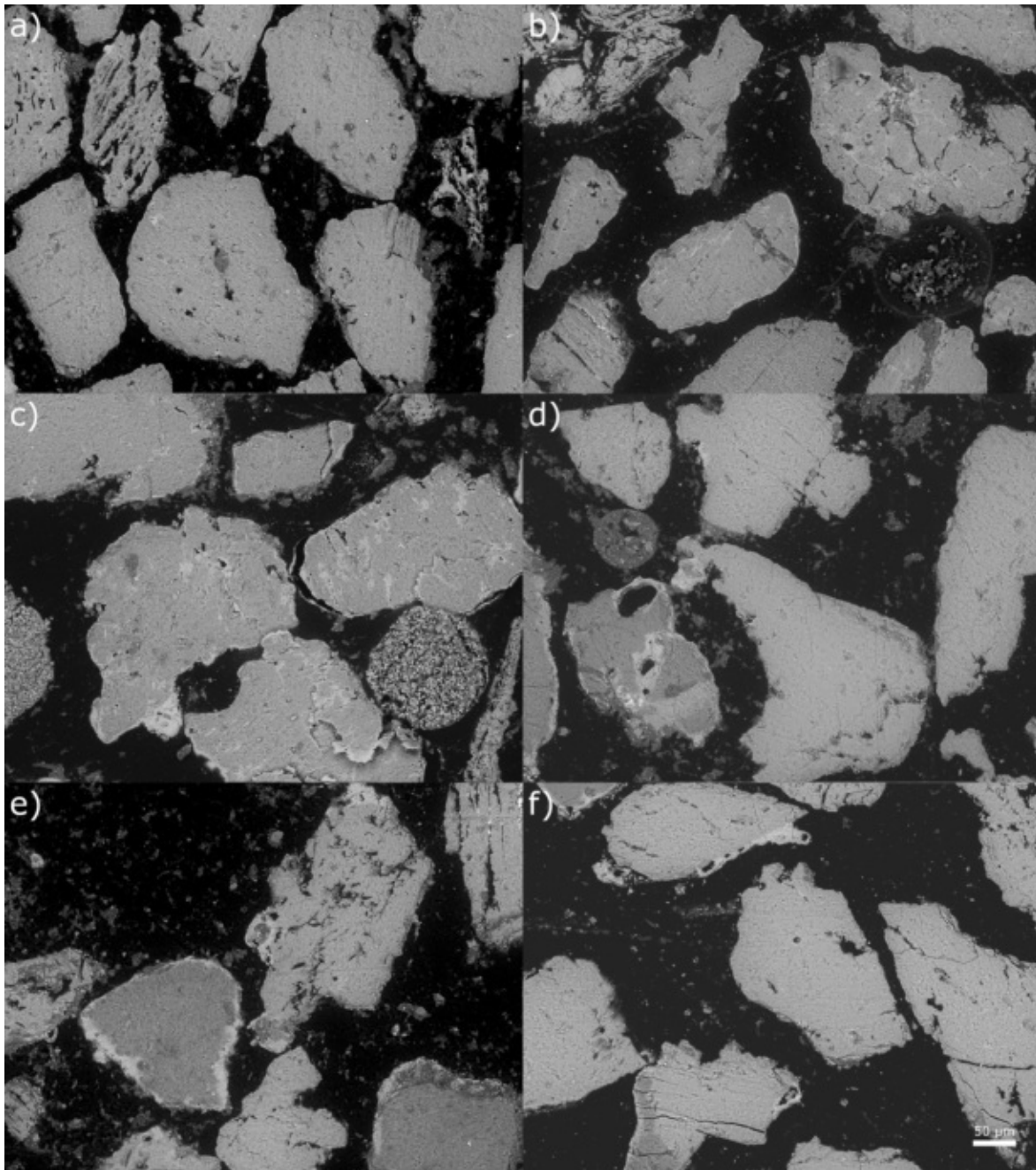


Figure 5.11: SEM images of bed material samples from CM combustion after a) 4 h, b) 8 h, c) 11 h, and S7C3 combustion after d) 4 h, e) 8 h, f) 9.5 h

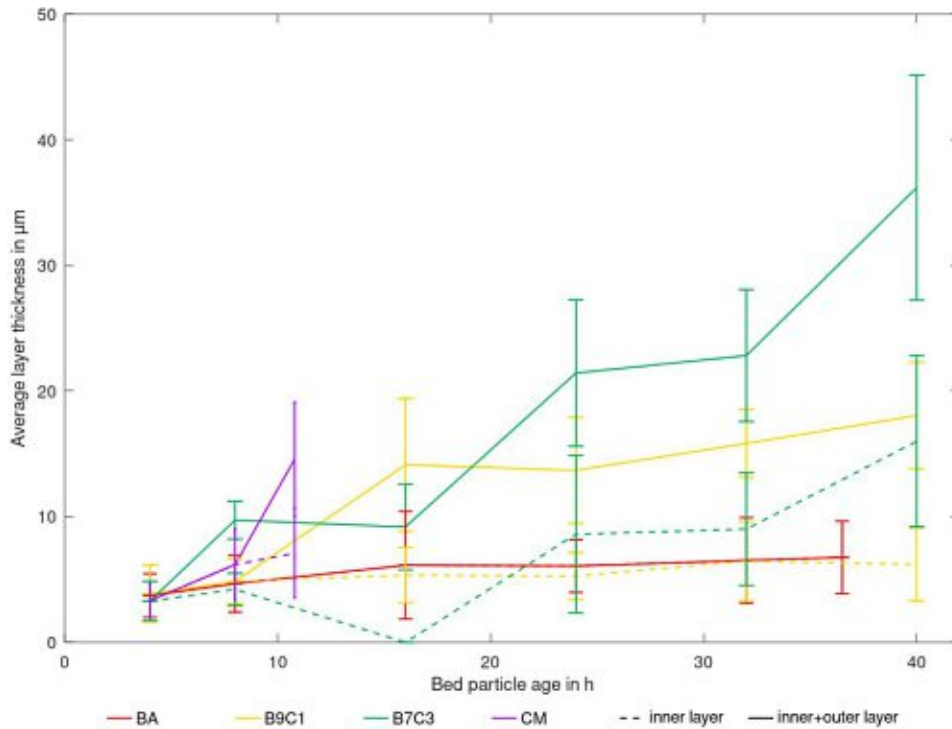


Figure 5.12: Growing layer thickness over time for BA, B9C1, B7C3 and CM. The dashed line gives the inner layer thickness (interaction layer) and the solid line indicates the thickness of both inner and outer layer combined. The standard deviation given for the line inner+outer layer shows the standard deviation for the outer layer only.

After 8 h a continuous layer formed around quartz impurities and initial layer formation can be observed for K-feldspar bed material particles. After 9.5 h, when the bed defluidised due to agglomeration, only some K-feldspar particles showed observable beginnings of layer formation.

5.2.3 Layer Thickness

Layer thicknesses of fuel ash layers were determined from EDS line scans for samples from BA, CM, B9C1 and B7C3 combustion. Figure 5.12 depicts the development of the layer thickness over particle age. Short operational times of the fluidised bed led to thin fuel ash layers and therefore to comparably large standard deviations of the average layer thickness. Figure 5.12 depicts both the inner layer thickness as well as the thickness of inner and outer layer combined. It must be stressed that the average total layer thickness detected is smaller than the sum of inner and outer layer since not all samples showed both an inner and outer layer. Due to clarity the actual average layer thickness is not depicted in Figure 5.12.

The layer thickness after 4 h is in the same range for all samples studied, probably caused

by the evaluation method used. Layers were assigned manually so a certain thickness has to be reached for a layer to be detectable. Additionally, layer starting and ending points were defined in the middle of the transition area between distinct concentration levels, therefore being the reason for the minimal layer thickness. For older particles a difference between layer thickness for BA, B9C1 and B7C3 can be discerned. As expected, the slowest layer growth was observed for BA, and B7C3 combustion showed the fastest layer growth. CM combustion showed fast layer growth as well, but due to the short operational time it is not possible to compare it to the other samples.

The layer composition of the inner layer detected for BA combustion is depicted in Figure 5.13. Bed materials from BA combustion exhibited no outer layer. This is in accordance with Faust et al. [56] who only observed a continuous outer layer after 51 h. The only element being added in a relevant amount is Ca. Starting at 16 h a depletion of K can be detected as well. The depletion of K is typical for woody biomass.

Figure 5.14 shows the inner and outer layer composition determined for B9C1 combustion. In contrast to BA combustion, no diffusion of K could be detected for the inner layer. Higher contents of P and Mg were detected for the inner layer as well. The outer layer shows an enrichment of P, Mg and S. Additionally, an addition of fuel ash K and Al can be assumed, since the Si:K and Si:Al ratios are lower than 3, deviating from K-feldspar.

Similar effects were observed during B7C3 combustion, see Figure 5.15. The only inconsistency is the inner layer for 40 h. This inner layer was detected to be significantly richer in Ca, P and Mg and the concentration of K-feldspar is reduced. For the outer layers formed during B7C3 combustion more K was detected compared to B9C1 combustion. This might be caused by the higher K content of B7C3 compared to B9C1. For the other elements the composition is similar to the outer layer from B9C1 combustion.

During CM combustion an outer layer was only detected after 10.8 h (Figure 5.16). For the inner layer only Ca and P were detected. The outer layer showed higher contents of Ca, P and Mg compared to the inner layer.

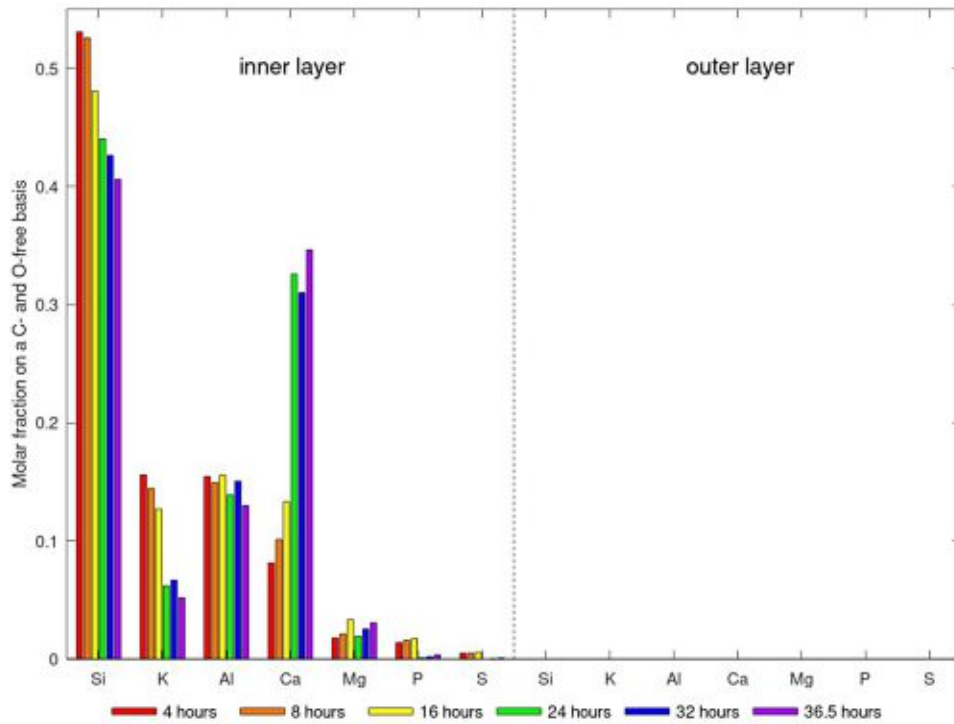


Figure 5.13: Layer composition over time during BA combustion. No outer layer could be detected during BA combustion.

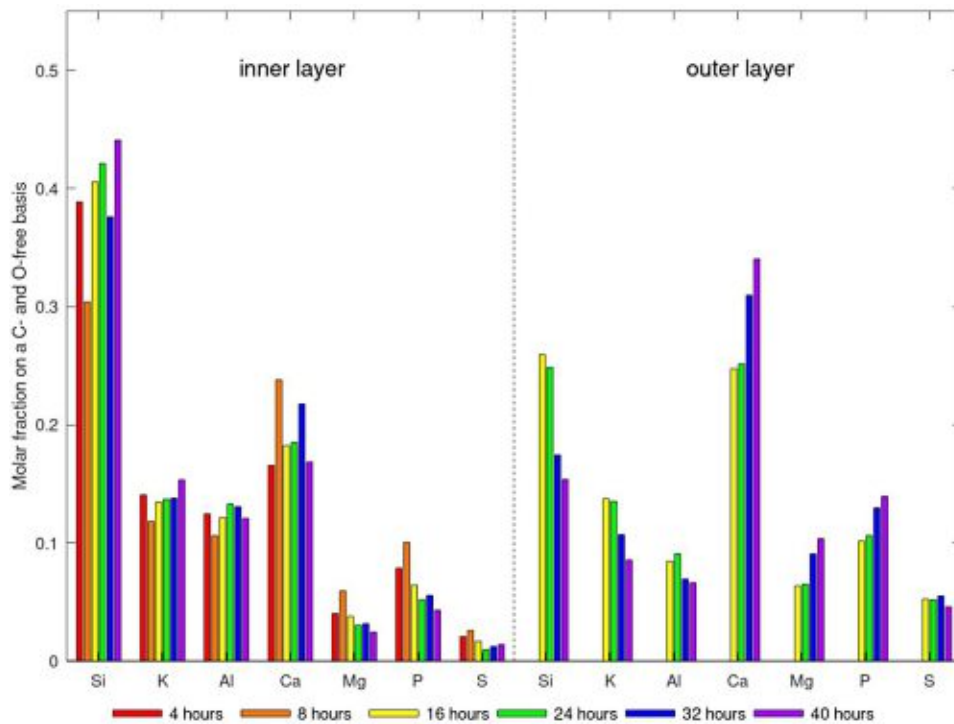


Figure 5.14: Layer composition over time during B9C1 combustion. Both an inner (left) and an outer (right) layer were detected for B9C1 combustion.

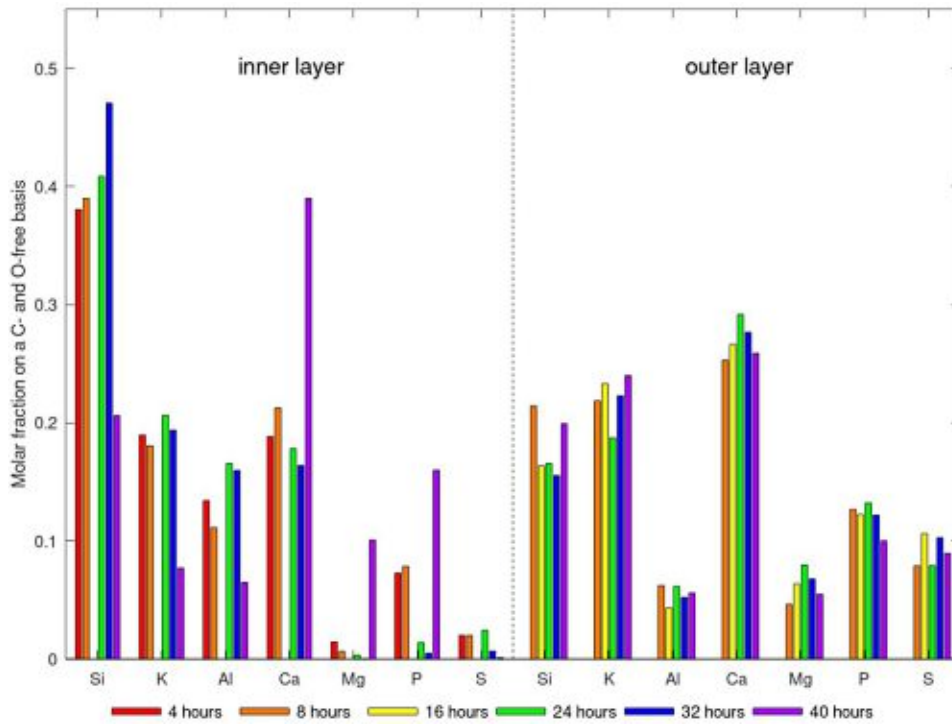


Figure 5.15: Layer composition over time during B7C3 combustion. Both an inner (left) and an outer (right) layer were detected for B7C3 combustion.

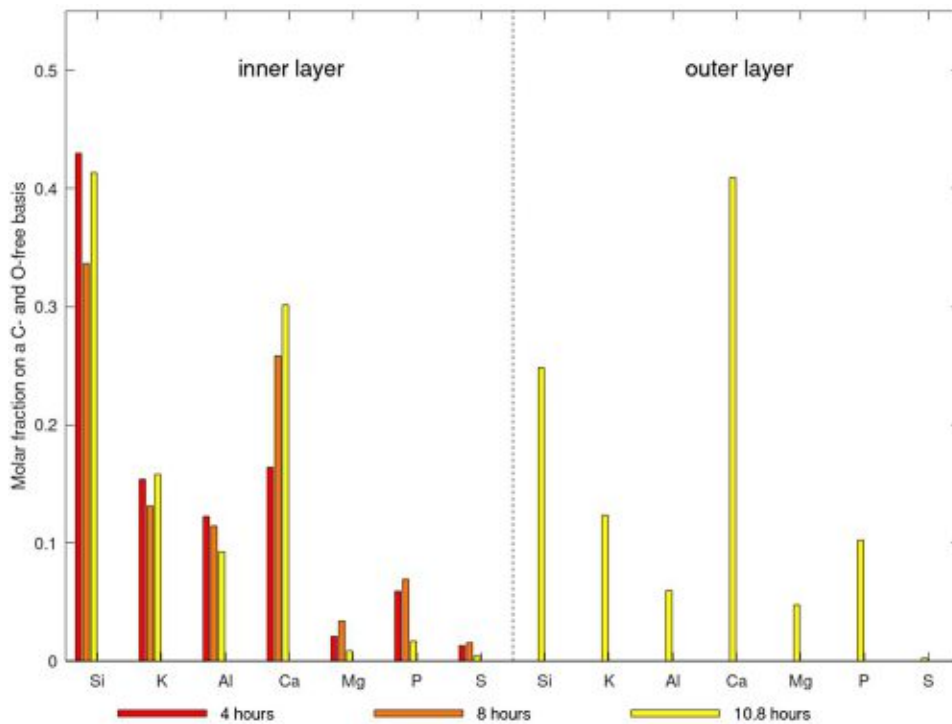


Figure 5.16: Layer composition over time during CM combustion. An outer layer was only detected for the final sample.

5.2.4 Surface Characterisation

The quantified results from BET analysis for BA, CM and B7C3 combustion are shown in Figure 5.17. No clear correlation can be seen for particle age and BET surface area. Still, for each separate sample an increase in surface area over particle age can be seen. The combustion of CM led to the fastest rise in surface area, probably caused by increased ash layer formation with ash-rich fuels. This is further supported by the fact that BA combustion led to the lowest increase in BET surface area. Layer formation might also explain the decrease in surface area observed after 4 h of BA combustion.

Figure 5.18 shows SEM images of the surface area of native K-feldspar, as well as samples after 8 h of BA, B7C3 and CM combustion, 32 h of BA combustion and 40 h of B7C3 combustion. The 8 h samples were selected since they were the last samples that were available for all experiments and the later samples for BA and B7C3 were selected since they were the last samples from scheduled sampling. Irregularities on the particle surface caused by the adhesion of fuel ash can be seen for all combustion samples. The irregular surface created by these ash particles is a further reason for the increase in BET surface area. Figure 5.18 a) shows the surface of fresh K-feldspar, where the crystal structure of K-feldspar on the surface is clearly observable. Figure 5.18 b) and c) show the result of

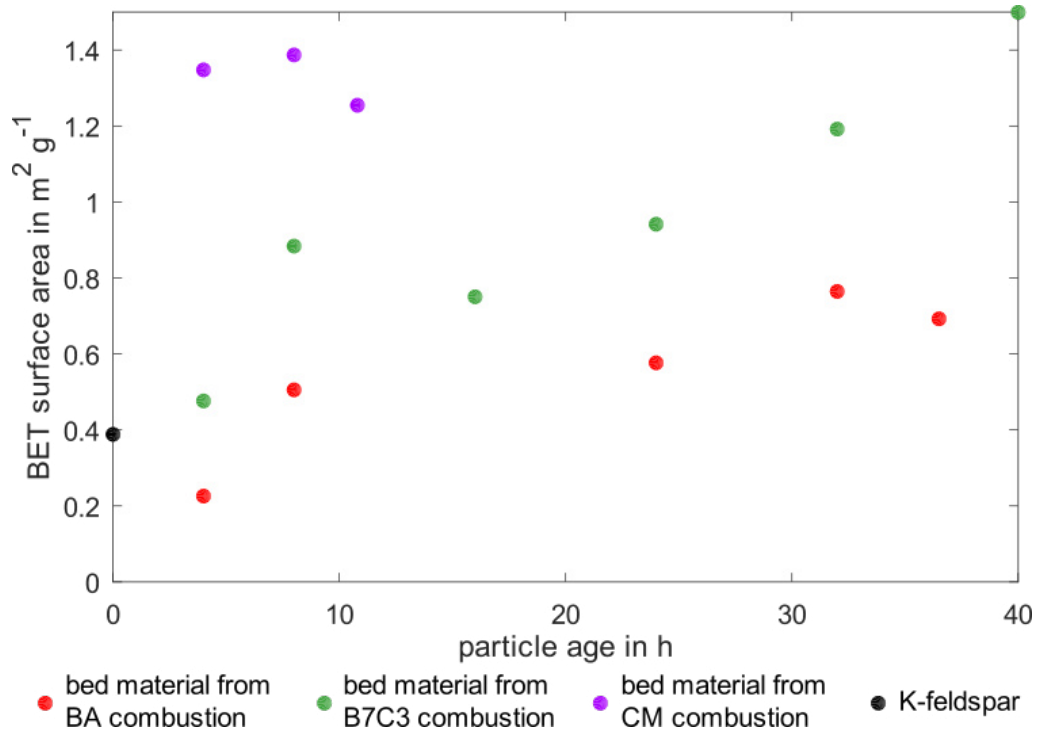


Figure 5.17: BET surface area measured for bed material samples from BA, CM, and B7C3 combustion.

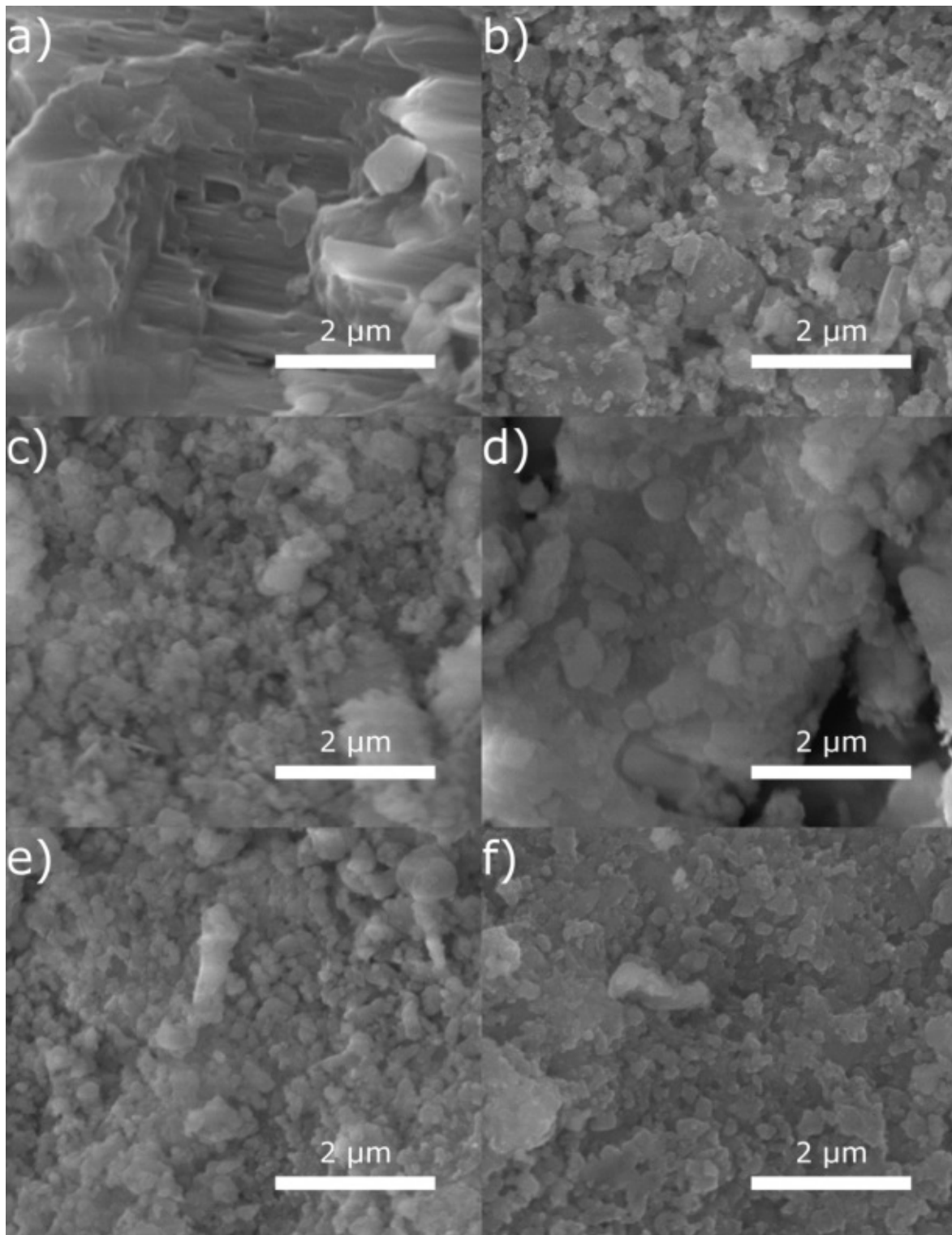


Figure 5.18: SEM images of the particle surface a) of fresh K-feldspar, b) after 8 h of interaction with BA, c) after 32 h of interaction with BA, d) after 8 h of interaction with CM, e) after 8 h of interaction with B7C3 and f) after 40 h of interaction with B7C3.

interaction of K-feldspar with BA ash after 8 h and 32 h, respectively, Figure 5.18 d) shows the particle surface of K-feldspar after 8 h of interaction with CM ash and Figure 5.18 e) and f) show the interaction with B7C3 ash after 8 h and 40 h of interaction, respectively. The SEM images of the surface at this magnification reveal ash particles adhering to the K-feldspar surface after interaction with fuel ash. Increasing the interaction time between K-feldspar and biomass, shown in Figure 5.18 c) for BA and in Figure 5.18 f) for B7C3, did not significantly influence the visible amount and size of ash particles observable with SEM.

5.2.5 Detailed Layer Formation Observations

Figure 5.19 depicts a close-up of a K-feldspar from B7C3 combustion. The SEM image shows three distinct layer regions which were not discernible by line analysis due to their low thickness. With EDS area analysis it is possible to discern the outer outer layer (▼) from the inner outer layer (■). The thin inner layer (▲) cannot be discerned with EDS area analysis. Intrusions of Ca into the particle can be detected as well.

Another close-up for B7C3 combustion is depicted in Figure 5.20. This particle only shows one outer layer (■) as well as the thin inner layer (▲). This close-up also shows precipitated crystals (★) inside the layer. These crystals highly deviate in composition from the fuel ash layers. The compositions determined for the layers and the crystals detected for Figure 5.19 and Figure 5.20 can be seen in Figure 5.21. The crystals are rich in K, Ca and Si. They additionally contain considerably higher contents of S as well as Na. The P content is similar to the content in the inner layers. All three outer layers (the outer outer and inner outer layer detected in Figure 5.19 and the outer layer detected in Figure 5.20) have a comparable composition. No measurable difference could be detected between inner outer and outer outer layer for the particle depicted in Figure 5.19. With the data currently available it is not possible to explain why the inner and outer outer layer are distinguishable with SEM but not with EDS.

The inner layers are richer in K, Al and Si indicating a higher fraction of native K-feldspar in this inner layer. Apart from K-feldspar a considerable amount of Ca as well as some P were detected as well. Overall the composition of these inner layers is comparable for both samples. It has to be mentioned that the K:Al ratio is close to 1 in both the inner and outer layers, indicating changes in layer formation compared to P-lean fuels.

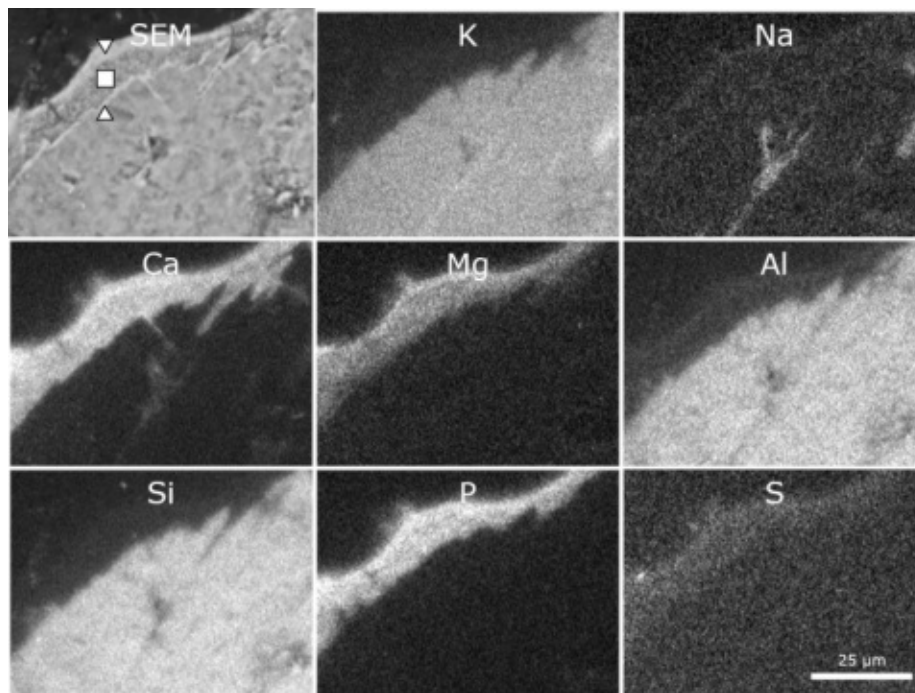


Figure 5.19: Close-up of a layer formed during B7C3 combustion. A SEM image as well as EDS area mappings for several elements are depicted. The detected layers are an outer outer layer (▼), an inner outer layer (■) and an inner layer(▲).

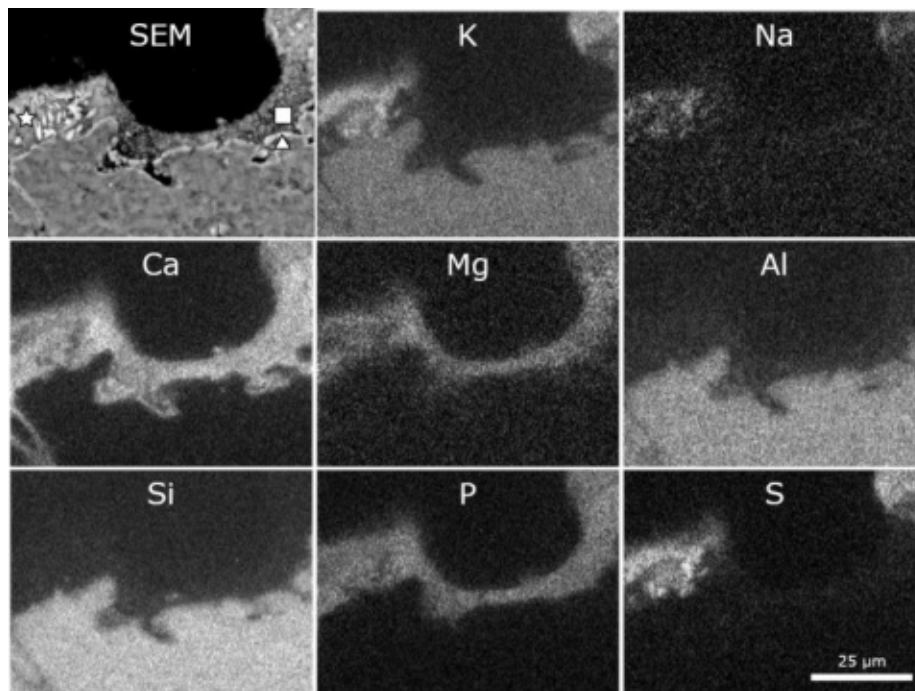


Figure 5.20: Close-up of a layer formed during B7C3 combustion. A SEM image as well as EDS area mappings for several elements are depicted. Precipitated crystals (★) can be distinguished in the fuel ash layers. The detected layers are an inner outer layer (■) and an inner layer(▲).

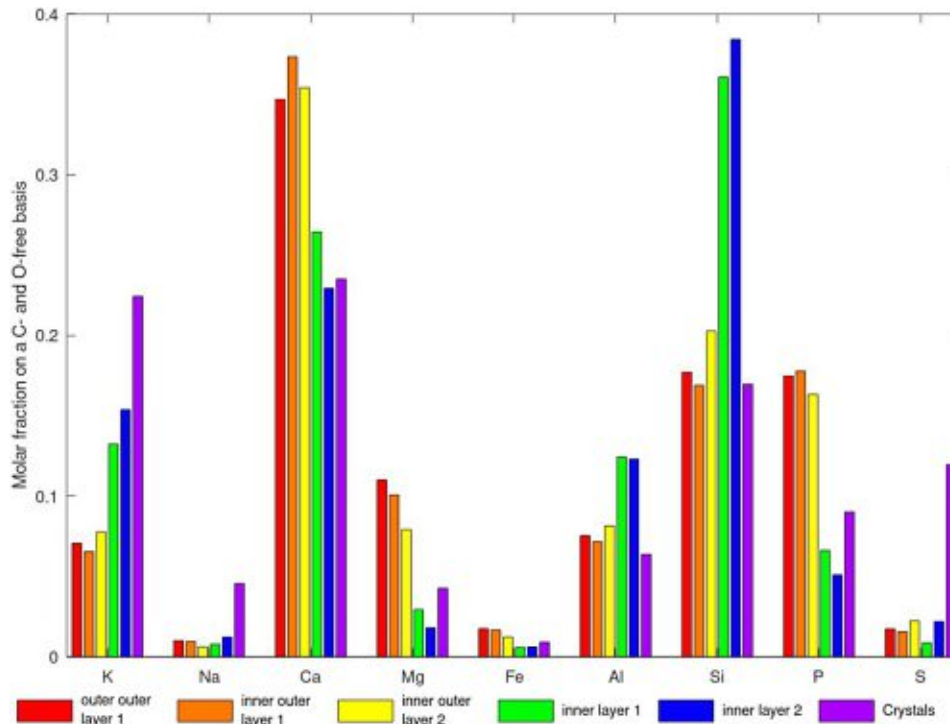


Figure 5.21: Elemental composition of several ash layer sections as well as the precipitated crystals detected in Figure 5.20 as collected from manually selected areas in EDS area mappings. The labelling of inner and outer layer was done according to the assumed layer formation mechanism underlying the formation of the relevant layer.

5.2.6 Proposed Layer Formation Process on K-Feldspar with P-rich Fuels

With the data collected throughout this thesis it is possible to propose a first layer formation mechanism for P-rich fuels on K-feldspar and compare it to the layer formation mechanism with P-lean fuels. Faust et al. [56] proposed three phases of layer formation, depicted in Figure 5.22 (top), with woody biomass on K-feldspar. Initially fuel ash deposits on the bed particle and Ca reacts with the bed material surface (first phase). The reaction of Ca with K-feldspar promotes the diffusion of Ca into the bed particle forming the Ca reaction layer (second phase). Simultaneously a diffusion of K out of the bed material is observed, indicated by a reduction of the K:Al ratio. The reactions of Ca with the K-feldspar lead to stresses inside the crystal structure and eventually to the development of cracks from the particle surface into the particle (third phase). The cracks open up new virgin surfaces for Ca to penetrate into the bed material.

When sufficient quantities of P are available in the fuel ash, P dominates the reactions occurring in the ash fraction due to the high stability of phosphates [52]. The first phase is similar

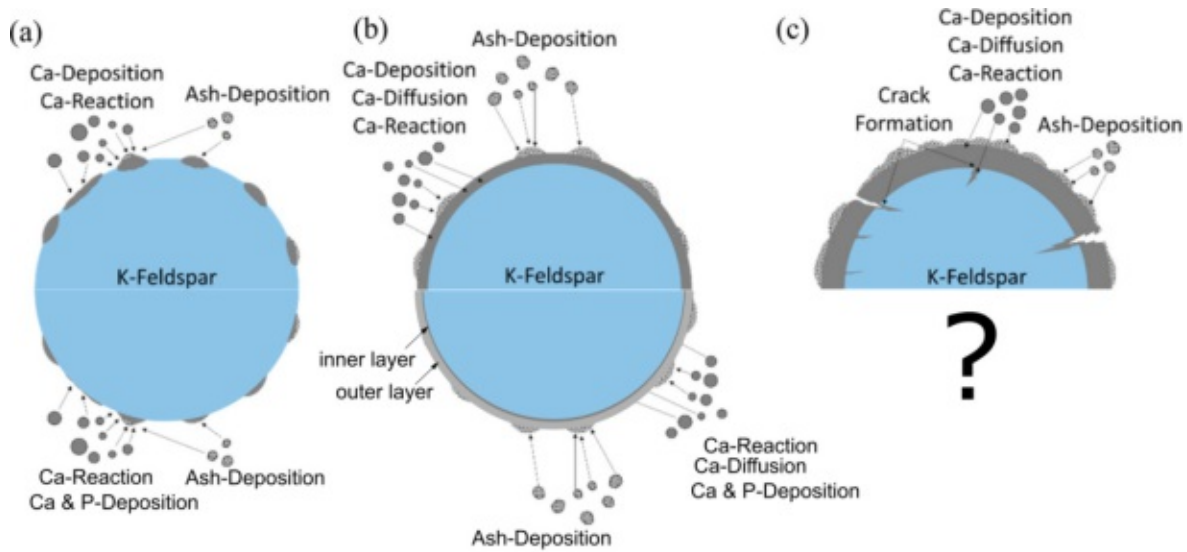


Figure 5.22: Layer formation mechanism on K-feldspar with woody biomass as proposed by Faust et al. [56] (top) and adapted for layer formation with P-rich fuels (bottom). (a) Initial accumulation of fuel ash elements. The major element reacting in this phase is Ca. This phase is comparable for P-lean and P-rich fuels. (b) Formation of continuous layers. During this phase mainly an inner layer forms for P-lean fuels while a thin inner layer and a thicker outer layer forms for P-rich fuels. Elements apart from Ca now also participate in layer formation. (c) Onset of crack layer formation and formation of a continuous outer layer for P-lean fuels. No crack formation has yet been observed for P-rich fuels due to shorter operational times.

to the first phase during layer formation with P-lean fuels. Ash deposits on the bed particle surface and interacts with the surface. Due to the interference of P less Ca is available for reactions with the particle surface, slowing down the development of a reaction layer. The second phase for P-rich fuels differs more from the case with P-lean fuels. Due to the decreased rate of reaction between Ca and K-feldspar, the inner layer develops considerably slower compared to P lean fuels. Figure 5.21 shows that an inner layer is in fact forming, which is mainly rich in K-feldspar and Ca, as well as P. Due to the presence of P in the inner layer it can be assumed that not only a variety of silicates make up the inner layer but also some phosphates can be found. The outer layers (ash deposition layers) contain a variety of elements. It has to be noted that the K:Al ratio is still around 1 in the outer layers leading to the assumption that less K is diffusing out of the K-feldspar particle.

During the operational time of 40 h it was not possible to observe crack formation on K-feldspar (third phase) with P-rich fuels. Since the overall interaction between fuel ash and bed material is reduced, it can be assumed that considerably longer operational times will be necessary with P-rich fuels for cracks to form, if any form at all. Further understanding the mechanisms underlying fuel ash - bed material interactions is of major importance when

broadening the fuels used during thermochemical applications. Long-term experiments will make it possible to broaden the understanding of fuel ash - bed material interactions with P-rich fuels and will make it possible to give a final recommendation about suitable fuels for gasification and thermochemical applications in general.

5.2.7 Differences to Fuel Ash Fractions

This subsection summarises Paper V and correlates it to the found observations of Paper III. Further analyses of the ash fractions from CM, B7C3 and S7C3 were performed to study the differences in compounds forming during the combustion of these fuels. Special attention was given to P during these analyses. The goal was to further understand the P-compounds forming and how to influence the P speciation to promote the formation of plant available compounds. The results of EDS analysis are summarised in Figure 5.23. For each experiment the composition of bed ash, cyclone ash and coarse particulate matter is nearly identical. This is probably caused by the fact that the cyclone ash and coarse particulate matter consist of the same compounds as the bed ash but are smaller particles produced by attrition that were subsequently discharged. Still, the bed ash contains a higher fraction of the bed material K-feldspar compared to the other ash fractions. The fine particulate matter mainly consisted of KCl for all experiments.

For B7C3 and CM combustion P was mainly detected in particles also rich in K, Ca, Mg, and S. Due to their smooth surface they are assumed to be melt precipitates and therefore amorphous. Table 5.3 also summarises the phases detected in the various ash fractions as well as in the bed material for CM and B7C3 combustion. During S7C3 combustion two types of particles were observed in the coarse ash. One of them is rich in K, Ca, Si and P and the other one is rich in K and Si. These particles can also be assumed to have been molten at some point during operation due to their shape and their composition. P in crystalline compounds was identified in apatite and whitlockite for CM and S7C3. Bark blends produced ash with P located in apatite. From a plant availability point of view, co-combustion of CM and WS is therefore an interesting route.

Compared to the fuel ash layers the composition of the ash fractions mainly deviates in Al and Si. Only low levels of Al were detected in the ash fractions. The high levels of Al in the fuel ash layers can be attributed to the Al in K-feldspar (KAlSi_3O_8). The differences in Si-concentration observed in the ash fractions for different fuels cannot be identified in the fuel ash layers, due to the high concentrations of Si originating from K-feldspar. The use of a Si-free bed material would be necessary to study the behaviour of fuel ash-originating Si in fuel ash layers.

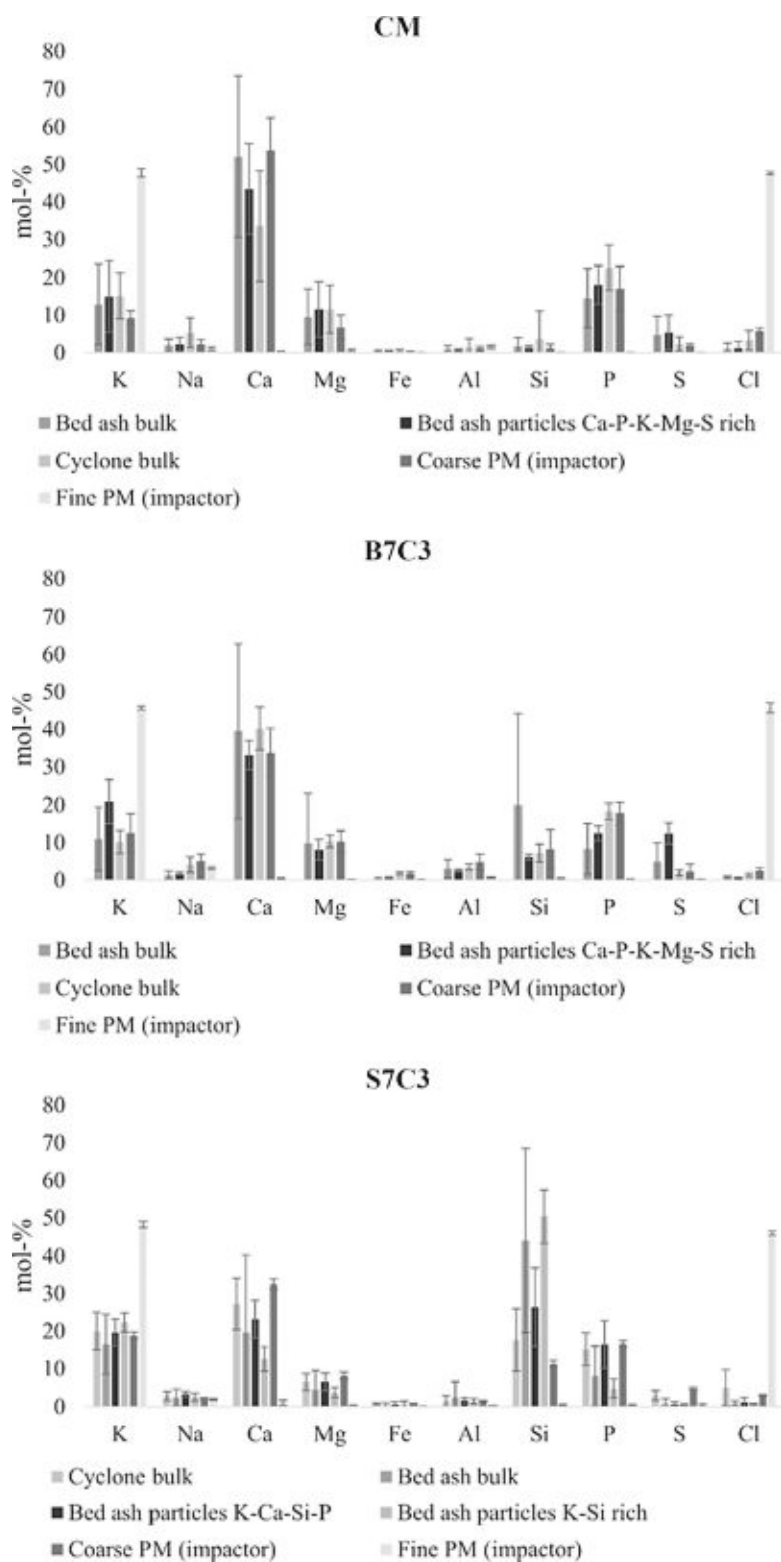


Figure 5.23: Average elemental composition (error bars show standard deviation) of major ash-forming elements for the bulk ash fractions and typical particles on a C- and O-free basis. Top: CM, Middle: B7C3, Bottom: S7C3.

Table 5.3: Detected phases in different ash and bed material fractions after CM and B7C3 combustion.

	CM			B7C3		
	Bed ash	Bed material 200 μm –250 μm	cyclone ash	Bed ash	Bed material 200 μm –250 μm	Cyclone ash
KAlSi_3O_8	XRD	XRD			XRD	
K_2SO_4	XRD	Raman	XRD	XRD	Raman	XRD
KCl			XRD			XRD
$\text{Na}_{0.5}\text{K}_{0.5}\text{Cl}$				XRD		
Na_2SO_4						XRD
$\text{Ca}_9\text{MgK}(\text{PO}_4)_7$			XRD			
Ca_2SiO_4		XRD			XRD	
CaSiO_3					XRD	
CaHPO_4		XPS			XPS	
$\text{Ca}_5(\text{PO}_4)_3\text{OH}$	XRD		XRD	XRD		XRD
CaCO_3		Raman	XRD		XRD	XRD
$\text{Ca}(\text{OH})_2$	XRD			XRD		
CaO	XRD	XRD, XPS Raman		XRD	Raman	
MgO	XRD	XRD		XRD		
SiO_2	XRD	XRD, XPS		XRD	XRD, XPS	XRD
$(\text{PO}_4)^{3-}$		XPS			XPS	
		Raman			Raman	
$(\text{CO}_3)^{2-}$		XPS			XPS	

Table 5.3 summarises the phases detected during the combustion of CM and B7C3 in the unsieved bed material sample (bed material and bed ash), the sieved fraction of 200 μm –250 μm from the bed material, and the cyclone ash.

The bed material sample was sieved to 200 μm –250 μm to mainly obtain K-feldspar bed material particles, which was sieved to this fraction before its use in the fluidised bed. Table 5.3 shows several silicates detected in the sieved bed material sample, which were not detected in the fuel ash. This is probably caused by the interaction of Si from the K-feldspar bed material with ash components. The bed material surface also shows less phases containing sulfur, compared to ash fractions. This indicates that sulfur is less available for layer formation compared to reactions in the ash phase.

5.2.8 Comparison to Layer Formation on Quartz and Limestone

This subsection summarises observations from Paper I and supervised Master Theses.

Figure 5.24 depicts EDS mappings of various quartz particles that were detected during

the combustion and gasification with K-feldspar as bed material. During these experiments layers rich in K, Ca, P and S formed. P and S were only detected in layers when CM or a mixture with CM was used as fuel. The mapping of WS combustion shows that quartz is involved in agglomeration phenomena to a high degree.

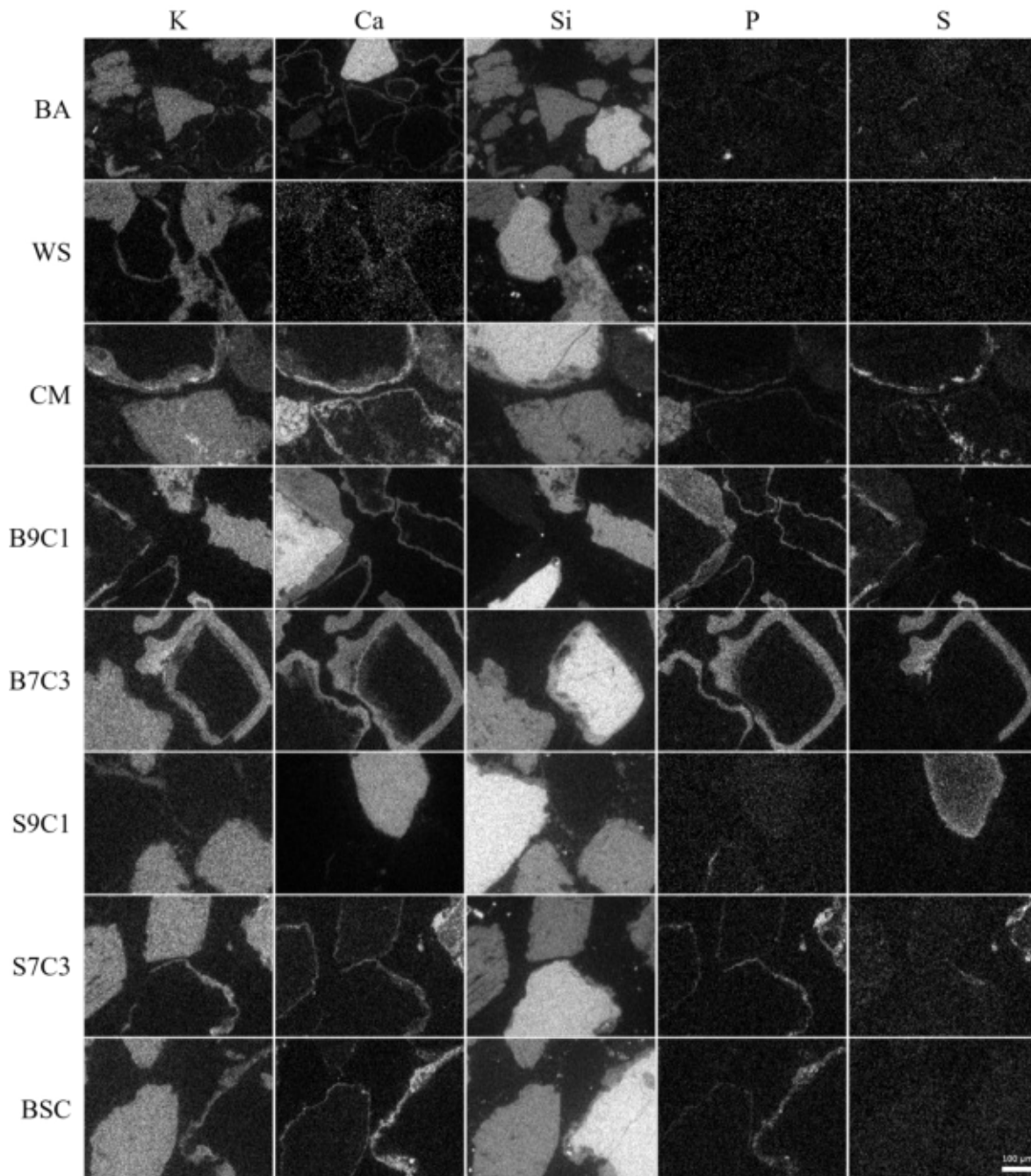


Figure 5.24: EDS mappings from quartz particles detected from the combustion experiments with K-feldspar (all but the last row) as well as the DFB steam gasification of 0.595 kg kg⁻¹ bark, 0.15 kg kg⁻¹ straw and 0.255 kg kg⁻¹ chicken manure on a dry basis (BSC) with pure K-feldspar.

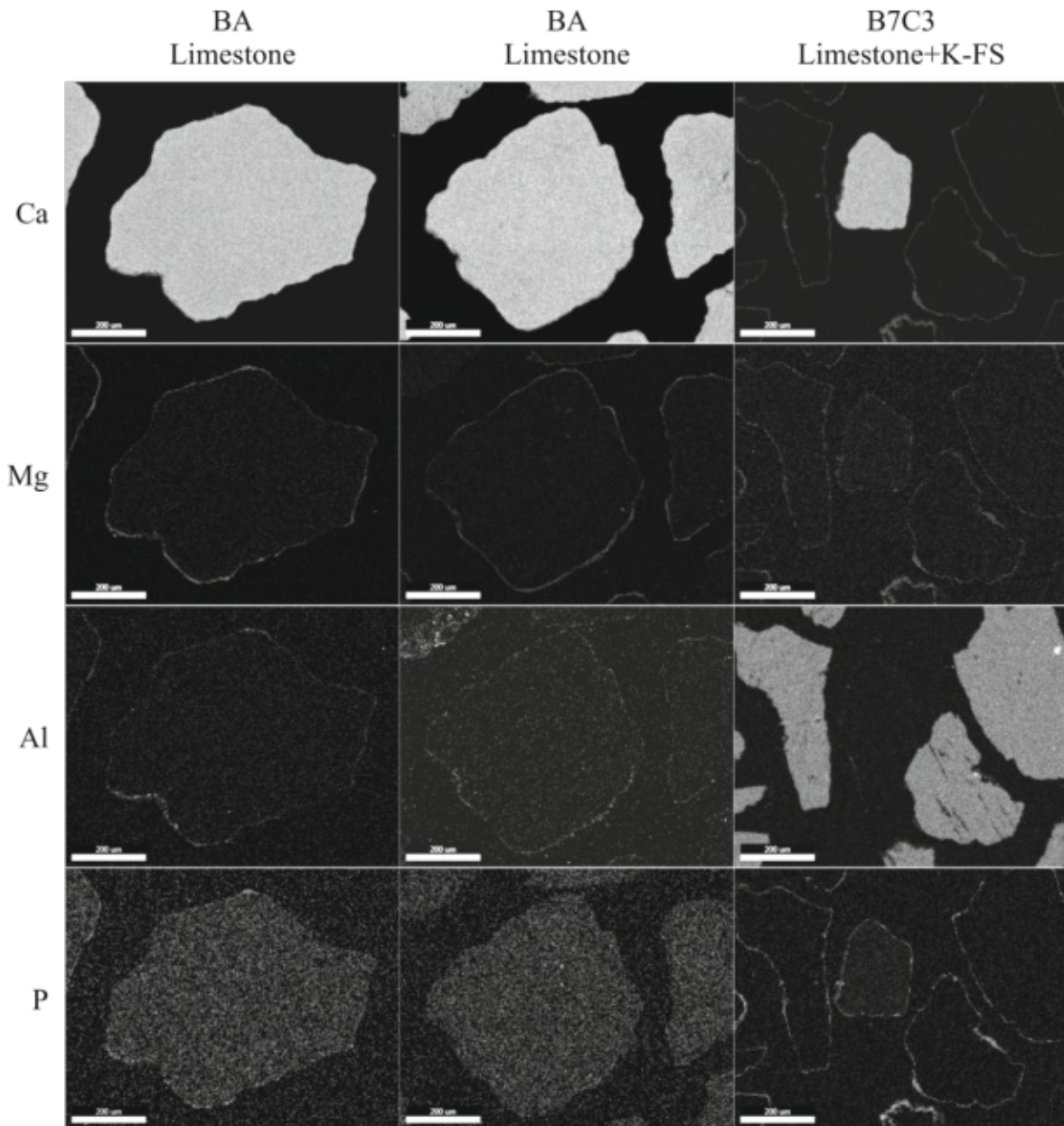


Figure 5.25: EDS mappings of limestone particles detected in bed material samples from DFB steam gasification.

The thickest layers formed on quartz during the combustion of CM and B7C3. For CM thick layers formed due to the high ash content of CM, for B7C3 the ash content as well as the long operational time played a major role. For these samples it is also possible to discern inner and outer layers on the quartz particles. The layers formed on quartz particles are also thicker compared to layers formed on K-feldspar. This indicates that K has a reduced layer formation tendency. This might lead to a prolonged time until negative effects of layer formation (i.e. crack formation) becomes relevant. Crack formation was attributed to increased bed material deposition in cyclones and therefore the necessity to regularly exchange the bed material [95].

Figure 5.25 shows several limestone particles detected from various DFB steam gasification experiments. Discontinuous layer accumulation of elements on the limestone surface could be detected. The clearest signs of initial layer formation can be seen for Mg and an enrichment of Al can be seen as well. P enrichment was only detected for B7C3 gasification, where sufficient P was available from the fuel ash.

Even though limestone is a soft mineral that is prone to attrition, it was possible to detect initial layer formation on the particles. Long-term experiments are necessary to determine what influence fuel ash layers have on the catalytic activity of limestone. Currently, literature indicates a negative effect of fuel ash layers, since fuel ash layers led to deactivation of dolomite [69]. This deactivation as well as the increased attrition of limestone makes long-term operation with limestone more challenging compared to K-feldspar.

5.3 Bed Material and Ash Layers Catalytic Activity

This section is based on results from Papers III and IV.

5.3.1 Catalytic Activity during Gasification

When new bed materials are first used for DFB steam gasification in the 100 kW DFB steam gasification pilot plant at TU Wien they are always tested with a fraction of limestone added as bed material first. This is done to ensure a certain level of catalytic activity and a reduction of tars in the system. The DFB steam gasification reactor can only handle certain amounts of tar due to design as a test-plant only in operation 1 day at a time. Therefore, K-feldspar was first tested in a K-Feldspar (0.9)/limestone (0.1) mixture with SW as fuel. These experiments showed a higher catalytic activity and lower tar contents than fresh olivine with SW. Due to these promising results experiments with pure K-feldspar as bed material were performed as well.

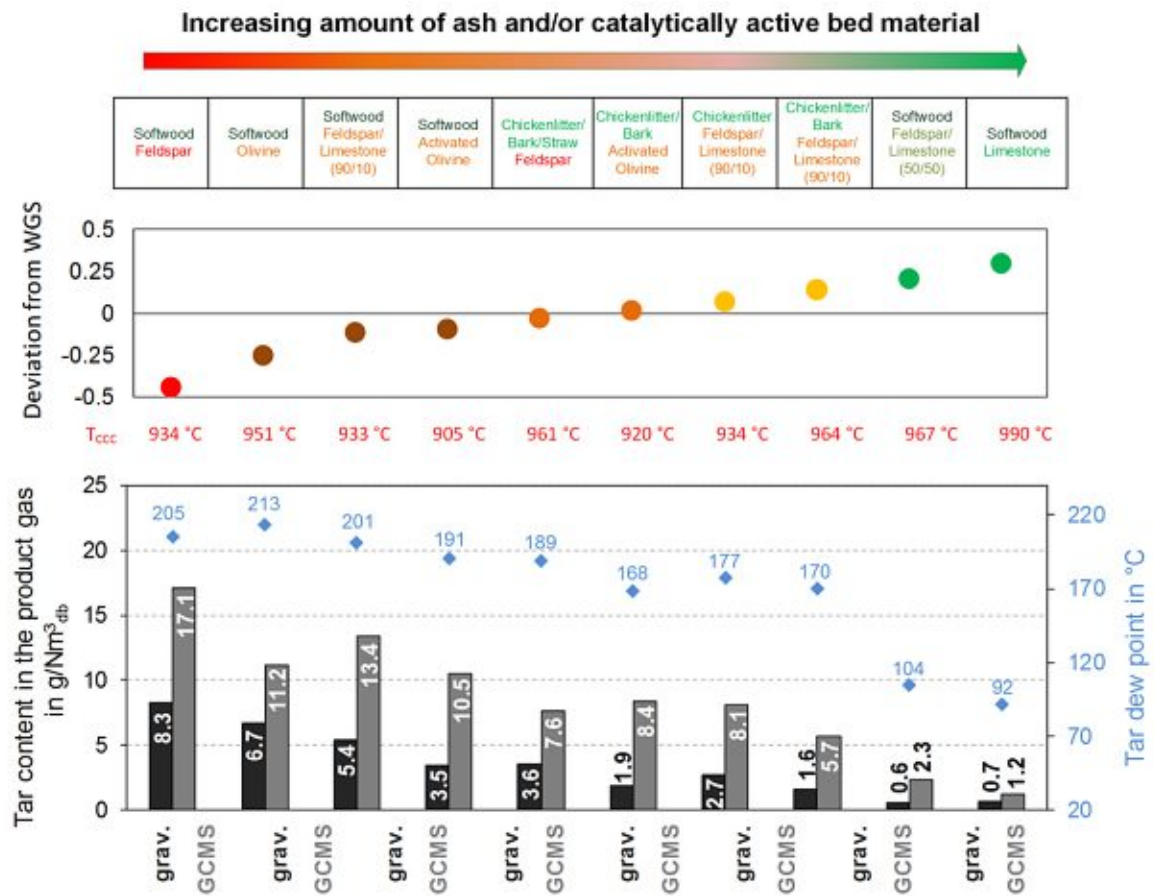


Figure 5.26: Summary of the performed gasification experiments. The experiments are sorted by their deviation from the WGS equilibrium (see upper picture). The lower image depicts the tar content in the product gas as well as the tar dew point.

As a reference gasification experiments were also performed with used olivine, pure limestone and a 50:50 mixture of K-feldspar and limestone. A comparison of all these experiments can be seen in Figure 5.26. The experiments were arranged according to their catalytic activity (indicated by the deviation from the WGS equilibrium). The upper part of the picture depicts the deviation from the WGS equilibrium, calculated according to Equation 4.1, as well as the temperature in the counter-current column closest to the gas sampling point. The WGS equilibrium was chosen as criterion to quantify the catalytic activity since it is possible to compare experiments performed at different temperatures easily. The WGS equilibrium is also an indicator on the $H_2:CO$ ratio, which is important for downstream synthesis. The lower part shows the corresponding tar contents measured for each experiment. It can be seen that, overall, an decrease in the deviation from the WGS equilibrium also means lower tar contents. Though it can be seen that the gasification temperature has an additional influence on the tar levels with higher temperatures further decreasing the tar content (see

SW with olivine and BSC with K-feldspar).

K-Feldspar (0.9)/limestone (0.1) mixture was also used as bed material for the gasification of B7C3. The use of B7C3 led to an increased occurrence of the WGS reaction, caused by an increased amount of fuel ash available compared to SW. The experiment was concluded with pure CM. While the use of CM also led to an increased occurrence of the WGS reaction the high ash contents of CM with 0.254 kg kg^{-1} led to problems with fluidization of the bed material. The reactor is not equipped with bottom ash removal, making long-term operation with ash-rich fuels challenging.

The next step in evaluating K-feldspar was using it as pure bed material, without the addition of limestone. During the experiment with SW the catalytic activity was reduced and the tar content was elevated compared to the experiments with limestone addition. The observed negative deviation of the WGS equilibrium as well as the high observed tar contents show that the used K-feldspar is an inactive bed material. Switching the fuel to ash-rich BSC showed a surprising behaviour. Even though the temperature inside the reactor was kept constant a rise in H_2 and a decline in CO was observed. A direct comparison between SW and BSC gasification can be seen in Figure 5.27. It becomes clear that the increased ash content of BSC is influencing the catalytic behaviour inside the reactor.

To further understand the significance of fuel ash layers on the catalytic activity, layered olivine from the DFB steam gasification plant in Senden, Germany was used in additional DFB steam gasification experiments. Experiments with SW showed that the negative deviation from the WGS equilibrium and the tar content is reduced compared to fresh olivine, proving the positive effect of fuel ash layers. The addition of the ash-rich fuel B7C3 only led to a small further increase in catalytic activity. Due to the already existing ash layer, a further addition of ash is only leading to a small increase in catalytic activity. During the subsequent experiment with CM no stable operation could be achieved. It was assumed that the high ash contents of CM led to problems with fluidization inside the reactor. No data evaluation regarding the gas composition could be performed for this experiment, and it is therefore not included in Figure 5.26.

Pure limestone as well as a 50:50 K-feldspar/limestone mixture were used as bed material with SW to complement the already performed experiments. As expected, limestone led to the lowest tar contents in the product gas followed by the 50:50 mixture.

The layers that developed during gasification are one reason for the increase in catalytic activity during operation [71]. This is especially clear for the experiments with fresh and layered olivine. Though, it can still be assumed that for the experiments presented in Figure 5.26 layer formation plays a minor role due to the short operational time. No change in product gas composition was yet observed during the course of the experiments, which

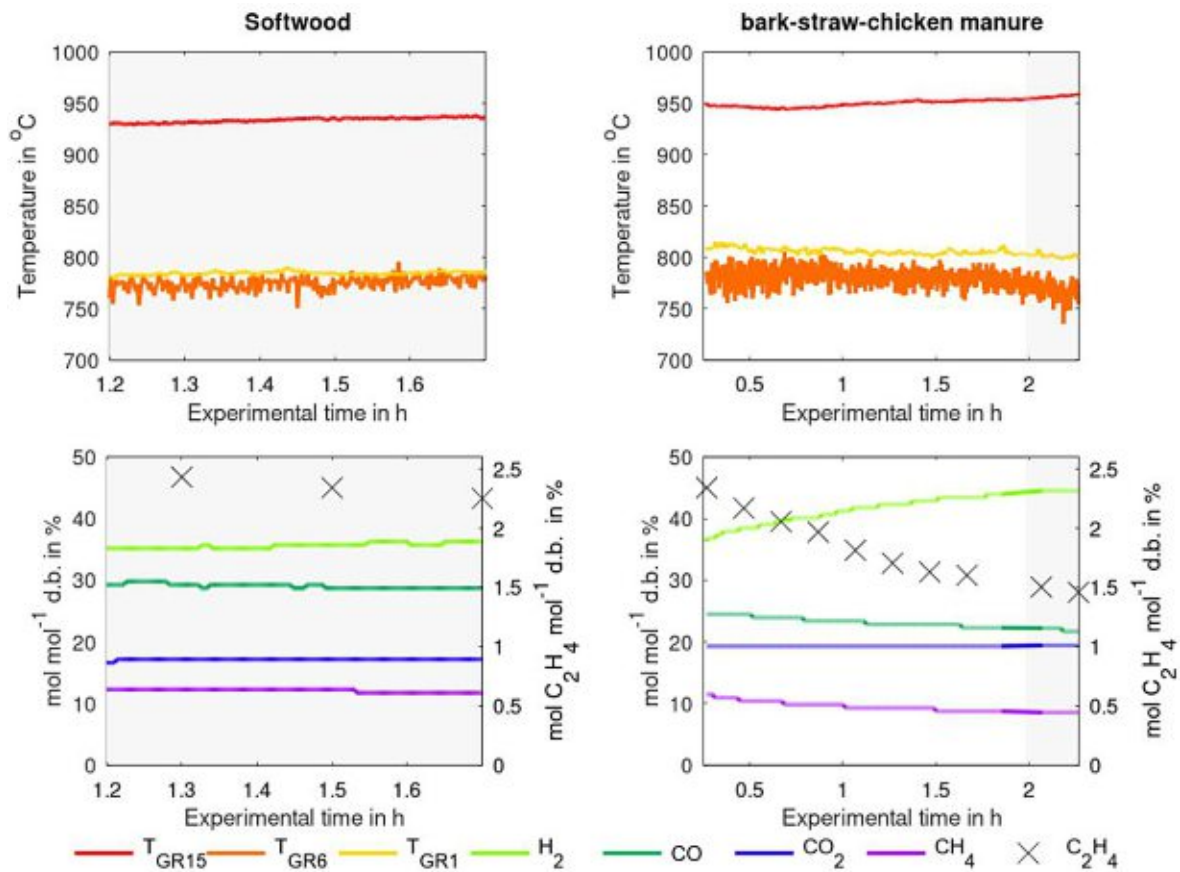


Figure 5.27: Comparison between operation with SW and a BSC with K-feldspar as bed material.

should occur, if sufficient layers had already formed during operation. The only exception was the experiment with K-feldspar and BSC where a change in product gas composition was observed over time (Figure 5.27) due to the low initial catalytic activity of K-feldspar. Therefore, in the first hours of operation the fuel ash and limestone fractions in the bed material have a considerably higher impact on the catalytic activity than the bed material K-feldspar and first layers forming on the bed material.

5.3.2 Activation of Different Bed Materials during Gasification

Several samples from DFB steam gasification were also examined in isolated WGS experiments. Sorting the experiments by the deviation from the WGS equilibrium yields Figure 5.28. Bottom ash samples were chosen for this investigation since they mainly consist of bed material and only low fractions of fuel ash, making it possible to focus on the bed material and fuel ash layers in more detail. Fresh bed materials and layered olivine were also tested in these experiments. They can be seen as approximation for DFB steam gasification with

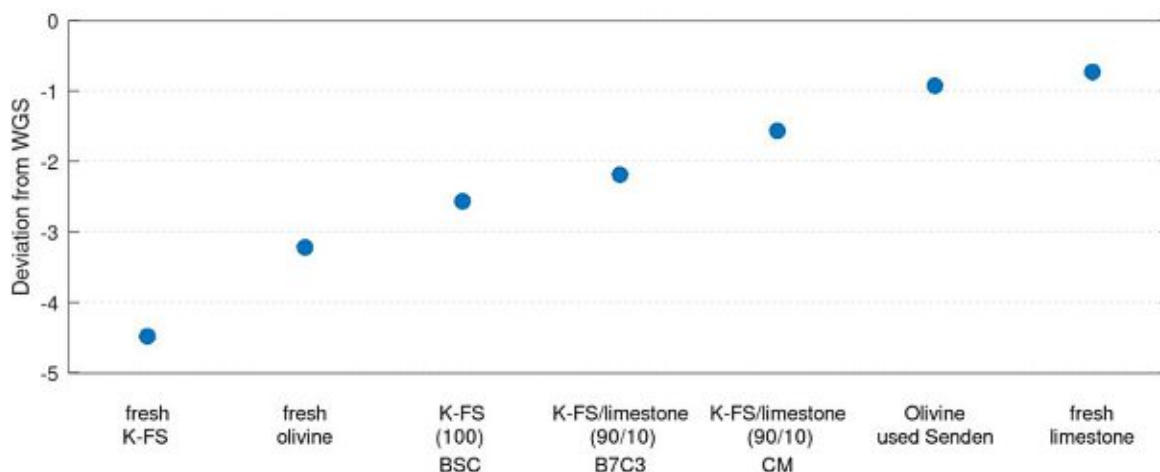


Figure 5.28: Deviation from the WGS equilibrium determined in isolated WGS experiments.

SW, since SW does not contain relevant amounts of ash.

Figure 5.28 shows a similar order of experiments compared to the catalytic activity observed during gasification (Figure 5.26). This highlights the relevance of the WGS reaction occurring during DFB steam gasification.

Layered olivine is the only sample that is more active than it should be according to the results obtained during DFB steam gasification. A possible explanation is that fuel ash layers might be especially catalytically active towards the WGS reaction, compared to other reactions occurring during gasification. Since fuel ash layers contain a considerable amount of Ca, this might also explain the high catalytic activity of limestone. Though, at this moment, no definite answer can be given why layered olivine shows a higher catalytic activity than predicted.

5.3.3 Time-Dependent Activation of Bed Material by Fuel Ash Layers

Experiments were conducted to determine the catalytic activation of layered K-feldspar over time from BA, CM and B7C3 combustion. As already established in subsection 5.2.1 layer formation during combustion and gasification is comparable. It is therefore possible to use samples from fluidised bed combustion to determine the catalytic activity for gasification. Figure 5.29 gives the deviation from WGS equilibrium when leading CO and H₂O over the bed material samples.

The correlation between particle age and WGS deviation was determined according to Kendall rank correlation. A τ value of 0.8 and a p-value well below 0.05 indicate a strong correlation between particle age and WGS deviation. The determined p-value has to be studied carefully, since the evaluation of the Kendall rank correlation with several data points of

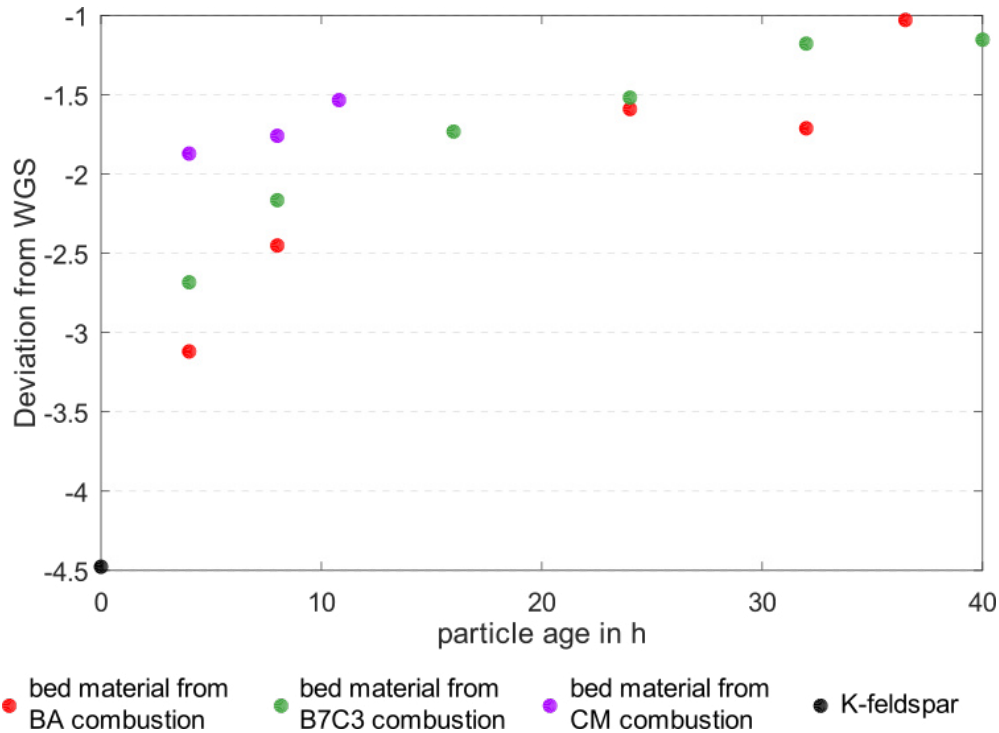


Figure 5.29: Catalytic activity determined for layered K-feldspar particles shown by the deviation from WGS equilibrium

the same x-value is only possible to a certain degree.

Fresh K-feldspar (0 h) showed nearly no catalytic activity but the other samples show a bed material activation. This observed activation effect that occurs due to bed material-ash interactions is well established [55, 72, 96]. Already short operational times of 4 h led to an observable increase in catalytic activity for all fuels. The catalytic activity further increased for longer operational times. After 10 h of combustion, the highest catalytic activity can be observed for the bed material samples from CM combustion. For operational times of more than 10 h, the samples from B7C3 and BA combustion reached a comparable WGS deviation.

With the samples available it was not possible to detect the final reachable deviation from WGS equilibrium possible with layered K-feldspar. The final WGS deviation reachable with long-term operation would give additional information on the suitability of ash-layered bed materials for biomass gasification.

Figure 5.30 depicts the correlation between the observed BET surface area (Figure 5.17) and deviation from WGS equilibrium (Figure 5.29).

Kendall rank correlation shows a strong correlation between BET surface area and the deviation from WGS equilibrium ($\tau=0.45$, $p=0.02$). Higher BET surface areas have a

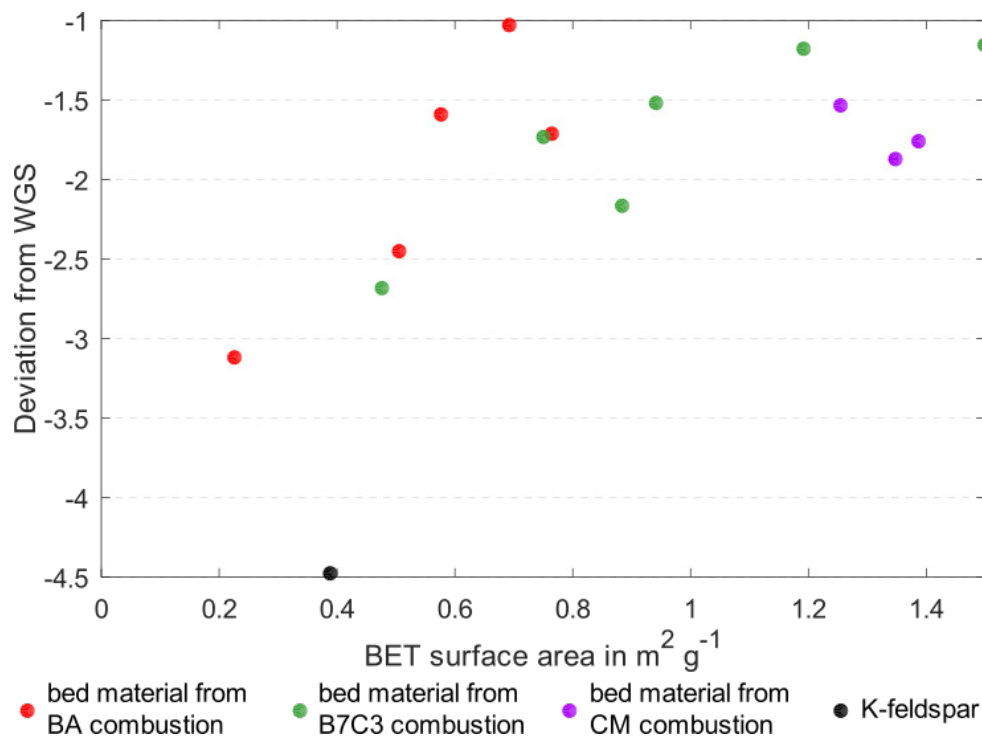


Figure 5.30: Correlation between BET surface area and catalytic activity, quantified by the H₂ yield regarding the WGS equilibrium

tendency to lead to a higher catalytic activity. This is in accordance with the fact that higher surface areas on catalysts lead to a higher yield. The deviations from a linear correlation can probably be traced back to the differences in surface composition caused by different fuels. It can be seen that layers formed by BA combustion lead to the same deviation from WGS equilibrium with lower BET surface areas compared to B7C3 and CM combustion. Studies focused on dolomite from air gasification observed a different connection between BET surface area and catalytic activity [69]. For used dolomite, the catalytic activity regarding benzene steam reforming was decreased by 24% compared to unused (but calcined) dolomite while the BET surface area increased from $0.4 \text{ m}^2 \text{ g}^{-1}$ – $19.5 \text{ m}^2 \text{ g}^{-1}$ during gasification. They explained the results by a deactivation of the CaO and MgO sites by SiO₂ deposition from the fuel ash.

In summary, layers forming on K-feldspar showed a similar catalytic activity to small admixtures of limestone to the bed material. The activation observed over time that was observed both in the DFB steam gasification pilot plant as well as WGS experiments with samples with fuel ash layers originating from combustion is promising for the further use of K-feldspar as bed material for DFB steam gasification.

Chapter 6

Future Work

Several steps have to be performed in the future before K-feldspar can be established as new bed material in DFB steam gasification plants. This chapter gives a short timeline for those steps.

6.1 K-feldspar as Bed Material in Industrial Plants

Before a final recommendation can be given regarding the suitability of K-feldspar it is necessary to perform long-term experiments. This can be carried out in two ways. One way is to substitute a part of active or activated bed material (e.g. layered olivine bed material) during operation of a DFB steam gasification plant using woody biomass and observe the changes in gas composition and tar content. When the performance of the gasification process is still satisfactory it is possible to substitute another part of the bed material by K-feldspar. This can be repeated until K-feldspar is substituted for all of the bed material and only has to be stopped if the product gas composition is not reaching desired qualities anymore. If it is possible to replace all olivine with K-feldspar without negative effects on the product gas composition K-feldspar proved to be a suitable bed material.

The other approach would be to use K-feldspar as bed material from the beginning and add additives like limestone during start-up and whenever necessary during operation. Ideally the frequency of limestone additions reduces during long-term operation and can be stopped as soon as sufficient layers formed on the K-feldspar bed material particles.

After using K-feldspar in an industrial plant for an extended period of time it will also be possible to study the long-term layer formation of K-feldspar. The final surface composition can be determined as well as the tendency of K-feldspar to form cracks. Cracks on bed material particles make it necessary to replace the bed material before pieces of the bed

material can break of. Therefore it is necessary to use a bed material with a low tendency for crack formation to prolong the life-time of bed material particles before they have to be replaced. Faust et al. [56] detected initial crack formation for K-feldspar after 51 h so it is necessary to focus attention to fragmentation of bed material occurring.

With samples from long-term exposure it will also be possible to determine the final reachable catalytic activity with K-feldspar and woody biomass. Comparing these results to layered olivine and limestone will further show the suitability of K-feldspar.

For combustion applications K-feldspar might also prove interesting to replace quartz bed materials. Due to its decreased interaction with the fuel ash the formation of cracks seems to be reduced. Replacing of used bed material can therefore be reduced compared to quartz, leading to lower costs of the bed material.

6.2 Long-term Experiments with Alternative Fuels

If the use of K-feldspar with woody biomass proofed successful it will next be necessary to use K-feldspar with ash-rich alternative fuels. The changes in ash content will make it necessary to further focus on ash removal both from inside the reactor as well as from the product gas stream. It might be possible to tackle the increased ash content with changes in operation alone but it could also be necessary to install additional cyclones or other ash removal equipment.

The influence of ash composition on both ash melting behaviour and ash layer formation are other aspects that have to be considered as soon as alternative fuels are being used. After successful operation with alternative fuels the influence of fuel ash composition on the final reachable catalytic activity can be studied. Fuel mixtures are one possibility to use otherwise problematic fuels like straw. By mixing problematic fuels with other fuels with high melting ash it might be possible to use these fuels at least in small quantities. The co-combustion of straw and chicken manure also led to the formation of plant available compounds that did not form during chicken manure mono-combustion.

6.2.1 Sewage Sludge

Sewage sludge is a waste stream that could be upgraded by gasification to a valuable product. It is also a challenging fuel due to its fuel properties. The heavy metal content as well as the increased water content have to be considered during operation. Sewage sludge also contains

considerable amounts of P. By using sewage sludge as fuel it might be possible to enrich P in the fuel ash by further treatment, making it more feasible to further utilise it.

6.3 Further Characterisation of Ash Fractions

The use of a heavy metal-free bed material makes it possible to further utilise the accruing ash fractions. One possible application is the use as fertiliser. First tests showed that ash from co-combustion of chicken manure and straw produces plant available P-compounds. More dedicated experiments are necessary to further understand how the speciation of ash elements in the ash can be influenced. Especially the influence of gasification atmosphere on the forming ash compounds has only been studied insufficiently until now.

6.4 Further Development of Micro-Scale Test-Rig

The WGS reaction tests on the micro-scale test-rig proved important for the characterisation of catalytic activity of bed materials. Though, the results showed that some differences in catalytic activity towards the WGS reaction can be observed during gasification and isolated WGS experiments. Understanding the causes for these differences might make these isolated experiments even more valuable since a wide variety of bed materials could be screened without using them in time-consuming gasification experiments. Further developing the method to include a variety of reactions (e.g. tar reforming) can also be an important factor in future characterisation of bed materials.



Die approbierte gedruckte Originalversion dieser Dissertation ist an der TU Wien Bibliothek verfügbar.
The approved original version of this doctoral thesis is available in print at TU Wien Bibliothek.

Chapter 7

Conclusions

K-feldspar was studied for its suitability as alternative bed material for fluidised bed applications. Combustion experiments with a variety of alternative fuels showed promising results regarding the applicability of K-feldspar as bed material as long as the ash melting point of the fuel ash isn't too low. DFB steam gasification and WGS experiments showed that K-feldspar is an inactive bed material regarding gasification reactions. Still, it was possible to observe activation of K-feldspar in a variety of experiments. In-situ activation of K-feldspar could be achieved with the aid of an ash-rich fuel mixture in the time-scale of several hours reaching similar catalytic activities to activated olivine, which is the current bed material in DFB bed steam gasification plants.

Several specific results could be obtained throughout this thesis:

- Combustion experiments dedicated to the formation of fuel ash layers were performed with a variety of alternative fuels to further study the influence of fuel ash composition on layer formation. The experiments showed that P originating from CM changes the layer formation mechanisms by promoting ash-ash reactions instead of ash-bed material reactions typical for P-lean fuels. The addition of CM to WS also showed an improvement in ash melting behaviour by elevating the ash melting point of the fuel.
- Experiments with pure CM highlighted the challenges of ash-rich fuel on the operation of fluidised bed systems. Both the combustion and the DFB steam gasification experiments exhibited problems due to the high ash content and had to be stopped prematurely due to it. Regular bottom ash removal has to be realised if CM or other ash-rich fuels are to be used in fluidised bed systems. Fly ash removal is not sufficient in removing enough ash from the system.

- Comparisons between layer formation during combustion and gasification showed no remarkable differences between those two operation modes. Differences in layer composition were only observed for different fuels. While woody biomass (BA, BA-rich logging residues) led to an exchange of K^+ with Ca^{2+} inside the particle no such exchange was observed for CM, B9C1 and B7C3. Due to the similarities in layer formation during combustion and gasification it was possible to use samples from fluidised bed combustion for further analysis regarding gasification suitability of layered K-feldspar.
- The addition of CM to BA led to the development of thicker layers in the same time-scale compared to pure BA combustion. Older particles showed a differentiation into inner and outer layer for the samples from CM, B9C1 and B7C3 manure combustion. BA combustion did only show inner layer formation. Inner layers were enriched in Ca for all samples but K depletion could only be detected for BA combustion. The outer layers were rich in Ca, P, Mg, S and often K.
- Dedicated experiments regarding the WGS reaction showed a catalytic activation of K-feldspar by bed material-fuel ash interactions. This effect was more pronounced for the samples from combustion, since they were performed for a longer time-frame. The bed material from CM combustion showed the fastest activation followed by the bed materials from B7C3 and BA combustion. During these experiments the catalytic activity still increased for the oldest samples so it was not possible to obtain the final reachable catalytic activity of layered K-feldspar. Longer experiments will be necessary to clarify this question.
- Several differences in composition were detected between fuel ash layers and ash fractions. The fine fly ash fraction mainly consisted of KCl while the bottom ash fraction was closer to the layers in composition. No Al could be detected in the ash fraction compared to the fuel ash layers where the Al originates from K-feldspar. S was only detected in the ash fraction indicating that it is less available for interactions with the bed material.
- The layer formation mechanism for K-feldspar with woody biomass proposed by He et al. [54] and Faust et al. [56] could be further confirmed. The presence of P in the fuel ash changed the layer formation mechanism from the development of an interaction layer to the formation of a deposition layer. Long-term experiments will be necessary to show the impact of the changes in layer formation on fluidised bed be-

haviour (agglomeration, bed material fragmentation) and the catalytic activity during gasification.

It was also possible to answer the set research questions of this thesis:

1. *Can K-feldspar be used as alternative bed material in DFB steam gasification to replace olivine?*

Overall, it was possible to use K-feldspar as bed material in fluidised bed applications. The fluidization problems observed during operation could all be related to the fuel ash and not the used bed material. It was also possible to obtain comparable catalytic activities with K-feldspar with an ash-rich fuel mixture (BSC) compared to activated olivine.

2. *What are the mechanisms behind fuel ash layer formation on K-feldspar?*

It was possible to further support the proposed layer formation for P-lean fuels, where layer formation is mainly promoted by Ca diffusion into and K diffusion out of the particle. The presence of P interferes with the diffusion of Ca into the particle, leading to thinner inner layers. Following, the formation of outer layers is more pronounced for P-rich fuels. The diffusion of K out of K-feldspar could also not be detected, further showing a reduced inner layer formation.

3. *How is the catalytic activity and time-dependent activation of fuel ash layers influenced by different fuels?*

Higher ash contents of the fuels generally led to a higher initial catalytic activity during DFB steam gasification. It could also be shown that the development of a layer on K-feldspar positively affects the catalytic activity of the bed material, suggesting that long-term performance with ash-rich fuels leads to further improvement of gasification performance.



Die approbierte gedruckte Originalversion dieser Dissertation ist an der TU Wien Bibliothek verfügbar.
The approved original version of this doctoral thesis is available in print at TU Wien Bibliothek.

List of Figures

1.1	Current status of seven from nine planetary boundaries as defined by Steffen et al. [1].	1
1.2	Top: CO ₂ emissions worldwide by sector in the years 1990 to 2016. Adapted from [6]. Bottom: Primary Energy consumption in million tonnes oil equivalent worldwide in the years 1990 to 2017. Adapted from [7].	2
2.1	Basic principle of DFB steam gasification [30].	9
2.2	Agglomeration types. (1) Coating-induced agglomeration, (2) Melt-induced agglomeration [41].	11
4.1	Fuel ash composition of the fuels used throughout this thesis.	22
4.2	Scheme of the fluidised bed combustion plant in Umeå [85].	24
4.3	Advanced design of the DFB steam gasification plant built at TU Wien [86].	25
4.4	Detailed flow sheet of the used micro-scale test-rig	27
5.1	SEM stitching showing a big section of the K-feldspar bed material sample obtained after BA combustion. Several particle types are marked throughout the image: ■ K-feldspar, ▲ quartz, ★ porous ash particle, ● Fe particles. Layers can be seen on K-feldspar and quartz particles, as well as on the porous ash particle.	35
5.2	SEM stitching showing a big section of the K-feldspar bed material sample obtained after WS combustion. Several particle types are marked throughout the image: ■ K-feldspar, ▲ quartz, + ash melt. A considerable share of quartz particles are involved in agglomeration formation with the ash melt. .	36

5.3	SEM stitching showing a big section of the K-feldspar bed material sample obtained after CM combustion. Several particle types are marked throughout the image: ■ K-feldspar, ▲ quartz, ★ porous ash particle, + ash melt. The ash melt and porous ash particles show the reason why the experiment had to be stopped prematurely.	36
5.4	SEM stitching showing a big section of the K-feldspar bed material sample obtained after S7C3 combustion. Several particle types are marked throughout the image: ■ K-feldspar, ▲ quartz, ★ porous ash particle, + ash melt. Big ash melt particles formed, causing the observed defluidisation.	37
5.5	SEM stitching showing a big section of the K-feldspar bed material sample obtained after B9C1 combustion. Several particle types are marked throughout the image: ■ K-feldspar, ▲ quartz, ★ porous ash particle. Bumps formed on the surface of K-feldspar particles giving the particles an irregular surface.	37
5.6	SEM stitching showing a big section of the K-feldspar bed material sample obtained after B7C3 combustion. Several particle types are marked throughout the image: ■ K-feldspar, ▲ quartz, ★ porous ash particle, + ash melt.	38
5.7	SEM and EDS analysis of K-feldspar particles for the experiments with BA, B7C3, and CM in combustion and gasification atmospheres.	41
5.8	Line scans measured on K-feldspar for samples from combustion and gasification of BA, B7C3 and CM. The given distance starts at the outside of the particle and points towards the core. The sample for the gasification of BA originates from a K-feldspar impurity from an olivine bed from Senden where gasification is performed with BA-rich logging residues.	42
5.9	SEM images of bed material samples from B7C3 combustion after a) 0 h, b) 2 h, c) 4 h, d) 8 h, e) 16 h, f) 24 h, g) 32 h, h) 40 h	44
5.10	SEM images of bed material samples from BA combustion after a) 4 h, b) 8 h, c) 16 h, d) 24 h, e) 32 h, f) 36.5 h	45
5.11	SEM images of bed material samples from CM combustion after a) 4 h, b) 8 h, c) 11 h, and S7C3 combustion after d) 4 h, e) 8 h, f) 9.5 h	46
5.12	Growing layer thickness over time for BA, B9C1, B7C3 and CM. The dashed line gives the inner layer thickness (interaction layer) and the solid line indicates the thickness of both inner and outer layer combined. The standard deviation given for the line inner+outer layer shows the standard deviation for the outer layer only.	47

5.13	Layer composition over time during BA combustion. No outer layer could be detected during BA combustion.	49
5.14	Layer composition over time during B9C1 combustion. Both an inner (left) and an outer (right) layer were detected for B9C1 combustion.	49
5.15	Layer composition over time during B7C3 combustion. Both an inner (left) and an outer (right) layer were detected for B7C3 combustion.	50
5.16	Layer composition over time during CM combustion. An outer layer was only detected for the final sample.	50
5.17	BET surface area measured for bed material samples from BA, CM, and B7C3 combustion.	51
5.18	SEM images of the particle surface a) of fresh K-feldspar, b) after 8 h of interaction with BA, c) after 32 h of interaction with BA, d) after 8 h of interaction with CM, e) after 8 h of interaction with B7C3 and f) after 40 h of interaction with B7C3.	52
5.19	Close-up of a layer formed during B7C3 combustion. A SEM image as well as EDS area mappings for several elements are depicted. The detected layers are an outer outer layer (▼), an inner outer layer (■) and an inner layer(▲).	54
5.20	Close-up of a layer formed during B7C3 combustion. A SEM image as well as EDS area mappings for several elements are depicted. Precipitated crystals (★) can be distinguished in the fuel ash layers. The detected layers are an inner outer layer (■) and an inner layer(▲).	54
5.21	Elemental composition of several ash layer sections as well as the precipitated crystals detected in Figure 5.20 as collected from manually selected areas in EDS area mappings. The labelling of inner and outer layer was done according to the assumed layer formation mechanism underlying the formation of the relevant layer.	55
5.22	Layer formation mechanism on K-feldspar with woody biomass as proposed by Faust et al. [56] (top) and adapted for layer formation with P-rich fuels (bottom). (a) Initial accumulation of fuel ash elements. The major element reacting in this phase is Ca. This phase is comparable for P-lean and P-rich fuels. (b) Formation of continuous layers. During this phase mainly an inner layer forms for P-lean fuels while a thin inner layer and a thicker outer layer forms for P-rich fuels. Elements apart from Ca now also participate in layer formation. (c) Onset of crack layer formation and formation of a continuous outer layer for P-lean fuels. No crack formation has yet been observed for P-rich fuels due to shorter operational times.	56

5.23	Average elemental composition (error bars show standard deviation) of major ash-forming elements for the bulk ash fractions and typical particles on a C- and O-free basis. Top: CM, Middle: B7C3, Bottom: S7C3.	58
5.24	EDS mappings from quartz particles detected from the combustion experiments with K-feldspar (all but the last row) as well as the DFB steam gasification of BSC with pure K-feldspar.	60
5.25	EDS mappings of limestone particles detected in bed material samples from DFB steam gasification.	61
5.26	Summary of the performed gasification experiments. The experiments are sorted by their deviation from the WGS equilibrium (see upper picture). The lower image depicts the tar content in the product gas as well as the tar dew point.	63
5.27	Comparison between operation with SW and a BSC with K-feldspar as bed material.	65
5.28	Deviation from the WGS equilibrium determined in isolated WGS experiments.	66
5.29	Catalytic activity determined for layered K-feldspar particles shown by the deviation from WGS equilibrium	67
5.30	Correlation between BET surface area and catalytic activity, quantified by the H ₂ yield regarding the WGS equilibrium	68

List of Tables

4.1	Summary of properties of the fuels used throughout this thesis.	22
4.2	Sauter diameter, density as well as hardness of the used bed materials. . . .	23
4.3	DFB steam gasification experiments performed throughout the course of this thesis	26
4.4	Set gas flows as well as used analysis equipment used during the experimental campaigns.	28
5.1	Experimental results of the combustion experiments. An X in the hour columns indicates an existing bed sample, - indicates that no sample could be taken due to stopped operation beforehand.	34
5.2	Experimental results of the gasification experiments. The experiment with CM and activated olivine did not achieve stable operation. Already published data was adapted from Mauerhofer et al. [65].	39
5.3	Detected phases in different ash and bed material fractions after CM and B7C3 combustion.	59



Die approbierte gedruckte Originalversion dieser Dissertation ist an der TU Wien Bibliothek verfügbar.
The approved original version of this doctoral thesis is available in print at TU Wien Bibliothek.

Nomenclature

Abbreviations and Acronyms

- B7C3** 0.7 kg kg⁻¹ bark and 0.3 kg kg⁻¹ chicken manure on a dry basis
- B9C1** 0.9 kg kg⁻¹ bark and 0.1 kg kg⁻¹ chicken manure on a dry basis
- BA** bark
- BET** Brunauer-Emmet-Teller
- BFB** bubbling fluidized bed
- BSC** 0.595 kg kg⁻¹ bark, 0.15 kg kg⁻¹ straw and 0.255 kg kg⁻¹ chicken manure on a dry basis
- CM** chicken manure
- CR** combustion reactor
- db** dry mass basis
- DFB** dual fluidised bed
- EDS** Energy-dispersive X-ray spectroscopy
- GR** gasification reactor
- K-FS** K-feldspar
- MFC** mass flow controller
- n.d.** not determined
- n.o.** not observed
- S7C3** 0.7 kg kg⁻¹ straw and 0.3 kg kg⁻¹ chicken manure on a dry basis
- S9C1** 0.9 kg kg⁻¹ straw and 0.1 kg kg⁻¹ chicken manure on a dry basis
- SEM** scanning electron microscopy
- SER** sorption enhanced reforming

- SW** softwood
T temperature
WGS Water-Gas-Shift
WS wheat straw
XRD X-ray diffraction
XRF X-ray fluorescence

Symbols

Symbol	Description	Unit
$K_p(T)$	Equilibrium constant of a specific chemical reaction (dependent on T)	-
p_i	Partial pressure of component i	bar
$p\delta_{eq,WGS}$	Logarithmic equilibrium deviation of the WGS reaction	-
T	temperature	K
λ	air excess number	-
ν_i	Stoichiometric factor of component i	-
τ	Kendall rank correlation coefficient	-

Bibliography

- [1] Will Steffen, Katherine Richardson, Johan Rockström, Sarah E. Cornell, Ingo Fetzer, Elena M. Bennett, Reinette Biggs, Stephen R. Carpenter, Wim de Vries, Cynthia A. de Wit, Carl Folke, Dieter Gerten, Jens Heinke, Georgina M. Mace, Linn M. Persson, Veerabhadran Ramanathan, Belinda Reyers, and Sverker Sörlin. “Planetary boundaries: Guiding human development on a changing planet”. In: *Science* 347.6223 (Feb. 13, 2015), p. 1259855. ISSN: 0036-8075, 1095-9203. DOI: 10.1126/science.1259855. URL: <http://science.sciencemag.org/content/347/6223/1259855> (visited on 08/14/2018).
- [2] United Nations - Framework Convention on Climate Change. “Adoption of the Paris Agreement”. In: *Conference of the Parties, 21st session*. Vol. 21932. 2015. URL: <https://unfccc.int/process-and-meetings/the-paris-agreement/the-paris-agreement>.
- [3] *Paris Agreement - Status of Ratification* | UNFCCC. United Nations Climate Change. URL: <https://unfccc.int/process/the-paris-agreement/status-of-ratification> (visited on 11/09/2020).
- [4] Long Cao and Ken Caldeira. “Atmospheric CO₂ stabilization and ocean acidification”. In: *Geophysical Research Letters* 35.19 (2008). ISSN: 1944-8007. DOI: 10.1029/2008GL035072. URL: <https://agupubs.onlinelibrary.wiley.com/doi/abs/10.1029/2008GL035072> (visited on 07/29/2020).
- [5] *Global Monthly Mean CO₂*. Global Monitoring Laboratory - Earth System Research Laboratories. Apr. 2020. URL: <https://www.esrl.noaa.gov/gmd/ccgg/trends/global.html> (visited on 07/29/2020).
- [6] Hannah Ritchie and Max Roser. *CO₂ and Greenhouse Gas Emissions*. Our World in Data. 2017. URL: <https://ourworldindata.org/co2-and-other-greenhouse-gas-emissions> (visited on 07/23/2020).

- [7] *Statistics | World - Total Primary Energy Supply (TPES) by source (chart)*. IEA. URL: <https://www.iea.org/data-and-statistics> (visited on 12/10/2019).
- [8] Martin Geissdoerfer, Paulo Savaget, Nancy M. P. Bocken, and Erik Jan Hultink. “The Circular Economy – A new sustainability paradigm?” In: *Journal of Cleaner Production* 143 (Feb. 1, 2017), pp. 757–768. ISSN: 0959-6526. DOI: 10.1016/j.jclepro.2016.12.048. URL: <http://www.sciencedirect.com/science/article/pii/S0959652616321023> (visited on 06/24/2020).
- [9] *Communication from the Commission to the European Parliament, the European Council, the Council, the European Economic and Social Committee and the Committee of the Regions - The European Green Deal*. Dec. 11, 2019. URL: <https://eur-lex.europa.eu/legal-content/EN/TXT/?qid=1588580774040&uri=CELEX:52019DC0640> (visited on 07/27/2020).
- [10] British Geological Survey, Bureau de Recherches Géologiques et Minières, Deloitte Sustainability, European Commission, Industry Directorate-General for Internal Market Entrepreneurship and SMEs, and Toegepast natuurwetenschappelijk onderzoek. *Study on the review of the list of critical raw materials: critical raw materials fact-sheets*. OCLC: 1111145995. 2017. ISBN: 978-92-79-72119-9. URL: <http://dx.publications.europa.eu/10.2873/398823> (visited on 05/20/2020).
- [11] Tina-Simone S. Neset and Dana Cordell. “Global phosphorus scarcity: identifying synergies for a sustainable future”. In: *Journal of the Science of Food and Agriculture* 92.1 (2012). _eprint: <https://onlinelibrary.wiley.com/doi/pdf/10.1002/jsfa.4650>, pp. 2–6. ISSN: 1097-0010. DOI: 10.1002/jsfa.4650. URL: <https://onlinelibrary.wiley.com/doi/abs/10.1002/jsfa.4650> (visited on 05/20/2020).
- [12] British Geological Survey, Bureau de Recherches Géologiques et Minières, Deloitte Sustainability, European Commission, Industry Directorate-General for Internal Market Entrepreneurship and SMEs, and Toegepast natuurwetenschappelijk onderzoek. *Study on the review of the list of critical raw materials: final report*. OCLC: 1111119694. 2017. ISBN: 978-92-79-47937-3. URL: <http://dx.publications.europa.eu/10.2873/876644> (visited on 05/20/2020).
- [13] Jurate Kumpiene, Evelina Brännvall, Martin Wolters, Nils Skoglund, Stasys Čirba, and Vladislovas Česlovas Aksamitauskas. “Phosphorus and cadmium availability in soil fertilized with biosolids and ashes”. In: *Chemosphere* 151 (May 1, 2016), pp. 124–

132. ISSN: 0045-6535. DOI: 10.1016/j.chemosphere.2016.02.069. URL: <http://www.sciencedirect.com/science/article/pii/S0045653516302284> (visited on 05/20/2020).
- [14] Katja Schiemenz and Bettina Eichler-Löbermann. “Biomass ashes and their phosphorus fertilizing effect on different crops”. In: *Nutrient Cycling in Agroecosystems* 87.3 (July 1, 2010), pp. 471–482. ISSN: 1573-0867. DOI: 10.1007/s10705-010-9353-9. URL: <https://doi.org/10.1007/s10705-010-9353-9> (visited on 05/28/2020).
- [15] Eton E. Codling, Rufus L. Chaney, and John Sherwell. “Poultry Litter Ash as a Potential Phosphorus Source for Agricultural Crops”. In: *Journal of Environmental Quality* 31.3 (2002), pp. 954–961. ISSN: 1537-2537. DOI: 10.2134/jeq2002.9540. URL: <https://access.onlinelibrary.wiley.com/doi/abs/10.2134/jeq2002.9540> (visited on 05/28/2020).
- [16] Martin Kaltschmitt, Hans Hartmann, and Hermann Hofbauer, eds. *Energie aus Biomasse: Grundlagen, Techniken und Verfahren*. 3., aktualisierte und erweiterte Auflage. OCLC: 948486478. Berlin Heidelberg: Springer Vieweg, 2016. 1867 pp. ISBN: 978-3-662-47438-9.
- [17] Efstathios Michaelides. *Alternative energy sources*. Green energy and technology. OCLC: ocn766342265. Heidelberg ; New York: Springer, 2012. 459 pp. ISBN: 978-3-642-20950-5 978-3-642-20951-2.
- [18] Prabir Basu. *Biomass gasification and pyrolysis: practical design and theory*. OCLC: ocn502035604. Burlington, MA: Academic Press, 2010. 365 pp. ISBN: 978-0-12-374988-8.
- [19] Reinhard Rauch, Alain Kiennemann, and Anca Sauciuc. “Chapter 12 - Fischer-Tropsch Synthesis to Biofuels (BtL Process)”. In: *The Role of Catalysis for the Sustainable Production of Bio-fuels and Bio-chemicals*. Ed. by Kostas S. Triantafyllidis, Angelos A. Lappas, and Michael Stöcker. Amsterdam: Elsevier, Jan. 1, 2013, pp. 397–443. ISBN: 978-0-444-56330-9. DOI: 10.1016/B978-0-444-56330-9.00012-7. URL: <http://www.sciencedirect.com/science/article/pii/B9780444563309000127> (visited on 03/18/2020).
- [20] Michiel J. A. Tijmensen, André P. C. Faaij, Carlo N. Hamelinck, and Martijn R. M. van Hardeveld. “Exploration of the possibilities for production of Fischer Tropsch liquids and power via biomass gasification”. In: *Biomass and Bioenergy* 23.2 (Aug. 1, 2002), pp. 129–152. ISSN: 0961-9534. DOI: 10.1016/S0961-9534(02)00037

- 5. URL: <http://www.sciencedirect.com/science/article/pii/S0961953402000375> (visited on 03/18/2020).
- [21] Michael Kraussler, Florian Pontzen, Matthias Müller-Hagedorn, Leopold Nenning, Markus Luisser, and Hermann Hofbauer. “Techno-economic assessment of biomass-based natural gas substitutes against the background of the EU 2018 renewable energy directive”. In: *Biomass Conversion and Biorefinery* 8.4 (Dec. 1, 2018), pp. 935–944. ISSN: 2190-6823. DOI: 10.1007/s13399-018-0333-7. URL: <https://doi.org/10.1007/s13399-018-0333-7> (visited on 05/14/2019).
- [22] Christiaan M. Van der Meijden, Hubert J. Veringa, and Luc P. L. M. Rabou. “The production of synthetic natural gas (SNG): A comparison of three wood gasification systems for energy balance and overall efficiency”. In: *Biomass and Bioenergy* 34.3 (Mar. 1, 2010), pp. 302–311. ISSN: 0961-9534. DOI: 10.1016/j.biombioe.2009.11.001. URL: <http://www.sciencedirect.com/science/article/pii/S096195340900230X> (visited on 01/25/2018).
- [23] M. Binder, R. Rauch, M. Koch, M. Summers, C. Aichernig, and H. Hofbauer. “Influence of Sulfur Components on the Catalytic Mixed Alcohol Synthesis Based on Wood Gas Derived from Biomass Steam Gasification”. In: *ETA-Florence Renewable Energies, 2017*. DOI: 10.5071/25theubce2017-3bv.3.14. URL: <http://www.etaflorence.it/proceedings?detail=13962> (visited on 08/24/2017).
- [24] Michael Kraussler, Matthias Binder, and Hermann Hofbauer. “2250-h long term operation of a water gas shift pilot plant processing tar-rich product gas from an industrial scale dual fluidized bed biomass steam gasification plant”. In: *International Journal of Hydrogen Energy* 41.15 (Apr. 2016), pp. 6247–6258. ISSN: 03603199. DOI: 10.1016/j.ijhydene.2016.02.137. URL: <http://linkinghub.elsevier.com/retrieve/pii/S0360319915308910> (visited on 02/21/2017).
- [25] Prabir Basu. *Combustion and Gasification in Fluidized Beds*. CRC Press, Feb. 17, 2006. 492 pp. ISBN: 978-1-4200-0515-8.
- [26] Stefan Kern, Christoph Pfeifer, and Hermann Hofbauer. “Reactivity tests of the water–gas shift reaction on fresh and used fluidized bed materials from industrial DFB biomass gasifiers”. In: *Biomass and Bioenergy* 55 (Aug. 1, 2013), pp. 227–233. ISSN: 0961-9534. DOI: 10.1016/j.biombioe.2013.02.001. URL: <http://www.sciencedirect.com/science/article/pii/S0961953413000500> (visited on 03/18/2020).

- [27] Kristina Göransson, Ulf Söderlind, Jie He, and Wennan Zhang. “Review of syngas production via biomass DFBGs”. In: *Renewable and Sustainable Energy Reviews* 15.1 (Jan. 1, 2011), pp. 482–492. ISSN: 1364-0321. DOI: 10.1016/j.rser.2010.09.032. URL: <http://www.sciencedirect.com/science/article/pii/S1364032110003199> (visited on 01/23/2019).
- [28] Stefan Kern, Christoph Pfeifer, and Hermann Hofbauer. “Gasification of wood in a dual fluidized bed gasifier: Influence of fuel feeding on process performance”. In: *Chemical Engineering Science* 90 (Mar. 7, 2013), pp. 284–298. ISSN: 0009-2509. DOI: 10.1016/j.ces.2012.12.044. URL: <http://www.sciencedirect.com/science/article/pii/S000925091200735X> (visited on 03/18/2020).
- [29] Florian Benedikt, Matthias Kuba, Johannes Christian Schmid, Stefan Müller, and Hermann Hofbauer. “Assessment of correlations between tar and product gas composition in dual fluidized bed steam gasification for online tar prediction”. In: *Applied Energy* 238 (Mar. 15, 2019), pp. 1138–1149. ISSN: 0306-2619. DOI: 10.1016/j.apenergy.2019.01.181. URL: <http://www.sciencedirect.com/science/article/pii/S0306261919301795> (visited on 03/29/2019).
- [30] Johannes Christian Schmid, Ute Wolfesberger, Stefan Koppatz, Christoph Pfeifer, and Hermann Hofbauer. “Variation of feedstock in a dual fluidized bed steam gasifier—influence on product gas, tar content, and composition”. In: *Environmental Progress & Sustainable Energy* 31.2 (July 1, 2012), pp. 205–215. ISSN: 1944-7450. DOI: 10.1002/ep.11607. URL: <https://onlinelibrary.wiley.com/doi/abs/10.1002/ep.11607> (visited on 08/14/2018).
- [31] Stephan Kraft, Matthias Kuba, and Hermann Hofbauer. “The behavior of biomass and char particles in a dual fluidized bed gasification system”. In: *Powder Technology* 338 (Oct. 1, 2018), pp. 887–897. ISSN: 0032-5910. DOI: 10.1016/j.powtec.2018.07.059. URL: <http://www.sciencedirect.com/science/article/pii/S0032591018305588> (visited on 03/29/2019).
- [32] Matthias Kuba, Fabian Havlik, Friedrich Kirnbauer, and Hermann Hofbauer. “Influence of bed material coatings on the water-gas-shift reaction and steam reforming of toluene as tar model compound of biomass gasification”. In: *Biomass and Bioenergy*. Biomass & Bioenergy special issue of the 23rd European Biomass Conference and Exhibition held in Vienna, June 2015 89 (Supplement C June 1, 2016), pp. 40–49. ISSN: 0961-9534. DOI: 10.1016/j.biombioe.2015.11.029. URL: <http://www>.

sciencedirect.com/science/article/pii/S0961953415301690
(visited on 01/08/2018).

- [33] H Hofbauer, R Rauch, G Loeffler, S Kaiser, E Fercher, and H Tremmel. “Six Years Experience with the FICFB-Gasification Process”. In: *12. European Conference on Biomass for Energy, Industry and Climate Protection*. Amsterdam, 2002. ISBN: 88-900442-5-X.
- [34] Matthias Kuba, Hanbing He, Friedrich Kirnbauer, Nils Skoglund, Dan Boström, Marcus Öhman, and Hermann Hofbauer. “Mechanism of Layer Formation on Olivine Bed Particles in Industrial-Scale Dual Fluid Bed Gasification of Wood”. In: *Energy & Fuels* 30.9 (Sept. 15, 2016), pp. 7410–7418. ISSN: 0887-0624. DOI: 10.1021/acs.energyfuels.6b01522. URL: <http://dx.doi.org/10.1021/acs.energyfuels.6b01522> (visited on 01/16/2018).
- [35] Reinhard Rauch, H Hofbauer, K Bosch, I Siefert, C Aichernig, H Tremmel, K Voigtlaender, R Koch, and R Lehner. “Steam Gasification of Biomass at CHP Plant Güssing – Status of the Demonstartion Plant”. In: (May 2004), pp. 1687–1690.
- [36] Matthias Kuba and Hermann Hofbauer. “Experimental parametric study on product gas and tar composition in dual fluid bed gasification of woody biomass”. In: *Biomass and Bioenergy* 115 (Aug. 1, 2018), pp. 35–44. ISSN: 0961-9534. DOI: 10.1016/j.biombioe.2018.04.007. URL: <http://www.sciencedirect.com/science/article/pii/S0961953418300965> (visited on 03/29/2019).
- [37] Task 33 / Thermal Gasification of Biomass. *Task 33 Database*. Task 33 Database - Gasification of Biomass and Waste. July 7, 2020. URL: http://task33.ieabioenergy.com/menus/show_database.
- [38] Matthias Kuba, Hanbing He, Friedrich Kirnbauer, Nils Skoglund, Dan Boström, Marcus Öhman, and Hermann Hofbauer. “Thermal Stability of Bed Particle Layers on Naturally Occurring Minerals from Dual Fluid Bed Gasification of Woody Biomass”. In: *Energy & Fuels* 30.10 (Oct. 20, 2016), pp. 8277–8285. ISSN: 0887-0624, 1520-5029. DOI: 10.1021/acs.energyfuels.6b01523. URL: <http://pubs.acs.org/doi/10.1021/acs.energyfuels.6b01523> (visited on 07/31/2018).
- [39] Hannes Gruber, Peter Groß, Reinhard Rauch, Alexander Reichhold, Richard Zweiler, Christian Aichernig, Stefan Müller, Nabeel Ataimisch, and Hermann Hofbauer. “Fischer-Tropsch products from biomass-derived syngas and renewable hydrogen”. In: *Biomass Conversion and Biorefinery* (June 22, 2019). ISSN:

- 2190-6823. DOI: 10 . 1007 / s13399 - 019 - 00459 - 5. URL: <https://doi.org/10.1007/s13399-019-00459-5> (visited on 11/29/2019).
- [40] Barbara Rehling, Hermann Hofbauer, Reinhard Rauch, and Christian Aichernig. “BioSNG - process simulation and comparison with first results from a 1 MW demonstration plant”. In: *Biomass Conversion and Biorefinery* 1.2 (July 1, 2011), pp. 111–119. ISSN: 2190-6815, 2190-6823. DOI: 10 . 1007 / s13399 - 011 - 0013 - 3. URL: <http://link.springer.com/article/10.1007/s13399-011-0013-3> (visited on 02/17/2017).
- [41] H. J. M. Visser, S. C. van Lith, and J. H. A. Kiel. “Biomass Ash-Bed Material Interactions Leading to Agglomeration in FBC”. In: *Journal of Energy Resources Technology* 130.1 (2008), p. 011801. ISSN: 01950738. DOI: 10 . 1115 / 1 . 2824247. URL: <http://EnergyResources.asmedigitalcollection.asme.org/article.aspx?articleid=1414770> (visited on 08/16/2018).
- [42] Jonathan D. Morris, Syed Sheraz Daood, Stephen Chilton, and William Nimmo. “Mechanisms and mitigation of agglomeration during fluidized bed combustion of biomass: A review”. In: *Fuel* 230 (Oct. 15, 2018), pp. 452–473. ISSN: 0016-2361. DOI: 10 . 1016 / j . fuel . 2018 . 04 . 098. URL: <http://www.sciencedirect.com/science/article/pii/S0016236118307300> (visited on 07/06/2020).
- [43] B. -M. Steenari and O. Lindqvist. “High-temperature reactions of straw ash and the anti-sintering additives kaolin and dolomite”. In: *Biomass and Bioenergy* 14.1 (Mar. 10, 1998), pp. 67–76. ISSN: 0961-9534. DOI: 10 . 1016 / S0961 - 9534 (97) 00035 - 4. URL: <http://www.sciencedirect.com/science/article/pii/S0961953497000354> (visited on 07/29/2020).
- [44] K. O. Davidsson, L. -E. Åmand, B. -M. Steenari, A. -L. Elled, D. Eskilsson, and B. Leckner. “Countermeasures against alkali-related problems during combustion of biomass in a circulating fluidized bed boiler”. In: *Chemical Engineering Science* 63.21 (Nov. 1, 2008), pp. 5314–5329. ISSN: 0009-2509. DOI: 10 . 1016 / j . ces . 2008 . 07 . 012. URL: <http://www.sciencedirect.com/science/article/pii/S000925090800362X> (visited on 06/19/2017).
- [45] Marcus Öhman and Anders Nordin. “The Role of Kaolin in Prevention of Bed Agglomeration during Fluidized Bed Combustion of Biomass Fuels”. In: *Energy & Fuels* 14.3 (May 2000), pp. 618–624. ISSN: 0887-0624. DOI: 10 . 1021 / ef990198c. URL: <http://dx.doi.org/10.1021/ef990198c> (visited on 06/19/2017).

- [46] Hari B Vuthaluru and Dong-ke Zhang. “Effect of Ca- and Mg-bearing minerals on particle agglomeration defluidisation during fluidised-bed combustion of a South Australian lignite”. In: *Fuel Processing Technology* 69.1 (Jan. 1, 2001), pp. 13–27. ISSN: 0378-3820. DOI: 10.1016/S0378-3820(00)00129-6. URL: <http://www.sciencedirect.com/science/article/pii/S0378382000001296> (visited on 07/24/2018).
- [47] H. B Vuthaluru and D. K Zhang. “Remediation of ash problems in fluidised-bed combustors”. In: *Fuel* 80.4 (Mar. 1, 2001), pp. 583–598. ISSN: 0016-2361. DOI: 10.1016/S0016-2361(00)00116-2. URL: <http://www.sciencedirect.com/science/article/pii/S0016236100001162> (visited on 07/24/2018).
- [48] Chunguang Zhou, Christer Rosén, and Klas Engvall. “Biomass oxygen/steam gasification in a pressurized bubbling fluidized bed: Agglomeration behavior”. In: *Applied Energy* 172 (June 15, 2016), pp. 230–250. ISSN: 0306-2619. DOI: 10.1016/j.apenergy.2016.03.106. URL: <http://www.sciencedirect.com/science/article/pii/S0306261916304408> (visited on 07/23/2018).
- [49] Gregor Markl and Michael Marks. *Minerale und Gesteine: Mineralogie - Petrologie - Geochemie*. 3. Aufl. OCLC: 894735684. Berlin: Springer Spektrum, 2015. 610 pp. ISBN: 978-3-662-44627-0 978-3-662-44628-7.
- [50] Marcus Öhman, Linda Pommer, and Anders Nordin. “Bed Agglomeration Characteristics and Mechanisms during Gasification and Combustion of Biomass Fuels”. In: *Energy & Fuels* 19.4 (July 1, 2005), pp. 1742–1748. ISSN: 0887-0624. DOI: 10.1021/ef040093w. URL: <https://doi.org/10.1021/ef040093w> (visited on 07/19/2018).
- [51] Elisabet Brus, Marcus Öhman, and Anders Nordin. “Mechanisms of Bed Agglomeration during Fluidized-Bed Combustion of Biomass Fuels”. In: *Energy & Fuels* 19.3 (May 2005), pp. 825–832. ISSN: 0887-0624, 1520-5029. DOI: 10.1021/ef0400868. URL: <https://pubs.acs.org/doi/10.1021/ef0400868> (visited on 03/27/2019).
- [52] Alejandro Grimm, Nils Skoglund, Dan Boström, and Marcus Öhman. “Bed Agglomeration Characteristics in Fluidized Quartz Bed Combustion of Phosphorus-Rich Biomass Fuels”. In: *Energy & Fuels* 25.3 (Mar. 17, 2011), pp. 937–947. ISSN: 0887-0624. DOI: 10.1021/ef101451e. URL: <https://doi.org/10.1021/ef101451e> (visited on 07/19/2018).

- [53] Dan Boström, Nils Skoglund, Alejandro Grimm, Christoffer Boman, Marcus Öhman, Markus Broström, and Rainer Backman. “Ash Transformation Chemistry during Combustion of Biomass”. In: *Energy & Fuels* 26.1 (Jan. 19, 2012), pp. 85–93. ISSN: 0887-0624. DOI: 10.1021/ef201205b. URL: <https://doi.org/10.1021/ef201205b> (visited on 07/20/2018).
- [54] Hanbing He, Nils Skoglund, and Marcus Öhman. “Time-Dependent Layer Formation on K-Feldspar Bed Particles during Fluidized Bed Combustion of Woody Fuels”. In: *Energy & Fuels* 31.11 (Nov. 16, 2017), pp. 12848–12856. ISSN: 0887-0624. DOI: 10.1021/acs.energyfuels.7b02386. URL: <https://doi.org/10.1021/acs.energyfuels.7b02386> (visited on 07/20/2018).
- [55] Nicolas Berguerand and Teresa Berdugo Vilches. “Alkali-Feldspar as a Catalyst for Biomass Gasification in a 2-MW Indirect Gasifier”. In: *Energy & Fuels* 31.2 (Feb. 16, 2017), pp. 1583–1592. ISSN: 0887-0624. DOI: 10.1021/acs.energyfuels.6b02312. URL: <https://doi.org/10.1021/acs.energyfuels.6b02312> (visited on 03/02/2018).
- [56] Robin Faust, Thomas Karl Hannl, Teresa Berdugo Vilches, Matthias Kuba, Marcus Öhman, Martin Seemann, and Pavleta Knutsson. “Layer Formation on Feldspar Bed Particles during Indirect Gasification of Wood. 1. K-Feldspar”. In: *Energy & Fuels* 33.8 (Aug. 15, 2019). Publisher: American Chemical Society, pp. 7321–7332. ISSN: 0887-0624. DOI: 10.1021/acs.energyfuels.9b01291. URL: <https://doi.org/10.1021/acs.energyfuels.9b01291> (visited on 03/24/2020).
- [57] Thomas Karl Hannl, Robin Faust, Matthias Kuba, Pavleta Knutsson, Teresa Berdugo Vilches, Martin Seemann, and Marcus Öhman. “Layer Formation on Feldspar Bed Particles during Indirect Gasification of Wood. 2. Na-Feldspar”. In: *Energy & Fuels* 33.8 (Aug. 15, 2019). Publisher: American Chemical Society, pp. 7333–7346. ISSN: 0887-0624. DOI: 10.1021/acs.energyfuels.9b01292. URL: <https://doi.org/10.1021/acs.energyfuels.9b01292> (visited on 03/24/2020).
- [58] Sigrid De Geyter, Marcus Öhman, Dan Boström, Morgan Eriksson, and Anders Nordin. “Effects of Non-Quartz Minerals in Natural Bed Sand on Agglomeration Characteristics during Fluidized Bed Combustion of Biomass Fuels”. In: *Energy & Fuels* 21.5 (Sept. 1, 2007), pp. 2663–2668. ISSN: 0887-0624. DOI: 10.1021/ef070162h. URL: <http://dx.doi.org/10.1021/ef070162h> (visited on 02/24/2017).

- [59] Friedrich Kirnbauer and Hermann Hofbauer. “Investigations on Bed Material Changes in a Dual Fluidized Bed Steam Gasification Plant in Güssing, Austria”. In: *Energy Fuels* 25.8 (July 11, 2011), pp. 3793–3798. DOI: 10.1021/ef200746c. URL: <https://pubs.acs.org/doi/abs/10.1021/ef200746c> (visited on 02/08/2018).
- [60] Alejandro Grimm, Marcus Öhman, Therése Lindberg, Andreas Fredriksson, and Dan Boström. “Bed Agglomeration Characteristics in Fluidized-Bed Combustion of Biomass Fuels Using Olivine as Bed Material”. In: *Energy & Fuels* 26.7 (July 19, 2012), pp. 4550–4559. ISSN: 0887-0624. DOI: 10.1021/ef300569n. URL: <http://dx.doi.org/10.1021/ef300569n> (visited on 02/24/2017).
- [61] Robin Faust, Jelena Maric, Teresa Berdugo Vilches, Britt-Marie Steenari, Martin Seemann, and Pavleta Knutsson. “Role of K and Ca for catalytic activation of bed material during biomass gasification”. In: *23rd International Conference on FBC*. International Conference on Fluidized Bed Conversion. Seoul, Korea, May 2018, pp. 1144–1154.
- [62] Matthias Kuba, Friedrich Kirnbauer, and Hermann Hofbauer. “Influence of coated olivine on the conversion of intermediate products from decomposition of biomass tars during gasification”. In: *Biomass Conversion and Biorefinery* 7.1 (Mar. 1, 2017), pp. 11–21. ISSN: 2190-6815, 2190-6823. DOI: 10.1007/s13399-016-0204-z. URL: <https://link.springer.com/article/10.1007/s13399-016-0204-z> (visited on 03/02/2018).
- [63] Nicolas Berguerand, Jelena Marinkovic, Teresa Berdugo Vilches, and Henrik Thunman. “Use of alkali-feldspar as bed material for upgrading a biomass-derived producer gas from a gasifier”. In: *Chemical Engineering Journal* 295 (July 1, 2016), pp. 80–91. ISSN: 1385-8947. DOI: 10.1016/j.cej.2016.02.060. URL: <http://www.sciencedirect.com/science/article/pii/S1385894716301619> (visited on 07/23/2018).
- [64] M. Kuba, F. Kirnbauer, and H. Hofbauer. “Influence of Calcium-Rich layers on the Catalytic Activity of Bed Materials in CO₂-Gasification of Biomass”. In: *European Biomass Conference and Exhibition Proceedings 24th EUBCE - Amsterdam 2016* (2016), pp. 823–827. ISSN: 2282-5819. DOI: 10.5071/24thEUBCE2016-2CV.3.8. URL: <http://www.etaflorence.it/proceedings/?detail=12633> (visited on 09/30/2019).
- [65] Anna Magdalena Mauerhofer, Florian Benedikt, Johannes Christian Schmid, Josef Fuchs, Stefan Müller, and Hermann Hofbauer. “Influence of different bed material

- mixtures on dual fluidized bed steam gasification”. In: *Energy* 157 (Aug. 15, 2018), pp. 957–968. ISSN: 0360-5442. DOI: 10.1016/j.energy.2018.05.158. URL: <http://www.sciencedirect.com/science/article/pii/S0360544218310028> (visited on 07/03/2018).
- [66] Florian Benedikt, Josef Fuchs, Johannes Christian Schmid, Stefan Müller, and Hermann Hofbauer. “Advanced dual fluidized bed steam gasification of wood and lignite with calcite as bed material”. In: *Korean Journal of Chemical Engineering* 34.9 (Sept. 1, 2017), pp. 2548–2558. ISSN: 1975-7220. DOI: 10.1007/s11814-017-0141-y. URL: <https://doi.org/10.1007/s11814-017-0141-y> (visited on 05/14/2019).
- [67] Josef Fuchs, Johannes C. Schmid, Stefan Müller, and Hermann Hofbauer. “Dual fluidized bed gasification of biomass with selective carbon dioxide removal and limestone as bed material: A review”. In: *Renewable and Sustainable Energy Reviews* 107 (June 1, 2019), pp. 212–231. ISSN: 1364-0321. DOI: 10.1016/j.rser.2019.03.013. URL: <http://www.sciencedirect.com/science/article/pii/S1364032119301467> (visited on 07/02/2019).
- [68] Jesús Delgado, María P. Aznar, and José Corella. “Biomass Gasification with Steam in Fluidized Bed: Effectiveness of CaO, MgO, and CaO-MgO for Hot Raw Gas Cleaning”. In: *Industrial & Engineering Chemistry Research* 36.5 (May 1997), pp. 1535–1543. ISSN: 0888-5885, 1520-5045. DOI: 10.1021/ie960273w. URL: <https://pubs.acs.org/doi/10.1021/ie960273w> (visited on 05/12/2020).
- [69] Maxime Hervy, Roberto Olcese, Mohammed M. Bettahar, Martine Mallet, Aurélien Renard, Libeth Maldonado, Damien Remy, Guillain Mauviel, and Anthony Dufour. “Evolution of dolomite composition and reactivity during biomass gasification”. In: *Applied Catalysis A: General* 572 (Feb. 25, 2019), pp. 97–106. ISSN: 0926-860X. DOI: 10.1016/j.apcata.2018.12.014. URL: <http://www.sciencedirect.com/science/article/pii/S0926860X18306100> (visited on 10/09/2019).
- [70] Teresa Berdugo Vilches, Jelena Marinkovic, Martin Seemann, and Henrik Thunman. “Comparing Active Bed Materials in a Dual Fluidized Bed Biomass Gasifier: Olivine, Bauxite, Quartz-Sand, and Ilmenite”. In: *Energy & Fuels* 30.6 (June 16, 2016), pp. 4848–4857. ISSN: 0887-0624. DOI: 10.1021/acs.energyfuels.6b00327. URL: <https://doi.org/10.1021/acs.energyfuels.6b00327> (visited on 07/16/2018).

- [71] Friedrich Kirnbauer, Veronika Wilk, Hannes Kitzler, Stefan Kern, and Hermann Hofbauer. “The positive effects of bed material coating on tar reduction in a dual fluidized bed gasifier”. In: *Fuel* 95 (May 1, 2012), pp. 553–562. ISSN: 0016-2361. DOI: 10 . 1016/j.fuel.2011.10.066. URL: <http://www.sciencedirect.com/science/article/pii/S0016236111006843> (visited on 06/09/2017).
- [72] Jelena Marinkovic, Henrik Thunman, Pavleta Knutsson, and Martin Seemann. “Characteristics of olivine as a bed material in an indirect biomass gasifier”. In: *Chemical Engineering Journal* 279 (Nov. 1, 2015), pp. 555–566. ISSN: 1385-8947. DOI: 10 . 1016/j.cej.2015.05.061. URL: <http://www.sciencedirect.com/science/article/pii/S1385894715007378> (visited on 08/02/2019).
- [73] Teresa Berdugo Vilches, Jelena Maric, Pavleta Knutsson, Daniel C. Rosenfeld, Henrik Thunman, and Martin Seemann. “Bed material as a catalyst for char gasification: The case of ash-coated olivine activated by K and S addition”. In: *Fuel* 224 (July 15, 2018), pp. 85–93. ISSN: 0016-2361. DOI: 10 . 1016/j.fuel.2018.03.079. URL: <http://www.sciencedirect.com/science/article/pii/S0016236118304873> (visited on 07/08/2019).
- [74] Robin Faust, Mohammad Sattari, Jelena Maric, Martin Seemann, and Pavleta Knutsson. “Microscopic investigation of layer growth during olivine bed material aging during indirect gasification of biomass”. In: *Fuel* 266 (Apr. 15, 2020), p. 117076. ISSN: 0016-2361. DOI: 10 . 1016/j.fuel.2020.117076. URL: <http://www.sciencedirect.com/science/article/pii/S0016236120300715> (visited on 01/29/2020).
- [75] Susanna Nilsson, Alberto Gómez-Barea, Diego Fuentes-Cano, Pedro Haro, and Guadalupe Pinna-Hernández. “Gasification of Olive Tree Pruning in Fluidized Bed: Experiments in a Laboratory-Scale Plant and Scale-up to Industrial Operation”. In: *Energy & Fuels* 31.1 (Jan. 19, 2017), pp. 542–554. ISSN: 0887-0624. DOI: 10 . 1021/acs.energyfuels.6b02039. URL: <https://doi.org/10.1021/acs.energyfuels.6b02039> (visited on 02/20/2020).
- [76] Johan M. Ahlström, Alberto Alamia, Anton Larsson, Claes Breitholtz, Simon Harvey, and Henrik Thunman. “Bark as feedstock for dual fluidized bed gasifiers- Operability, efficiency, and economics”. In: *International Journal of Energy Research* 43.3 (2019). _eprint: <https://onlinelibrary.wiley.com/doi/pdf/10.1002/er.4349>, pp. 1171–1190. ISSN: 1099-114X. DOI: 10 . 1002/er.4349. URL: <https://onlinelibrary.wiley.com/doi/abs/10.1002/er.4349> (visited on 05/11/2020).

- [77] Jean Taillon, Andras Horvath, and Antti Oksman. “Replacement of fossil fuel with biomass in pulp mill lime kilns”. In: *O papel* 79.3 (2018), pp. 85–89.
- [78] Zimeng He, Daniel J. Lane, Woei L. Saw, Philip J. van Eyk, Graham J. Nathan, and Peter J. Ashman. “Ash–Bed Material Interaction during the Combustion and Steam Gasification of Australian Agricultural Residues”. In: *Energy & Fuels* 32.4 (Apr. 19, 2018), pp. 4278–4290. ISSN: 0887-0624. DOI: 10.1021/acs.energyfuels.7b03129. URL: <https://doi.org/10.1021/acs.energyfuels.7b03129> (visited on 07/24/2018).
- [79] L. E. Fryda, K. D. Panopoulos, and E. Kakaras. “Agglomeration in fluidised bed gasification of biomass”. In: *Powder Technology* 181.3 (Feb. 12, 2008), pp. 307–320. ISSN: 0032-5910. DOI: 10.1016/j.powtec.2007.05.022. URL: <http://www.sciencedirect.com/science/article/pii/S0032591007002793> (visited on 11/09/2020).
- [80] Sylvie Valin, Serge Ravel, Philippe Pons de Vincent, Sébastien Thiery, Hélène Miller, Françoise Defoort, and Maguelone Gâteau. “Fluidised Bed Gasification of Diverse Biomass Feedstocks and Blends—An Overall Performance Study”. In: *Energies* 13.14 (July 18, 2020), p. 3706. ISSN: 1996-1073. DOI: 10.3390/en13143706. URL: <https://www.mdpi.com/1996-1073/13/14/3706> (visited on 07/27/2020).
- [81] Nils Skoglund, Alejandro Grimm, Marcus Öhman, and Dan Boström. “Combustion of Biosolids in a Bubbling Fluidized Bed, Part 1: Main Ash-Forming Elements and Ash Distribution with a Focus on Phosphorus”. In: *Energy & Fuels* 28.2 (Feb. 20, 2014). Publisher: American Chemical Society, pp. 1183–1190. ISSN: 0887-0624. DOI: 10.1021/ef402320q. URL: <https://doi.org/10.1021/ef402320q> (visited on 05/28/2020).
- [82] Wei Cheng Ng, Siming You, Ran Ling, Karina Yew-Hoong Gin, Yanjun Dai, and Chi-Hwa Wang. “Co-gasification of woody biomass and chicken manure: Syngas production, biochar reutilization, and cost-benefit analysis”. In: *Energy* 139 (Nov. 15, 2017), pp. 732–742. ISSN: 0360-5442. DOI: 10.1016/j.energy.2017.07.165. URL: <http://www.sciencedirect.com/science/article/pii/S0360544217313592> (visited on 02/20/2020).
- [83] Alen Horvat, Daya Shankar Pandey, Marzena Kwapinska, Barbara B. Mello, Alberto Gómez-Barea, Lydia E. Fryda, Luc P. L. M. Rabou, Witold Kwapinski, and James J. Leahy. “Tar yield and composition from poultry litter gasification in a fluidised bed reactor: effects of equivalence ratio, temperature and limestone addition”. In: *RSC*

- Advances* 9.23 (2019), pp. 13283–13296. DOI: 10.1039/C9RA02548K. URL: <https://pubs.rsc.org/en/content/articlelanding/2019/ra/c9ra02548k> (visited on 02/20/2020).
- [84] Daya Shankar Pandey, Marzena Kwapinska, Alberto Gómez-Barea, Alen Horvat, Lydia E. Fryda, Luc P. L. M. Rabou, James J. Leahy, and Witold Kwapinski. “Poultry Litter Gasification in a Fluidized Bed Reactor: Effects of Gasifying Agent and Limestone Addition”. In: *Energy & Fuels* 30.4 (Apr. 21, 2016), pp. 3085–3096. ISSN: 0887-0624. DOI: 10.1021/acs.energyfuels.6b00058. URL: <https://doi.org/10.1021/acs.energyfuels.6b00058> (visited on 02/20/2020).
- [85] Marcus Öhman and Anders Nordin. “A New Method for Quantification of Fluidized Bed Agglomeration Tendencies: A Sensivity Analysis”. In: *Energy & Fuels* 12.1 (Jan. 1, 1998), pp. 90–94. ISSN: 0887-0624. DOI: 10.1021/ef970049z. URL: <https://doi.org/10.1021/ef970049z> (visited on 07/11/2019).
- [86] Johannes Christian Schmid. “Development of a novel dual fluidized bed gasification system for increased fuel flexibility”. PhD thesis. Institute of Chemical Engineering, Vienna University of Technology, 2014.
- [87] Stefan Koppatz, Christoph Pfeifer, and Hermann Hofbauer. “Comparison of the performance behaviour of silica sand and olivine in a dual fluidised bed reactor system for steam gasification of biomass at pilot plant scale”. In: *Chemical Engineering Journal* 175 (Nov. 2011), pp. 468–483. ISSN: 13858947. DOI: 10.1016/j.cej.2011.09.071. URL: <http://linkinghub.elsevier.com/retrieve/pii/S1385894711011442> (visited on 05/29/2017).
- [88] Josef Fuchs, Johannes Christian Schmid, Stefan Müller, Anna Magdalena Mauerhofer, Florian Benedikt, and Hermann Hofbauer. “The impact of gasification temperature on the process characteristics of sorption enhanced reforming of biomass”. In: *Biomass Conversion and Biorefinery* (May 31, 2019). ISSN: 2190-6823. DOI: 10.1007/s13399-019-00439-9. URL: <https://doi.org/10.1007/s13399-019-00439-9> (visited on 03/27/2020).
- [89] A. Roine. *HSC Chemistry [Software]*. Pori. URL: www.outotec.com/HSC.
- [90] Thomas Degen, Mustapha Sadki, Egbert Bron, Uwe König, and Gwilherm Nénert. “The HighScore suite”. In: *Powder Diffraction* 29 (S2 Dec. 2014), S13–S18. ISSN: 0885-7156, 1945-7413. DOI: 10.1017/S0885715614000840. URL: <https://www.cambridge.org/core/journals/powder-diffraction/>

article/highscore-suite/C5F7C0DD3DA96EA5E0CFF1A0C9C87DF3 (visited on 08/27/2019).

- [91] Stacy Gates-Rector and Thomas Blanton. “The Powder Diffraction File: a quality materials characterization database”. In: *Powder Diffraction* 34.4 (Dec. 2019). Publisher: Cambridge University Press, pp. 352–360. ISSN: 0885-7156, 1945-7413. DOI: 10.1017/S0885715619000812. URL: <https://www.cambridge.org/core/journals/powder-diffraction/article/powder-diffraction-file-a-quality-materials-characterization-database/3C1FDF449C7A82A8E6FBC8F76342187A> (visited on 05/21/2020).
- [92] Brian H. O’Connor and Mark D. Raven. “Application of the Rietveld Refinement Procedure in Assaying Powdered Mixtures”. In: *Powder Diffraction* 3.1 (Mar. 1988). Publisher: Cambridge University Press, pp. 2–6. ISSN: 1945-7413, 0885-7156. DOI: 10.1017/S0885715600013026. URL: <https://www.cambridge.org/core/journals/powder-diffraction/article/application-of-the-rietveld-refinement-procedure-in-assaying-powdered-mixtures/6580BAA56C9A5833623CCDBEE52B5209> (visited on 05/21/2020).
- [93] Martin Ester, Hans-Peter Kriegel, Jörg Sander, Xiaowei Xu, et al. “A density-based algorithm for discovering clusters in large spatial databases with noise.” In: *Kdd*. Vol. 96. 1996, pp. 226–231.
- [94] M He, B Xiao, Z Hu, S Liu, X Guo, and S Luo. “Syngas production from catalytic gasification of waste polyethylene: Influence of temperature on gas yield and composition”. In: *International Journal of Hydrogen Energy* 34.3 (Feb. 2009), pp. 1342–1348. ISSN: 03603199. DOI: 10.1016/j.ijhydene.2008.12.023. URL: <https://linkinghub.elsevier.com/retrieve/pii/S0360319908016844> (visited on 07/20/2020).
- [95] Hanbing He, Nils Skoglund, and Marcus Öhman. “Time-Dependent Crack Layer Formation in Quartz Bed Particles during Fluidized Bed Combustion of Woody Biomass”. In: *Energy & Fuels* 31.2 (Feb. 16, 2017), pp. 1672–1677. ISSN: 0887-0624. DOI: 10.1021/acs.energyfuels.6b02980. URL: <https://doi.org/10.1021/acs.energyfuels.6b02980> (visited on 07/20/2018).
- [96] R Rauch, K Bosch, H Hofbauer, D Świerczyński, C Courson, and A Kiennemann. “Comparison of different olivines for biomass steam gasification”. In: *Proceedings of the Conference for Science in Thermal and Chemical Biomass Conversion*. Conference for Science in Thermal and Chemical Biomass Conversion. Vol. 1. Victoria,

Canada, Sept. 30, 2004, pp. 677–690. URL: https://www.academia.edu/24146148/Comparison_of_different_olivines_for_biomass_steam_gasification.